TABLE OF CONTENTS

LIST OF FIGURES

LIST OF TABLES

SCIENTIFIC CONTRIBUTIONS

Publications

- **Mhuka V,** Dube S, Nindi MM, "Chemical, structural and thermal properties of *Gonometa postic*a silk fibroin, a potential biomaterial*", Int. J. Biol. Macromol.* 52, 2013, 305-11.

- **Mhuka V,** Dube S, Nindi MM, Torto N, "Fabrication and structural characterization of electrospun nanofibres from *Gonometa postica and Gonometa rufobrunnae* regenerated silk fibroin", *Macromol Res*, 21, 2013, 995-1003.

CHAPTER ONE

1.1   General Introduction

Numerous innovative designs and technologies that have contributed to the improvement of human life have been derived from imitating materials found in nature. Observation of shelled creatures and architectural structures has resulted in the development of body armour and net materials (e.g. fishing nets, bandages, sieves) respectively [1]. Most of these natural materials are protein and polysaccharide polymers arranged individually or as composites with other elements or minerals to obtain various functionalities [2]. These polymers are hierarchically organized to dimensions as low as nanoscale level and exhibit several appealing properties for material scientists. Industries are thus targeting natural polymers, especially those patterned at nano level, for use in numerous medical and technical applications. Silk, collagen, elastin and keratin are some of the protein biopolymers that serve a variety of purposes in nature, mostly as structural materials in various systems [3]. Silks in particular are produced by spiders and several insect species, mostly as building materials for a wide variety of purposes [4]. The most well-known types are from the spiders due to their unparalleled mechanical strength [5] and silkworm which has been valued as a luxury textile fibre for many centuries [6]. Like other natural polymers, silk fibres show considerable variability dependent on the species, silk spinning conditions and the environment of the animals [7, 8]. The increased knowledge of silkworm silk properties and processing has contributed to it being rated as an excellent biopolymer for the development of biomedical devices. The possibilities presented by the silk at nanoscale levels have the potential to revolutionize the field of tissue engineering.

1.2 Background

A greater need for repair of damaged tissues and organs has demanded innovations centred on bio-based materials. Biomaterials are prized for their inherent properties such as biocompatibility, non-toxicity and biodegradability which are critical for biomedical and biotechnological designs. There has thus been increased interest in natural fibres, especially proteins and polysaccharides, which possess biomaterial properties that can be of use in the biomedical and biotechnology sectors [9, 10]. Amongst the natural protein fibres, silk fibroin has emerged as one of the most promising biomaterials for human tissue engineering and/or regeneration. SF offers a unique combination of features that are unmatched by most other biopolymers. Its highly impressive mechanical properties provide support for regeneration of various tissues coupled with good biocompatibility, low inflammatory response, good gas permeability and tailored biodegradation [11].

Versatility in processing and chemical modification options offered by SF strengthens its preferential use in applications requiring biocompatible polymeric materials. Broad applicability of SF can also be realized through utilization of different formats such as films, hydrogels, powders, foams, micro and nanoparticles, membranes and 3D-scaffolds [11-13]. Three dimensional porous materials, particularly in the form of nanofibres, have greater potential as scaffolds for tissue engineering compared to two dimensional ones. Strongly resembling the natural extracellular matrix (ECM) of organisms, the high porosity and large surface area of nanofibres allows for cell attachment, transport of nutrients and gaseous exchange. In addition, a broad range of activity can be introduced into the nanofibre matrix by functionalizing or adding single or multiple bioactive components such as antibiotics, antimicrobials and growth factors [14, 15].

Amongst the techniques used for producing three dimensional nanostructured materials, electrospinning outclasses the rest due to its simplicity, cost-effectiveness, ability to produce nanofibres from various types of polymers and scale up capability [16]. Several reviews have been published highlighting the vast opportunities offered by electrospinning [17-19]. Nanofibres produced from various biomaterials have proven to be excellent in many biomedical applications. SF electrospun nanofibre scaffolds in particular have been recommended for growth and repairing of various tissues such as blood vessels, skin, nerves, tendons, bone and cartilage [11, 14, 20].

1.3   Motivation of the study

In order for fibroin to be effectively applied in various fields, there has to be a good understanding of its chemical and structural features which affect its performance. Studies conducted show that SF is generally a large molecular weight (200–350 kDa or more) polymer composed of 18 amino acids arranged mostly in repetitive hydrophobic domains interspaced with small hydrophilic regions [21]. SF from the domesticated *Bombyx mori* species has been extensively characterized over many decades [22-24] and as such it has been the most applied as a biomaterial. SF extracted from other species has displayed different chemical properties and variability in primary structures and physical properties [25]. This diversity has been attributed to distinctions in the amino acid sequences of the different silks. For example, *Antheraea* silks are composed primarily of alanine-alanine (Ala-Ala)$_n$ polypeptides whereas the *B. mori* silks are mainly comprised of glycine –alanine (Gly-Ala)$_n$ polypeptides [26].

Information on the diverse properties offered by SF from other species has resulted in increased interest in their use as biomaterials. Their performance in some biomaterial

applications has been found to be superior to *B. mori* SF owing to differences in their physicochemical properties. In one study, films prepared from *A. mylitta* fibroin showed better cell growth and proliferation than films made from *B. mori* fibroin [27]. This was attributed to a tripeptide sequence, arganine–glycine–aspartic acid present in *A. mylitta* and not in *B. mori* fibroin. In addition to performance, the type of SF has also been found to influence key processes such as dissolution [28] and also has an impact on biomaterial fabrication [29, 30]. The clear fact is that each type of silk therefore has to be studied extensively to assess its processing and potential use as a biomaterial as this varies between species.

These and other studies highlighting the potential of silk other than that from *B. mori* have motivated research of less studied silks such as those from uncommon silkworm species, bees, scorpions and mites in order to identify the unique properties that may be valuable for biomaterial and/or textile applications [31-33]. Africa is home to a number of the less studied silkworm species from different families such as the *Saturniidae*, *Thaumetopoeidae* and *Lasiocampidae* families. Limited studies have focused on identifying their chemical and physical properties [34-36] and more have been from a biodiversity, entomological and textile perspective [37-41]. There have/has actually been no studies on the processing and fabrication of applicable biomaterial formats of silk fibroin from silkworm species indigenous to Africa; thus their use has not gone beyond textiles. Understanding properties and processing of silk fibroin from African species will be key in identifying their place in biomaterial and biotechnological applications. Moreover, it will extend knowledge of the relationship between structure and functional properties of natural fibrous polymers.

1.4 Objectives

Against this background, the overall objective of the presented work was to determine the properties of silk fibroin from African silkworm species and to explore their potential use as biomaterials. This was achieved under the following specific objectives:

1. Chemical and physical characterization of fibroin derived from the African silkworm species *Gonometa rufobrunnae, Gonometa postica, Argema mimosae, Epiphora bahuniae* and *Anaphe panda*

2. Fabrication and characterization of electrospun nanofibres from fibroin derived from African silkworm species

3. Application of fabricated fibroin nanofibres as biomedical scaffolds.

1.5 Layout of the Thesis

Chapter 1 introduces the work and presents the motivation and objectives for the work.

Chapters 2 and 3 provide literature review. Chapter 2 focuses on reviewing work done on the characterization of silk proteins. It also discusses properties of silk fibroin that make it attractive as a biomaterial. Chapter 3 discusses the electrospinning technique and its use in the fabrication of SF nanofibres. The use of electrospun SF nanofibres in different applications is also discussed.

Chapter 4 covers the experimental procedures and characterization techniques used in the study.

Chapters 5 and 6 contain results of the experiments conducted in the study. Chapter 5 focuses on the results of the chemical and physical characterization of the African silk fibroins. Chapter 6 shows results on the electrospinning of *Gonometa* SF. We also present results on

adsorption of the natural polyphenol resveratrol onto silk nanofibres for potential biomedical application.

Chapter 7 presents conclusions of the research undertaken in this study. Proposals are also put forward for recommended future work.

CHAPTER TWO

SILK AND ITS PROPERTIES

2.1   Introduction

Silks are protein polymers that are spun into fibres by some arthropods such as silkworms, spiders, scorpions and mites [42, 43]. These organisms produce silks for different purposes such as protective shelters, structural supports and capturing food [42, 44]. Silkworms in particular spin silk cocoons for protection from environmental elements and predators during metamorphosis. Silkworm silk is the most explored due to its success in textiles, historical medical use and availability as compared to silks from other organisms [44]. Classification of silk producing moths is often according to their different families e.g. *Bombycidae*, *Saturniidae*, *Lasiocampidae*, *Thaumetopoeidae*, etc., as summarized in Table 2.1. Though there are over 400 species of silk moths found in the world [45], only a few have been successfully explored for commercial production of silk.

Silk production is typically associated with Asia, where silk processing was first developed over 4,500 years ago in China. Commercial silks are broadly classified as mulberry (cultivated) silk and non-mulberry (wild) silk. The *Bombyx mori* species which feeds on mulberry leaves is the best example of cultivated silk. *B. mori* silkworms have the highest fibre production thus providing the bulk of commercial silk fibre to date [46]. However, the silks produced by wild silkworms have found a place in the global market because of their rare feel and colour [50]. Unlike the *B. mori* silkworms that are reared in a controlled environment and nutrition, the wild silkworms feed and spin cocoons on a variety of host plants in their natural habitats. The quality of silk they produce is different and mainly attributed to their polyphagous nature, which has been found to influence the type of cocoon

produced [51]. Most of the wild silks species are from the *Saturniidae*, *Lasiocompidae* and *Thaumetopoeidae* families such as *Antheraea pernyi*, *Antheraea mylitta*, *Antheraea yamamai* and *Samia Cynthia ricini* [52].

Table 2.1.   Classification of some silkmoths found around the world

Silkworm species	Host plants	Distribution	Reference
Bombycidae			
Bombyx mori *B. mandarina*	Mulberry	China, India, Japan, Korea	[46]
Saturniidae			
Antheraea mylitta	*Terminalia tomentosa, Terminalia arjuna, Shrea robusta*	India, Korea, Japan,	[47]
A. assemensis	*Persea bombycina, Litsea polhantha, L. salicifolia, L. citrate*		
Lasiocampidae			
Gonometa postica	*Acacia erioloba, A. tortillis, A. mellifera, Burkea africana, Prosopis glandulosa, Brachystegia species*	Southern Africa, Kenya	[37, 38]
G. rufobrunnae	*Colophospermum mopane*	Botswana, Zimbabwe, Namibia	[37]
Thaumetopoeidae			
Anaphe infracta , A. venata, A. panda A. reticulata A. moloneyi	*Bridelia minrantha, Pseudolachnostylis maprouneifolia, Cynometra ulexandri, Triumfetta manrophylla*	Nigeria, Uganda, Kenya, Cameroon, Congo, and Togo	[39, 48, 49]

Developing countries, including some in Africa, have taken up wild silk production to generate employment as part of poverty alleviation projects for poor rural societies. Africa is home to a number of wild silk species and some of them such as *Gonometa postica*, *Gonometa rufobrunnae* and *Anaphe panda* have shown they have potential use in the textile industry [37-39, 53, 54].

2.2   Composition of the silk thread

Silk proteins are synthesized in specialized glands of the silkworm and fibres are formed by stretching the liquid silk through the head movement of the silkworm [55-57]. Sericin and fibroin are the two main proteins produced by the silkworm. Fibroin makes up the bulk of the silk fibre with almost 80% composition whilst sericin constitutes 20–30% of the silk fibre, depending on the species [55, 58]. The fibroin, which is made up of two bundle cores (called brins), is synthesized in the posterior silk gland and then transferred into the middle silk gland where it is stored prior to spinning. Sericin is produced in the middle silk gland and is secreted into the lumen. It coats the fibroin during spinning and acts as a gum binder to maintain the structural integrity of the cocoon [55, 58]. The rest of the cocoon consists of other small proteins, waxes, fats, salts and ash [59].

2.3   Chemical characterization of silk proteins

Proteins are essentially polymers of different length amino acid chains. Every amino acid possesses three groups; an amine group, a carboxyl group and a hydrogen atom bound to an alpha-carbon. The fourth group is the side chain ("R" group) which varies from one amino acid to the other. The unique amino acid composition of proteins results in their different sizes, structural arrangement and chemical reactivity. Silk proteins can thus be identified by the type and quantity of amino acids in their structure.

Chemical and structural studies on silk proteins have been primarily done on fragments isolated from *B. mori* species as early as the 1930s [60]. The same 18 amino acids have been identified in both sericin and fibroin. However, owing to the different roles of the two proteins, they have easily distinguishable chemical compositions. Fibroins generally have around 80% non-polar amino acids rendering them insoluble in hot water. *B. mori* fibroin has

a large average molecular weight comprised of a heavy (350 kDa) and light (25 kDa) chain. These chains are linked together through a disulphide bond and the glycoprotein P25 (30 kDa). Each P25 protein is bound through hydrophobic interaction to six heavy and light chains [61, 62]. The H-chain has a highly repetitive sequence of approximately 5263 amino acid residues typically rich in glycine, alanine and serine [23]. The L-chain polypeptide has about 262 amino acid residues dominated by leucine, isoleucine, valine and acidic amino acids. Fibroin extracted from wild silkworms indicates similarity to *B. mori* fibroin in that the predominant amino acids are glycine, alanine and serine, though there is variability in composition and size of the protein. Datta and co-workers established that *A. mylitta* fibroin is composed of two similar sized polypeptides approximately 197 kDa each [25]. This assembly appears to be characteristic of silk secreted by the *Saturniidae* family where L-fibroin and P25 are absent [63]. Table 2.2 shows the amino acid composition of fibroins from different silk species.

Sericin has a very different composition from fibroin. Studies have shown more than 5 different sized polypeptides ranging from 20 to over 300 kDa in both mulberry and non-mulberry sericin [24, 65, 66]. Most of the amino acids in sericin have strong polar (hydroxyl, carboxyl and amino) side groups such as serine and aspartic acid. Similar to observations for fibroin, sericin from wild cocoons has shown differences to *B. mori* sericin (Table 2.3). Exposure to various external stresses and harsh environments has been one of the reasons cited for differences in chemical composition in mulberry and wild cocoons [66]. Diet and differing genetics have also been implicated as contributors to these differences [67].

Table. 2.2.   Amino acid composition of fibroins from different silk species

Amino acid	Mole (%) composition				
	Bombyx mori [64]	*Anthereae mylitta* [25]	*Philosamia cynthia ricini* [64]	*Anaphe infracta* [64]	*Gonometa rufobrunnae* [34]
Glycine	42.8	30.89	27.8	28.6	35.95
Alanine	32.4	27.7	50.5	61.5	23.75
Serine	14.7	13.72	7.0	5.80	12.88
Tyrosine	11.8	9.37	10.7	2.85	5.11
Arganine	0.90	3.4	3.81	1.76	6.07
Aspartic acid[a]	1.73	5.39	4.48	2.13	7.06
Glutamic acid[b]	1.74	1.26	1.23	1.93	1.84
Threonine	1.51	3.4	0.72	0.52	1.08
Proline	0.63	0.05	0.55	0.86	2.07
Histidine	0.32	1.36	1.74	1.16	0.13
Phenylalanine	1.15	0.21	0.35	0.28	0.53
Valine	3.03	1.57	0.58	0.54	1.12
Leucine	0.68	0.79	0.50	0.91	1.04
Lysine	0.45	0.26	0.46	0.23	0.49
Isoleucine	0.87	0.28	0.68	0.40	0.74
Cystine	0.03	ND	0.01	0.01	0.06
Tryptophan	0.36	ND	0.70	0.51	-
Methionine	0.1	0.05	0.02	0.11	0.12

ND = not detected; - = not determined

A few characterization studies on proteins from the African silk worm species have been reported in literature. The first report was by Freddi and co-workers conducted on G*onometa rufobrunnae* [34]. The fibroin, typical to those from other species, had large amounts of glycine and alanine.   In the same study, *G. rufobrunnae* sericin also contained a lot of acidic and hydroxyl amino acids with serine being the most abundant amino acid. There has been also a report on the chemical composition and rheological behaviour of *Gonometa postica* fibroin extracted directly from the silkworm glands [70]. Part of the work presented in this thesis on the *Gonometa* species has also been published [71]. Some data on *Anaphe panda* silk has been recently reported by researchers in Kenya [72]. There is however still a lot of work that needs to be done regarding the study of the chemical composition of silk proteins from other African silkworm species such as *A. mimosae* and *E. bahuniae*.

Table 2.3.   Amino acid composition of sericin from different silk species

Amino acid	Mole (%) composition			
	Bombyx mori (250kDa) [68]	*Antheraea mylitta* [64]	*Cricula trifenestrata* [69]	*Gonometa rufobrunnae* [34]
Glycine	14.3	14.91	20.8	20.59
Alanine	5.5	2.73	5.9	11.52
Serine	39.0	23.21	39.8	21.51
Tyrosine	0.70	4.33	7.1	2.90
Arganine	2.90	6.11	2.9	3.67
Aspartic acid[a]	13.3	14.15	2.6	18.08
Glutamic acid[b]	12.8	6.03	1.5	8.95
Threonine	3.3	13.16	13.1	1.29
Proline	ND	1.09	2.5	1.55
Histidine	1.0	2.41	-	1.06
Phenylalanine	0.4	2.47	-	2.28
Valine	0.7	0.79	-	1.80
Leucine	0.5	0.55	1.1	2.13
Lysine	5.4	2.01	0.7	1.13
Isoleucine	0.2	0.39	0.8	1.41
Cystine	0.1	Traces	-	Traces
Tryptophan	-	-	-	-
Methionine	ND	Traces	-	0.16

ND = not detected; - = not determined

2.3.1   Amino acid analysis

The types and quantities of amino acids present in silk fibroin have a notable impact the physical and chemical properties of silks. This is because the amino acids influence sequencing which then determines protein orientation and conformation of the protein chains [73].

Amino acid analysis (AAA) is therefore an important step in characterizing silks and typically involves four main steps; hydrolysis, derivatization, separation and data interpretation. Hydrolysis is the process of breaking down the peptide bonds in the protein to release individual amino acids reflecting the composition of the parent protein [74]. Acid

hydrolysis using hydrochloric acid (HCl) is mostly used for protein/peptide hydrolysis. Derivatization involves modification of analytes with the aim of imparting more suitable analytical characteristics to the analytes [75]. Specifically in AAA, derivatization is done for detection purposes as most amino acids suffer from the lack of strong chromophores (for UV detection) or fluorophores (for fluorescence detection). Phenylisothiocyanate (PITC) is a very good derivatization reagent for amino acids forming a cyclic 3-phenyl-2-thiohydantoin (PTH) or phenylthiocarbamyl (PTC) labelled product [76, 77] detectable at 254 nm (maximum absorbance) using UV detection.

Though all the stages highlighted above are important, this study focused more on the separation and quantification of the derivatized amino acids. Separation of amino acids in complex matrices such as fibroin presents challenges as amino acids share common aspects of their chemical structure and hence have similar chemical properties. Each has a carboxylic acid and an amino functional group attached to the same tetrahedral carbon atom. Variances are found in the nature of their side groups (R) such as long or short chain alkyl groups, phenyl groups or polar entities (Table 2.4).

Early methods developed for the separation, detection and quantification of amino acids were based on ion exchange chromatography (IEC), high performance liquid chromatography (HPLC) and gas chromatography (GC) [78-80]. Capillary electrophoresis (CE) later became a well appreciated technique in amino acid profiling as it offers intrinsic advantages such as high separation efficiency, small sample volumes and low consumption of solvents [81-83]. CE is an electrophoretic separation technique that employs an electric field to separate charged ions. Partitioning is primarily based on differences in solute size and charge at a given pH [82].

Table 2.4.   Structure and properties of amino acids found in silk [84]

Amino Acid	Abbreviation	R	pKa-NH$_3^+$	pKa-CO$_2$H	pKa-Side chain
Glycine	Gly	-H	9.6	2.34	-
Alanine	Ala	-CH$_3$	9.69	2.35	-
Valine	Val	-CH(CH$_3$)$_2$	9.62	2.32	-
Leucine	Leu	CH$_2$CH(CH$_3$)2	9.60	2.36	-
Isoleucine	Ile	CH(CH$_3$)CH$_2$CH$_3$	9.68	2.36	-
Phenylalanine	Phe	—CH$_2$—⟨phenyl⟩	9.13	1.83	-
Tryptophan	Trp	—CH$_2$—⟨indole⟩	9.39	2.38	-
Tyrosine	Tyr	—CH$_2$—⟨phenol⟩—OH	9.11	2.20	10.07
Histidine	His	—CH$_2$—⟨imidazole⟩	9.17	1.82	6.0
Serine	Ser	CH$_2$OH	9.15	2.21	-
Threonine	Thr	CH(CH$_3$)-OH	10.43	2.63	-
Methionine	Met	CH$_2$CH$_2$SCH$_3$	9.21	2.28	-
Cysteine	Cys	CH$_2$SH	8.33	1.71	10.78
Aspartic Acid	Asp	CH$_2$CO$_2$H	9.82	2.09	3.86
Glutamic Acid	Glu	CH$_2$CH$_2$CO$_2$H	9.67	2.19	4.25
Asparagine	Asn	CH$_2$CONH$_2$	8.08	2.02	-
Glutamine	Gln	CH$_2$CH$_2$CONH$_2$	9.13	2.17	-
Lysine	Lys	(CH$_2$)4NH$_2$	8.95	2.18	10.53
Arginine	Arg	-(CH$_2$)$_3$-NH-C(=NH)NH$_2$	9.04	2.17	12.48
Proline	Pro	⟨pyrrolidine⟩-CO$_2^-$	10.60	1.99	-
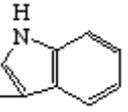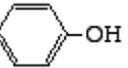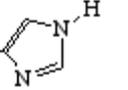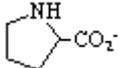
The variances result in different migration velocities of the analytes when voltage is applied; thus they are separated as depicted in Figure 2.1a. However, separation solely based on charge to mass ratios is not very successful in separating neutral or similar structured amino

acids such as the isomers leucine and isoleucine which have almost identical pKa values (Table 2.4).
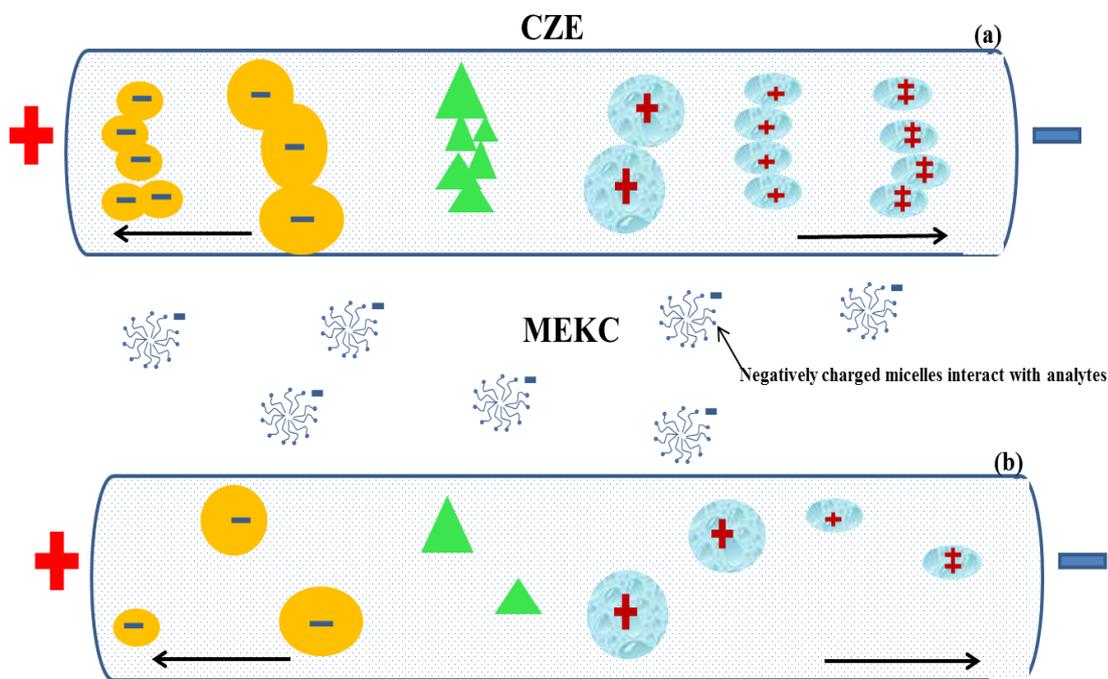
Figure 2.1. Illustration of separation in (a) CZE mode and improved resolution in (b) using MEKC mode

Modified electrophoresis techniques such as micellar electrokinetic chromatography (MEKC) offer added advantages in the separation of complex mixtures comprised of acidic, neutral, and basic amino acids. MEKC makes use of charged micelles to separate neutral and charged analytes by means of a pseudo-micellar phase that is created through hydrophobic interactions between solute molecules and the surfactant [85]. Analytes migrate based on their partitioning between the bulk buffer solution and micelles thus adding selectivity in the separation process (Figure 2.1b). Iadarola *et al.* extensively reviewed MEKC as a separation tool for amino acids from various biological matrices [86]. The review highlights MEKC as a reliable analytical technique for the analysis of amino acids in real samples and it was therefore the method of choice for determining amino acid composition of silk proteins in this work.

2.4   Primary and secondary structure of silk proteins

The variation in amino acid composition between sericin and fibroin results in considerable differences in their primary and secondary configurations. Sericin is primarily amorphous and has no organized structure. Silk fibroin, on the other hand, is highly ordered due to a repetitive primary structure based predominantly on the amino acids glycine, alanine and serine [87, 88]. The recurring subunits of these short chain amino acids permit close packing between the molecular chains resulting in extensive crystalline regions in fibroin [87]. Most of the amino acid residues with bulky and polar side chains are found in the minor non-crystalline (amorphous) areas. This region is made up of various disordered structures with varying degrees of hydrogen bonding [89]. The structures observed for SF in the solid state are the Silk I, Silk II and Silk III structures. These structures have been investigated using several analytical techniques that include X-ray diffraction [22, 90], electron diffraction [91-93], conformational energy calculations [94, 95], Infrared spectroscopy [90, 96] and NMR [97-99].

Of the three structures, Silk III is the relatively newly discovered structure. It is described as a threefold helical crystal structure adopted by fibroin at the air–water interface, separating the hydrophobic alanine residues from the hydrophilic serine residues [100-102]. The Silk I structure is that found in the silk gland before spinning and is water-soluble. This structure is unstable as it transforms to the more common Silk II structure when subjected to physical stress such as drawing and shearing or upon exposure to heat and organic solvents [103, 104]. The lack of orientation and the ease with which Silk I converts to Silk II has made its study difficult though some researchers have proposed possible structural models for it [105].

The Silk II (β-sheet) structure is the dominant secondary structure of fibroin which is well documented as it has been thoroughly studied for decades. The key element of this structure is the extensive hydrogen bonding between adjacent polypeptide chains forming large interconnected sheets (Figure 2.2). Marsh *et al.* proposed the antiparallel hydrogen bonded β-sheet arrangement in which all of the polypeptide's methyl groups are found on one side of the protein sheet for the Silk II structure of *B. mori* fibroin [22]. On the basis of this structure, Warwicker categorized fibroin from the different species into several groups. These groups have different intersheet spacings dependent on varying amounts of glycine and alanine in the crystalline areas [106].
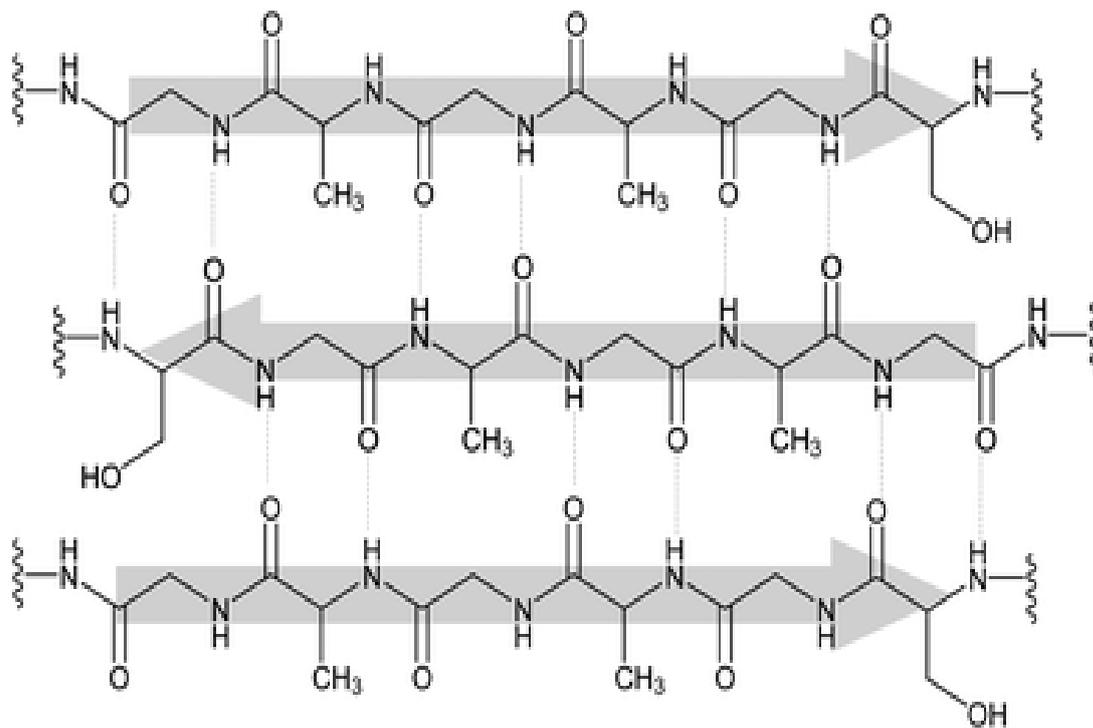
Figure 2.2.   Interaction between polypeptide chains forming the β-sheet structure [109]

The general conclusion from various studies is that the repetitive regions of the Silk II crystalline structure of *B. mori* SF are made up of -Gly-Ala-Gly-X$_{.n.}$ units, with X as Ser or Tyr while those of the wild *Saturniidae* silks are mainly of polyalanine (Ala)$_n$ repeats [26,107,108].

2.5 Physical properties of silk fibroin

Both the crystalline and amorphous regions play an important role in determining the physical properties of the silks. The crystalline domains are responsible for the strength and toughness of the fibroin as the high fraction of β-sheets reinforce the structure which contributes to the stability of silk. The amorphous domains allow the crystalline domains to orient under strain thereby introducing elasticity and flexibility and also further increasing the strength of the material [11, 110]. The overall result is silk fibres possessing exceptional mechanical properties as compared to other natural and synthetic fibres, which is one of their most outstanding features. The hydrophobic domains of fibroins also contribute to its thermal stability at very low as well as very high temperatures [110, 111].

2.6 Silk fibroin as a biomaterial

One of the more common definitions of a biomaterial is "any substance (other than a drug) or combination of substances synthetic or natural in origin, which can be used any time, as a whole or as a part of a system which treats, augments, or replaces any tissue, organ or function of the body"[112]. Fibroin originally found use as a biomaterial in suturing of wounds after surgeries [113]. With continued research, fibroin use has extended to other biotechnological and biomedical applications. This is mainly because, in addition to its excellent physical properties, silk fibroin possesses biocompatible properties that render it useful as a biomaterial as summarized in Figure 2.3.

18
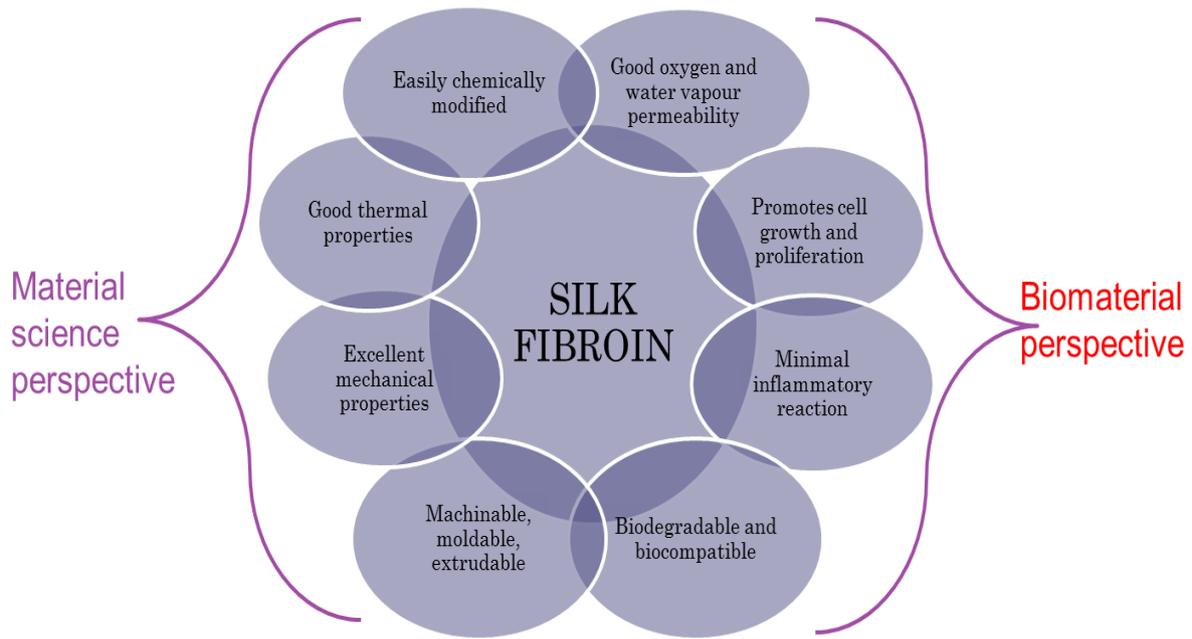
Figure 2.3.   Properties of silk fibroin

Fibroin has exceptional biocompatibility, biodegradability, low inflammatory response and good oxygen/water vapour permeability [114-116]. Biocompatibility is a vital property for biomaterials to ensure biological integration without causing harm to the host organism. Fibroin prepared in different formats has shown biocompatibility and has been successful in culturing a number of cell types with good adhesion and growth, similar or enhanced when compared to other biomaterials [117-120].

To ensure the desired physiological integration of a biomaterial device, its biodegradability must match its intended function in the organism. As a protein, fibroin degrades in a biological environment as a result of proteolysis. The rate and extent of silk biodegradation reportedly varies with different proteolytic enzymes such as chymotrypsin, protease, actinase and carboxylase [114, 121, 122]. Degradation rate is variable, depending on factors such as structural and morphological features of the fibroin, processing conditions, characteristics of

the biological environment at the location of implantation, and presence of different mechanical and chemical stresses [123]. It can be concluded that properties such as biodegradability and biocompatibility are influenced by the molecular arrangement or conformation of the silk fibroin.

2.7   Preparation of silk fibroin matrices for biomaterial applications

The chemical and material properties of silk fibroin allow it to be processed into a variety of formats with potential for surface modifications suiting a wide range of applications. Silk fibroin biomaterial formats are mostly made from silk fibroin solutions. These solutions can be obtained by dispersing liquid silk from the silk gland of matured larvae in water, or by dissolving degummed silk fibres from cocoons [124]. The latter method is more practical for yielding large quantities of silk at once, though a number of steps are involved in processing the cocoons. The initial step is degumming where sericin is separated from the fibroin. The sericin is easily removed due to its hydrophilic nature which renders it soluble in hot water, alkali or acid solutions. Sodium carbonate (Na_2CO_3) or sodium hydrogen carbonate ($NaHCO_3$) solutions are typically used for degumming [125]. The degummed fibres are then washed and dried before dissolving them to yield a fibroin solution.

Dissolution of SF is often challenging as solvent molecules have to penetrate and break down the highly crystallized structure of the protein. SF is therefore insoluble in common solvents such as water, dilute acids and alkalis. Traditional methods of fibroin dissolution employ concentrated solutions of aqueous, organic and aqueous-organic solution of salts such as lithium thiocyanate (LiCNS), lithium bromide (LiBr), calcium chloride ($CaCl_2$), zinc chloride ($ZnCl_2$), and calcium nitrate ($Ca(NO_3)_2$) [126-128]. More recently, ionic liquids have proven to be effective environmentally friendly solvents in dissolving fibroin [129, 130].

After dissolution, the fibroin solution is subjected to filtration and dialysis to remove any debris and the salt ions to produce an aqueous fibroin solution. The 'redissolved' aqueous fibroin solution is often termed regenerated silk fibroin (RSF). From RSF, fibroin can be used alone, blended and/or functionalized with other materials to fabricate different formats such as films [131-133], membranes [134], hydrogels [135, 136], sponges [121], powders [137], 3D scaffolds [138, 139], fibres and nanofibres [140-144].

The properties of the silk fibroin greatly influence its preparation into the different applicable designs and also affect its performance as a biomaterial. Studies on the attachment and growth of fibroblast cells (L-929) on the matrices of silk fibroin made from *B. mori* and *A. pernyi* showed that *A. pernyi* silk fibroin exhibited better cell attachment and growth [145] *A. pernyi* fibroin molecules contain the arganine–glycine–aspartic acid (RGD) tri-peptide sequences and consist of more amino acids with positive charge, which favours cell attachment. Acharya *et al*. reported that *A. mylitta* films had better mechanical strength, lower hydrophilicity and better support for cell growth as compared to *B. mori* films [146, 147]. Each silk therefore has to be studied extensively to assess its potential use as a biomaterial as this varies from species to species. This, combined with the need for materials with varied functionality biomedical and biotechnological applications, has prompted the study of the chemical, physical and biomaterial properties of unstudied silks [148-150]. These unstudied species include many of those found in Africa that are subject to research in this work.

CHAPTER THREE

ELECTROSPINNING AND SILK FIBROIN NANOFIBRES

3.1   Introduction

Fibres serve different purposes in nature and have also found use in numerous technological applications. When these fibres are reduced to nano-scale dimensions, new and/or improved physicochemical properties are realized such as high surface area to volume ratio, superior thermal and electrical properties and mechanical strength [18, 151]. Nanofibres have thus found application in various industries including reinforcement of composites [152], protective textiles [153], filtration [154], catalysis [155], tissue engineering [156, 157] energy storage [158], sensors [159] and enzyme immobilization [160].

Table 3.1   Comparison of nanofibre fabricating techniques [161]

Process	Production scale	Advantages	Disadvantages
Drawing	Laboratory	Minimum equipment required	Discontinuous process, difficult to control fibre dimensions
Template synthesis	Laboratory	Different fibre dimensions easily achieved by using different templates	Process cannot be scaled up from laboratory
Phase separation	Laboratory	Minimum equipment required, Batch to batch consistency is easily achieved	Limited to specific polymers
Self assembly	Laboratory	Good for obtaining smaller nanofibres	Complex process
Electrospinning	Laboratory and industrial scale	Cost effective, wide applicability using both natural and synthetic polymers long continuous nanofibres can be produced	Jet instability

Fabrication of nanofibres can be achieved using several techniques such as the template method [162], self assembly [163], phase separation [164], drawing [165], melt blowing [166], ultrasonic techniques [167], nanolithography [168] and electrospinning [157-159].

From a practical view point, most of the above mentioned techniques have limitations with respect to cost, production rate and the variety of polymers that can be processed (Table 3.1). Electrospinning is the only process that can easily produce large volumes of nanofibres from a wide range of synthetic and natural polymers at a reasonably low cost. It has thus become the most studied and developed nanostructuring technique by many tertiary and research institutes worldwide. Several companies worldwide, such as eSpin Technologies (United States) and Elmarco (Czech Republic), have harnessed this technology for materials production and have been successful in commercializing electrospun products [169-171].

3.2   Background of electrospinning

Electrospinning, originally termed electrostatic spinning, involves the generation of nanofibres from a polymer solution or melt using electrostatic force. Cooley and Moore filed patents that depicted apparatus for spraying of liquids using electrical charges over a 100 years ago [172]. The more famous patent was filed by Formhals in which he described the electrospinning of plastics [173]. A few decades later, there was a renewed interest in the process with a discovery made by Taylor named after himself, the "Taylor cone". This phenomenon is the deformation of the droplet at the end of the tip into a conical shape after application of the electrical field [174]. Reneker and co-workers then made significant contributions in understanding the process as they explored electrospinning of many different polymers [175, 176]. Over the years, knowledge and application of the process has evolved with continued research and development. Several review articles have been published

describing the numerous advancements that have been made in various aspects of the technique [177-179].

3.3 Electrospinning setup and process

The most basic electrospinning setup is shown in Figure 3.1. It consists of a high voltage power supply, syringe pump, collector, and a syringe fitted with a needle. The polymer solution or melt is pumped through the needle and charged with a large electric potential. When voltage is applied and the electric potential reaches a critical level, the electrostatic repulsion of the polymer solution overcomes the surface tension at the tip of the spinneret, and a fine jet of entangled polymer chains is drawn out [178]. This jet whips through the air towards the grounded target, creating a dry fibre that collects on the target as the solvent evaporates.
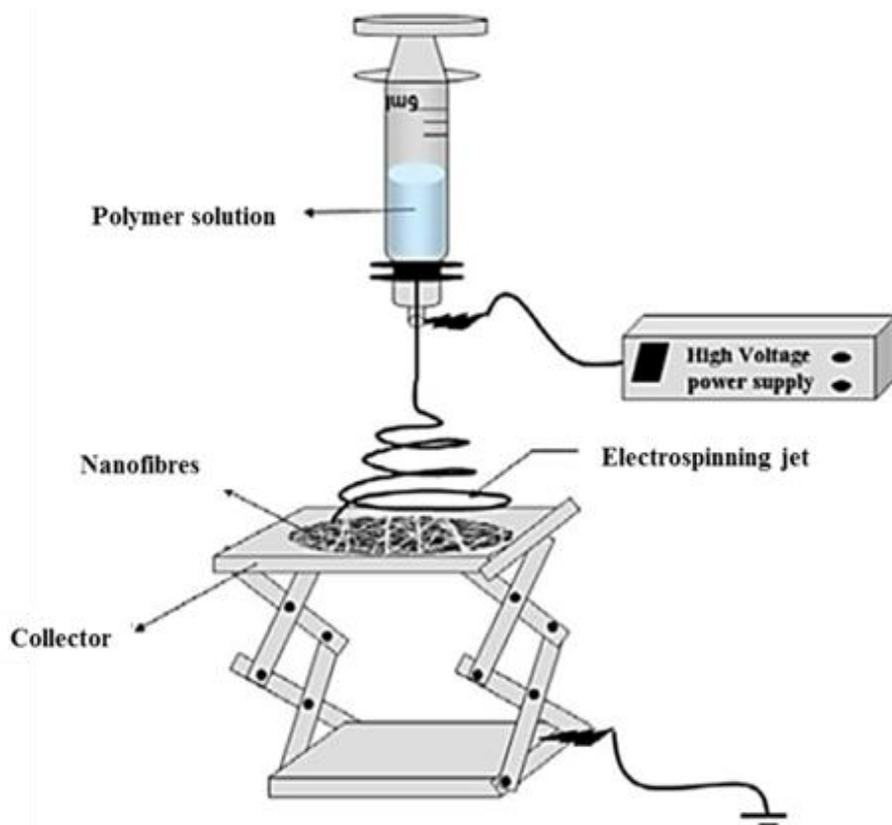
Figure 3.1.   General electrospinning setup [180]

Characteristics such as nanofibre diameter and morphology can be controlled by varying parameters that affect the electrospinning process. These parameters include processing, solution and ambient conditions [161, 181]. These parameters interact and influence each other during the electrospinning process and have to be optimized for nanofibres to form. Table 3.2 highlights how these parameters have affected nanofibre formation using different polymers.

Apart from the different parameters affecting electrospinning, some applications require tailoring of nanofibres to suit specific functions. Electrospinning offers multiple possibilities in fabricating customized nanofibrous structures by modification of components such as the needle system [193] and the collecting manifold [194].

3.4   Electrospinning of silk fibroin

In addition to its other attractive material properties, regenerated silk fibroin (RSF) is extrudable, making it a good candidate for electrospinning. It can also be easily chemically modified or blended with other polymers to improve electrospinnability.

Early recorded reports on electrospinning of silk were by Zarkoob and co-workers where they prepared nanofibres from *Bombyx mori* silk and spider dragline silk from *Nephila clavipes* [195]. From then, Sukigara and co-workers successfully employed electrospinning to prepare silk nanofibres whilst also studying how the various electrospinning parameters impact on the properties of the nanofibres [184, 189, 196]. The studies determined that silk concentration was the most important parameter for successful fabrication of silk nanofibres [184].

Table 3.2. Parameters affecting electrospinning

Parameters	Condition	Effect on fibre morphology	References
Solution parameters			
Viscosity	The viscosity of the solution is related to the extent of polymer chain entanglements in the solution that prevent the electrical jet from breaking up	Increase in viscosity results in low bead generation and increase in fibre diameter.	[182]
		High viscosity hinders pumping of the polymer solution through the syringe needle	[183]
Polymer concentration	A minimum concentration is required for sufficient polymer chain entanglements within the solution necessary to maintain the continuity of the electrical jet	Increase in fibre diameter with increase in concentration	[184]
Molecular weight of polymer	Polymer length also influences the extent of polymer chain entanglements in the solvent	Reduction in the number of beads and droplets with increase in molecular weight	[185]
Conductivity	An increase in conductivity of the solution allows for more charges to be carried by the electrospinning jet.	Decrease in fibre diameter with increase in conductivity	[186]
Surface tension	Charges on the polymer solution must be high enough to overcome the surface tension of the solution.	No conclusive link, high surface tension results in instability of jets	[187]

Processing parameters			
Applied voltage	Electrostatic force applied must overcome the surface tension of the solution	Decrease in fibre diameter with increase in voltage There is a greater tendency for beads formation with too low and too high voltage	[188]
Tip to collector distance	For independent fibres to form, sufficient distance is needed to allow time for the solvent to evaporate	Beads generated when distance is too small or too large Increasing the distance results in a decrease of the average fibre diameter	[189]
Feed rate	Feed rate should be proportional to the rate the polymer solution is ejected from the tip of the needle	Decrease in fibre diameter with decrease in flow rate, generation of beads with too high flow rate	[190]
Ambient parameters Humidity	-	High humidity results in circular pores in the fibres	[191]
Temperature	-	Increase in temperature results in decrease of fibre diameter	[192]

Though SF from a number of different silk species has been successfully electrospun, the electrospinnability has been greatly influenced by the type of silk as the molecular weight varies for different silk species. Ohgo *et al.* highlighted this when they found different spinning concentrations for *B. mori*, *Samia Cynthia ricini* and genetically engineered recombinant silk fibroins using hexafluoroacetone hydrate as an electrospinning solvent [197]. In other work, indigenous Thai silkworms (Nang-Lai) and Chinese/Japanese hybrid silkworms showed different electrospinnability [198]. In addition to differences in electrospinnability, *B. mori* silk fibroin, Tussah silk fibroin (TSF) and (SF/TSF) hybrid nanofibres showed differences in properties such as moisture absorption as well as cell attachment and spreading [199]. Other studies have shown that electrospinning of SF is also dependent on the processing methods used for regeneration of the silk. Wadbua and co-workers reported different electrospinning concentrations when they electrospun nanofibres from separated light-chain and heavy-chain fibroins [200]. The nanofibres produced from light-chain and heavy chain fibroins also exhibited differences in properties such as hydrophilic nature, water uptake ability, degradation rate and cell adhesion. It is therefore important to study electrospinning of SF from different species individually as they may require different conditions to produce nanofibres and/or produce nanofibres exhibiting varied properties.

Table 3.3 highlights extensive work done on electrospinning of SF, alone or blended with various polymers or active agents, for different applications and studies. The most utilized solvents for electrospinning silk fibroin shown in Table 3.3 include formic acid (FA), hexafluoro-2-propanol (HFIP), trifluoroacetic acid (TFA), hexafluoroacetone (HFA) and trifluoroethanol (TFE). The use of these harsh organic solvents was put under the spotlight for potentially compromising the biocompatibility and mechanical properties of the silk nanofibres.

28

Table 3.3.   Examples of electrospinning of silk fibroin nanofibres and their applications

Polymer(s)	Additives	Solvent(s)	Application	References
B. mori SF & spider dragline silk	-	HFIP	-	[195]
B. mori SF	-	98-100% FA	-	[184, 201]
B. mori, SF, *S.C. ricini* SF, hybrid silk	-	HFA	-	[197]
B. mori SF	TMOS, (nHA)	HFIP, 98% FA	Bone tissue engineering	[202]
B. mori SF/Chitin	-	HFIP	Wound healing/tissue engineering	[203]
B. mori SF	Curcumin	100% TFA	Drug delivery	[204]
B. mori SF	-	H_2O	-	[205-207]
B. mori SF/PEO	-	H_2O	Cell culture	[208]
B. mori SF	-	Imidazolium based ionic liquids	-	[209]
B. mori SF/carbon nanotubes	-	Imidazolium based ionic liquids	-	[209]
B. mori SF/ (MWNTs)	-	H_2O	Tissue engineering	[210]
B. mori SF/chitosan	-	HFIP,TFE	-	[211]
B. mori SF/CA	-	TFA	Heavy metal ion adsorption	[212]
B. mori SF	-	98% FA	Skin regeneration	[213]
SF/ PLA	Aspirin	TFA/ dichloromethane 70/30)	Drug delivery	[214]
B. mori SF/PEO	Epidermal growth factor (EGF)	H_2O	Wound healing	[215]
B. mori SF	Vitamin C	H_2O	Skin regeneration, Wound dressings, anti-aging cosmetics.	[216]
B. mori SF/Chitosan	-	HFIP / TFA	Wound dressing	[217]
B. mori SF/Chitosan	-	TFA/DCM (7:3)	bone tissue engineering	[218]
A. pernyi SF	-	HFIP	Tissue engineering	[219]
B. mori SF	Au NPs, (RGD) peptide		Tissue engineering	[220]
SF, type I collagen, PLAGA	-	HFIP	Tissue engineering	[221]
Thai *B. mori* and Chinese/Japanese Hybrid *B. mori* SF	-	85% FA	Bone tissue engineering	[222]
B. mori SF	BMP-2	H_2O	Bone tissue engineering	[223]
B. mori & Thai SF	-	HFIP	Nerve regeneration	[224]

Tussah SF	-	98% FA, HFIP	Nerve tissue engineering	[225]
B. mori SF	-	98-100% FA	Enzyme immobilization	[226]
B. mori SF/gelatin	-	FA	Blood vessel engineering	[227]
B. mori SF/PVA	Ag		Antimicrobial scaffold	[228]
SF/SS	-		-	[229]
B. mori silk gland SF/PEO	Green fluorescent protein	H_2O		[230]

TMOS = tetramethyl orthosilicate, (nHA)= nanohydroxyapatite, SWNTs = single walled nanotubes, MWNTs = multi-walled nanotubes, PLAGA = polylactic-co-glycolic acid, BMP-2 = bone morphogenetic protein-2, PLA = polylactic acid, PVA = polyvinyl alcohol, CA = cellulose acetate

Although it has since been deduced that proper removal these solvents do not compromise the use of silk fibroin nanofibres in biological environments, the concern over them still resulted in studies being conducted to determine more 'bio-friendly' electrospinning solvents. Water was the solvent of choice and a number of researchers successfully electrospun fibroin aqueous solutions [205-207]. A general observation is that in aqueous media, higher SF concentrations are required for producing good nanofibres. Ionic liquids are powerful solvents that are considered to be environmentally friendly and some researchers have successfully utilized them for electrospinning silk fibroin [209].

3.5   Post treatment of silk nanofibres

The crystalline structure of fibroin is degraded during processing into regenerated silk fibroin (RSF) used to produce biomaterial formats such as nanofibres. RSF structure is mainly composed of α-helix and random coil conformations resulting in poor mechanical property and water resistance. Mechanical integrity is significant in many applications such as tissue and vessel engineering. RSF matrices therefore require post treatment mostly to restore and/or enhance their mechanical properties and water resistance. The common way of improving mechanical properties of silk fibroin matrices is by inducing crystallinity using

30

polar protonic organic solvents such as methanol, ethanol, propanol and isopropanol. The solvents bring about aggregation of the fibroin molecule chains resulting in structural transition from random coil and α-helix to mainly β-sheet conformation [231]. Improved mechanical properties have been observed for different SF matrices such as films [232] and nanofibres [143]. Methanol is widely reported as the most used solvent for treating SF matrices. It has however been found to induce crystallization of SF in an uncontrollable manner, forming extensive β-sheet structures which result in very brittle matrices [104]. Ethanol has been reported to have a similar but milder effect to methanol as the transition is to a smaller extent [143, 233]. Similar to immersion methods, solvent vapour treatment is also a fast and effective way to alter the secondary structure of SF nanofibres [104]. Water vapour also successfully induced structural transition comparable to the organic solvents. Time and temperature of the treatment were the influential parameters determining the extent of structural change [213].

Recently, cross-linking agents such as glutaraldehyde and genipin have been used to achieve structural transition in SF matrices [234-236]. The advantage these compounds have is that they can be incorporated into the electrospinning thereby enabling conformational transition in one step and eliminating the post spinning treatment. The secondary structure of SF scaffolds is an important factor to consider as it has an impact on properties such as degradation [237], thermal behaviour [232], water absorption [134] as well as oxygen and water vapour permeability [134, 238]. Silk II is the most important and exploited structure in biomaterial applications as it can be tailored to suit various uses.

Alternative to structural modification, blending of SF with other polymers can help improve mechanical properties. SF blend nanofibres with polyethylene oxide (PEO) [239], carbon nanotubes [209], chitosan [211] and cellulose acetate (CA) [212] all exhibited better mechanical properties as compared to pure SF nanofibres. Besides improving and/or

modifying structural and physical properties, post treatment for SF matrices can serve as a method for removing residual solvents used in the electrospinning process [30].

3.6   Application of electrospun SF in wound healing

Electrospun SF nanofibres find use in many applications such as those highlighted in Table 3.3. Regenerative medicine is one of the major areas where there has been significant utilization of SF nanofibres. From a structural perspective, the porous three-dimensional nature of electrospun nanofibres resembles the nanoscale fibrous composition of the extracellular matrix (ECM) of living systems (Figure 3.2). The high surface area provided by nanofibres enables functions such as cell attachment and migration, which are key for regeneration of tissues and organs [240- 242]. The ECM is also composed of many proteins such as collagen, fibronectins, laminin and vitronectin thus making SF a prime material to be used in various facets of regenerative medicine.
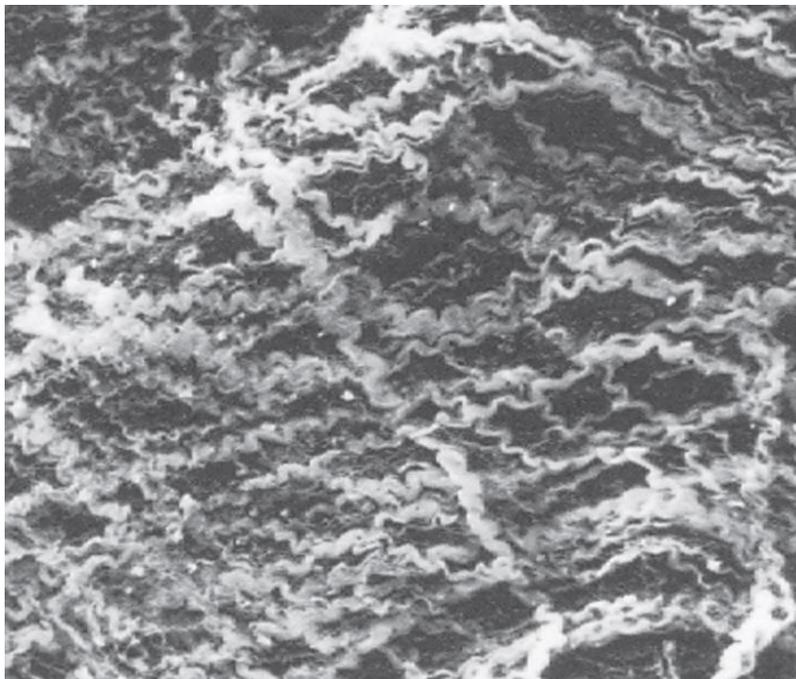
Figure 3.2.   Structure of the extracellular matrix (ECM) surrounding cells in living tissues [243]

Several articles have highlighted the use of SF in many areas of regenerative medicine; however, this review will focus on its applications in wound healing and regeneration. Wound healing involves the restoration or regeneration of dermal and epidermal tissues after an individual has been wounded [244]. The healing process itself is complex and several aspects need to be carefully considered when trying to create an ideal wound dressing. However, the basic desirable properties for a wound dressing are to create an optimum environment to allow reepithelialisation, allow effective gaseous exchange and create a barrier against harmful microorganisms [245, 246].

As wound dressings are in contact with biological environments, biopolymers are mostly more effective as wound dressings and accelerate the wound healing process compared to synthetic polymers [247]. One of the most important steps in wound healing is the closure of the wounded area by epithelial cells, a process that restores the epidermal barrier and protects the underlying tissue. Fibroin has shown potential in this regard by successfully supporting adhesion and growth of human keratinocytes which are the skin cells responsible for reepitheliazation of wounds [203, 213, 248, 249]. Fibroin has also been reported to promote growth and proliferation of human skin fibroblasts, which are also important in the wound healing process [249-253]. Min *et al.* further examined the effect of the nature of the SF matrices on the cell adhesion and spreading. They determined that the nanofibres are better suited for applications such as wound dressings and tissue engineering scaffolds than films and microfibre matrices [248].

3.7   Bioactive agents in wound dressings

For several decades, researchers have been searching for ways of improving the wound healing process. Advances in cellular and molecular biology have brought about knowledge that has made it possible for improvement and development of new therapies for treatment of

wounds. A major advancement are the new generation 'smart' wound dressings that incorporate single or a combination of therapeutic agents that can target different aspects of wound healing. The bioactive agents may be antibiotics [254], antibacterials [255], analgesics [256], growth factors [215], vitamins [216], antifungals [257], or a combination [258].

There are, however, some current drawbacks in wound healing regarding some commonly used additives such as toxicity and increased antibiotic resistance. For example, silver is the active agent in several commercial antimicrobial wound dressings. However, it has been reported that prolonged use of silver particles and nanoparticles may be toxic to DNA and mitochondria [259, 260]. In addition to this, silver in wound dressings is the cause of some irritation and discoloration of wounds and surrounding tissue [261]. This therefore raises concerns regarding safety in long term use of silver. There are also major concerns regarding the increase of antibiotic resistant bacterial strains. Bacterial resistance has been observed with various groups of drugs such as tetracyclines, sulphonamides, macrolides and aminoglycosides [262, 263]. There is also evidence of some microbes also having developed resistance to silver [264].

These illustrations highlight the great need for new or alternative topical bioactive agents to address the shortcomings of the current ones. In our opinion, biological active components derived from plants are significant and important as new drugs that are likely to lead to better treatments for various ailments and diseases.

3.7.1 Plant phenolics in wound dressings

Phenolics are secondary metabolites found commonly in many foods that are integral in the human diet such as vegetables, fruits, grains, teas, herbs and fruits [265]. The compounds are classified under several groups though their commonality lies in each compound possessing a phenol group in its structure. One of the groups of phenolics, the polyphenols, exhibit an

array of valuable biological activities, including antiviral, antibacterial, antioxidant, anti-inflammatory, and anti-carcinogenic activity [266] and have great prospects as medicinal products. Major emphasis has been placed on polyphenols being taken orally as dietary supplements. The same multiple benefits can be afforded to the skin when polyphenols are applied topically [267, 268] as they possess a number of properties beneficial for wound healing and combating a wide range of skin disorders. It is often necessary for these compounds to be carried in formulations or in materials to be delivered to their targets. Fibroin is attractive and has success as a carrier for bioactive molecules due to its chemical and structural properties. A wide range of molecules can thus be encapsulated and stabilized within the fibroin through hydrophilic and/or hydrophobic interactions [356, 357].

SF matrices functionalized with polyphenols have provided scaffolds that are excellent candidates for wound healing and tissue engineering materials. Polyphenolic extracts from the plants *Pistacia terebinthus*, *Pistacia lentiscus*, and *Hypericum empetrifolium* were adsorbed on silk fibroin/chitosan blend films resulting in a scaffold with both antibacterial and antioxidant properties [269]. Kasoju & Bora prepared a curcumin releasing porous SF scaffold that can be used as a wound dressing or for therapy against cancerous tumours [270]. In addition to the inherent properties of SF, the high surface area and porosity of SF nanofibres make them great candidates for carrying compounds such as polyphenols. However, there are few reports on tissue engineering applications of SF nanofibres with polyphenolic compounds. Elakkiya *et al.* described fabrication of curcumin loaded SF nanofibres by coelectrospinning for drug delivery applications. The scaffold was reported to have high porosity (85%) and water uptake (150%) [204]. In vitro release studies showed at least 80% release after 10 days for formulations with up to 1.5 wt % curcumin. This report is based on *B. mori* SF and SF from African silkworm species have not been studied in this capacity.

Resveratrol (3,4',5-Trihydroxystilbene) is one of the more potent phenolics that can be found in grapes, berries and peanuts and red wine [271]. Resveratrol exists as two isomers; cis- and trans-resveratrol. Trans-resveratrol (Figure 3.3) is the natural form of the compound and is more active and stable than the cis- isomer [272]. Resveratrol has been found to be active against several species of bacteria and dermatophytes that cause infections and a variety of skin conditions [273-275]. However, its applications have mostly been centred on its anti-inflammatory and anti-cancer properties [276, 277]. For topical applications, fibroin promotes cell growth and proliferation but lacks other properties required for wound healing specific to mitigation of bacterial and pathogen growth. SF blended with polyphenolic compounds such as resveratrol provides a great opportunity to exploit the combined benefits of these natural products. As far as we could ascertain, there have been no recorded studies on the incorporation of resveratrol into silk nanofibres for any applications.
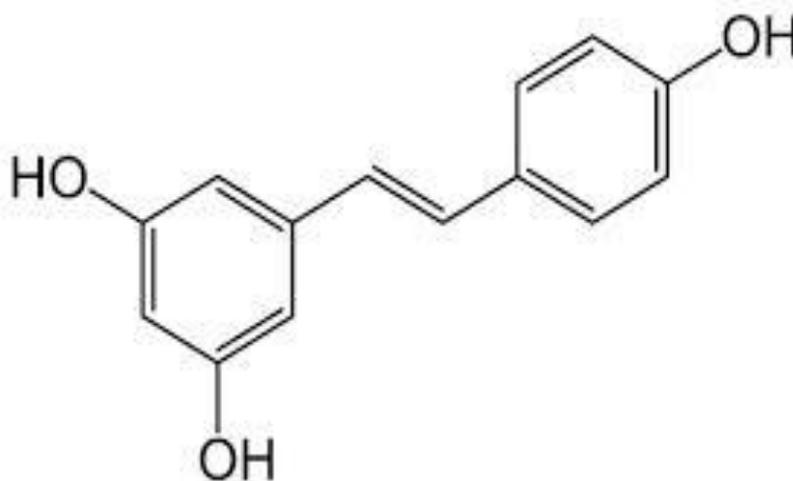
Figure 3.3   Structure of trans-resveratrol

3.8   Techniques for incorporating bioactive compounds onto nanofibres

Therapeutic compounds can be integrated into a biomaterial matrix via adsorption, covalent bonding to the matrix polymer, or physical entrapment or encapsulation. Encapsulation can be effected by co-electrospinning the compounds with the carrier polymer [278]. This procedure is very easy and convenient though it may result in diminished activity of the sensitive compounds when harsh electrospinning conditions are used. It can also be challenging to homogeneously mix some compounds in the polymer solution. Addition of some compounds can actually alter polymer solution properties, thus influencing the electrospinning process. For instance, the incorporation of the antibiotic cefazolin into poly(lactic-co-glycolic acid) (PLGA) resulted in larger nanofibre diameters as compared to as-spun PLGA nanofibres [279].

It is also possible to load compounds on prefabricated nanofibres via physical adsorption or chemical immobilization methods. Physical adsorption is a straightforward and easy technique for loading bioactive molecules on nanofibrous scaffolds due to the high surface area to volume ratio of nanofibres. The nanofibre mat is simply placed in a solution with the bioactive agents or the solution poured onto the nanofibres for adsorption to occur [280]. The compounds bind onto the nanofibre scaffold by non-covalent interactions such as van der Waals forces, hydrogen bonding, or hydrophobic interactions. Introduction of bioactive materials in this manner often prevents degradation or loss of activity of the bioactive molecules [280]. The chemical immobilization method involves covalent attachment of the bioactive molecules onto the surface of electrospun nanofibres. The disadvantage, however, is that the technique may result is some partial inactivation of the immobilized molecules as some active sites can become chemically modified during the process [281].

With co-electrospinning, solubility of the bioactive compound in the polymer will influence its distribution in the nanofibre scaffold as well as the drug release [282]. A rapid drug release profile has been observed with drugs loaded using the adsorption technique and these scaffolds are particular useful in early treatment [280]. In the case of chemical immobilization, the drugs are not as easily released from the surface of the nanofibres when incubated over an extended period. The drugs covalently bonded to the polymers are released over an extended period of time as opposed to the burst release offered by simple adsorption. Other factors that affect the release of drugs from nanofibre are the morphology of the fibres and additional interactions with the drug [283]. The concentration of the drug in the fibres also has an effect on the drug release kinetics. A pronounced burst has been observed with higher concentration, which is attributed to enrichment of the drug on the surface [283]. Using the above techniques, scaffolds for both local and sustained drug delivery can be produced depending on the compounds and polymers being used.

CHAPTER FOUR

EXPERIMENTAL PROCEDURES

4.1   Introduction

This chapter details the materials and procedures used in the experimental work. Firstly, silk fibroins from different silkworm species were purified and tests were conducted to determine their physical and chemical properties. Fibroin based nanofibres were fabricated via electrospinning. Parameters affecting the electrospinning process and the properties of the resultant nanofibres were investigated. Resveratrol, a potent antimicrobial and antioxidant agent, was incorporated onto the silk nanofibre matrix via adsorption. Parameters affecting the loading of resveratrol onto the nanofibres were studied. Physical and biological properties of the resveratrol loaded silk fibroin nanofibres were then investigated. Figure 4.1 depicts the experimental work and the characterizations done at the different stages of the work.

PARAMETERS STUDIED   **PROCESS**   **CHARACTERIZATION**

Silkworm cocoons

SEM

Degumming

Raw silk fibres

Amino acid analysis, SEM, FT-IR, RAMAN, DSC, TGA, DMA, Mechanical tests

- Type of salt
- Salt concentration
- Salt-organic mixtures
- Dissolution time

Dissolution & Dialysis

Silk fibroin solution

MeOH treatment

Freeze drying

Regenerated silk fibroin (RSF) powder

- Solvent
- Fibroin concentration
- Voltage
- Feed rate
- Tip to collector distance

Electrospinning

Silk nanofibres

SEM, FT-IR,RAMAN, DSC, TGA, BET, DMA, Solubility, degradability, Biomedical tests

- Time
- Initial loading concentration
- Temperature
- Shaking

Resveratrol loading

Solvent treatment

Solvent treated nanofibres

Resveratrol loaded nanofibres

Figure 4.1.   Block diagram showing the various stages of silk processing, parameters studied and characterization done in this study

4.2   Materials

4.2.1   Reagents and Chemicals

Unless stated otherwise, all chemical reagents used in the experiments had a purity of at least 98 % and were purchased from Sigma Aldrich (St Louis, USA). These chemicals were used without any further purification. Buffers and all aqueous solutions were prepared in ultra-high purity (UHP) water (18.2 mΩ) from a Millipore MilliQ water purification system (Molsheim, France).

4.2.2   Sampling of silkworm cocoons

Silkworm cocoons used in the study (shown in Figure 4.2) were randomly collected after the moths had emerged from the cocoons. Silkworm cocoons used in the study (shown in Figure 4.2) were randomly collected after the moths had emerged from the cocoons. *Gonometa rufobrunnae* cocoons were obtained from Gwanda, Zimbabwe and from Shashe in Botswana. Samples of *Gonometa postica* cocoons were collected from Eastern Cape Province in South Africa. *Argema mimosae* cocoons were obtained from Manzini district in Swaziland. Additional samples of *Argema mimosae*, together with *Epiphora bahuniae* and *Anaphe panda* cocoons, were donated by Mr. Addis Teshome from the ICIPE (International Centre of Insect Physiology and Ecology) in Kenya. *B. mori* cocoons reared in South Africa were donated by Elster Vermeulen.

4.3   Processing of silk fibroin

4.3.1   Degumming of silkworm cocoons

Silk cocoons were treated according to their species and location. For example, *Gonometa postica* and *Argema mimosae* cocoons were batched   separately. Also, *Gonometa*

rufobrunnae samples from different locations i.e. from Botswana and Zimbabwe, were also batched separately.

Fibroin samples were obtained by removing sericin via degumming. Briefly, cocoons were boiled using a two-step procedure. The cocoons were boiled in 1.1 g/L Na_2CO_3 for 1 h followed by 0.5 g/L Na_2CO_3 for another hour. *Epiphora bahuniae* and *Anaphe panda* cocoons required harsher degumming conditions firstly using 2.5 g/L Na_2CO_3 solution for an hour followed by 0.5 g/L Na_2CO_3 for another hour. For *B. mori* cocoons, degumming was achieved in one step by boiling in 1.1 g/L Na_2CO_3 solution for an hour. The cocoon to water ratio was 1:40 in the degumming procedures. After the degumming, the fibroin was thoroughly rinsed with warm distilled water and air dried. The fibroin (Figure 4.3) was kept in a cool dry cupboard until analysis.
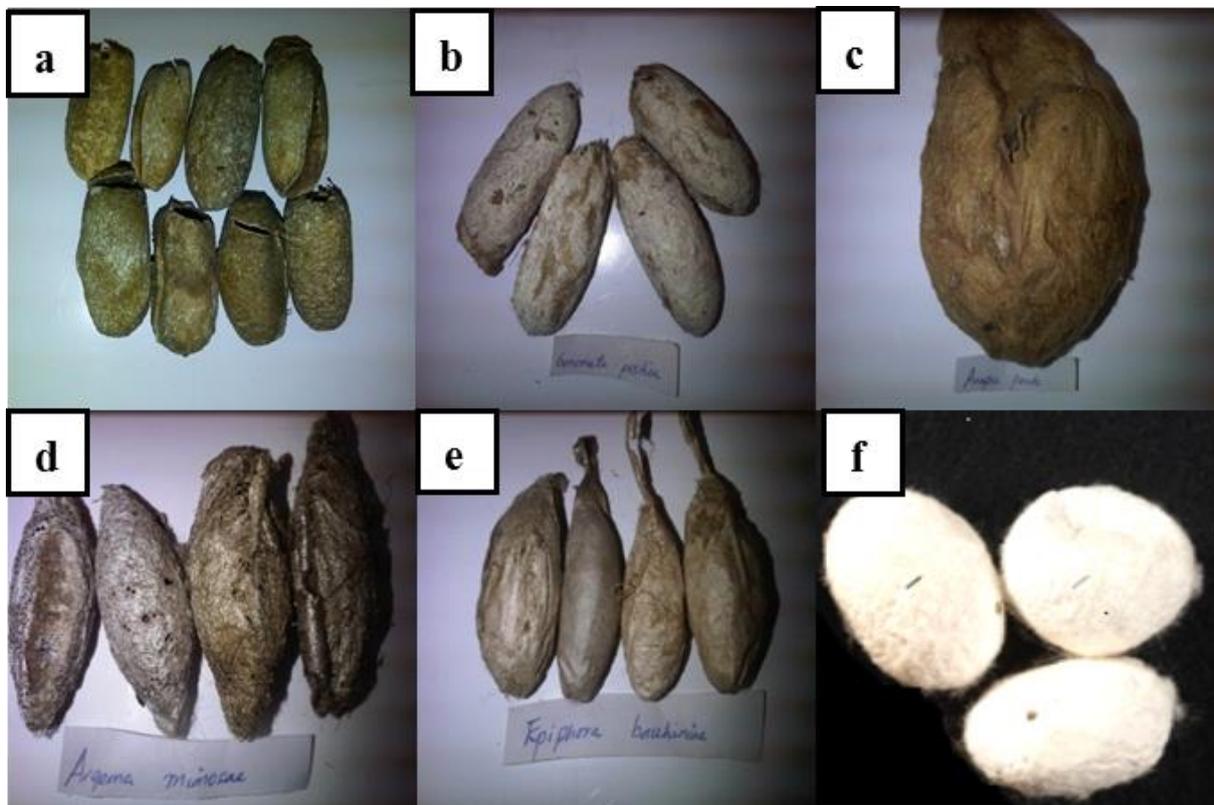
Figure 4.2.   Samples of a) *G. rufobrunnae* b) *G. postica* c) *A. panda* d) *A. mimosae* e) *E. bahuniae* and f) *B. mori* silkworm cocoons used in the study

4.3.2   Dissolution of silk fibroin

The effect of different salts, salt concentration and influence of organic solvents on the solubility of degummed silk fibroin from different species was investigated. Commonly used solvent systems listed below were investigated;

i.   9.5 M LiBr (aq)

ii.   9.5 M LiCl (aq)

iii.   10 M Ca(NO$_3$)$_2$ (aq)

iv.   Saturated CaCl$_2$ (aq) solution

v.   LiBr:EtOH:H$_2$O (4:4:1)

vi.   LiCl: EtOH: H$_2$O (4:4:1)

vii.   Ca(NO$_3$)$_2$:H$_2$O:MeOH (1:4:2)

viii. CaCl$_2$:EtOH:H$_2$O (1:2:8)

Figure 4.3.   Degummed *G. rufobrunnae* silk fibres

Aqueous/alcohol solvent systems were prepared by mixing the salts in water/alcohol mixtures according to the molar ratios indicated for each system. Dissolution of the salts was achieved by stirring the mixture at room temperature for about 30 min. Dissolution temperature of 80°C was used for the fibroins in the various solvent systems with the aid of magnetic stirring. Using between 10 and 20 mL of solvent, dissolution times up to 6 hours were studied. Fibroin was added to the solvents in 1 % increments starting from 0.5 % w/v concentrations. The point at which fibroin could no longer be dissolved in the solutions was noted as the maximum dissolution concentration. Undissolved material was removed by centrifugation and filtration to obtain clear brown fibroin solutions (Figure 4.4).
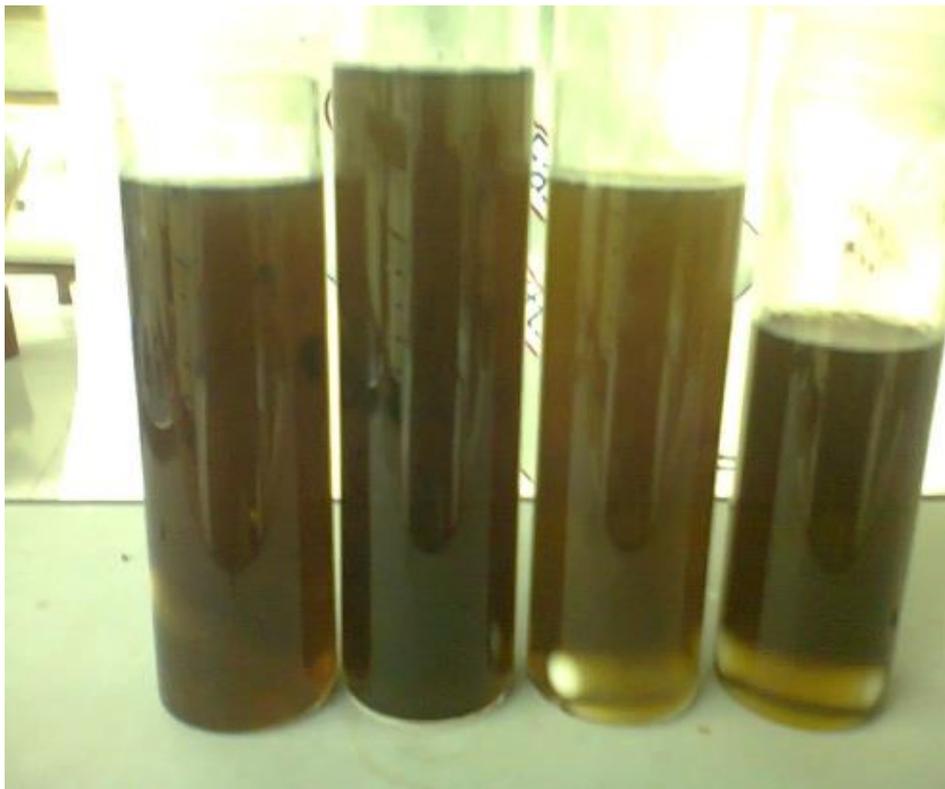
Figure 4.4.   Dissolved *Gonometa rufobrunnae* and *Gonometa postica* silk fibroin

4.3.3   Preparation of Regenerated Silk Fibroin (RSF)

Dialysis is an important step by which the salts used in the dissolution process are removed from the silk solution. Silk fibroin (SF) solutions were dialyzed for three days against UHP using Snakeskin dialysis tubing with a molecular weight cut-off of 3,500 Da (Thermo Scientific, Illinois, USA). The resultant aqueous fibroin solutions (Figure 4.5) were frozen at -20 °C for at least 24 h. RSF powders were prepared by either freeze drying or via rotary evaporation. For freeze drying, samples were placed in a freezer (-80 °C) for 1 h to ensure they were completely frozen before freeze drying at -80 °C for 3 days. For rotary evaporation, the frozen RSF solutions were thawed and the water layer was decanted leaving behind the fibroin. The fibroin was then immersed in neat methanol for 5 min prior to drying using a rotary evaporator at room temperature. The RSF powders obtained from both methods were stored in a dessicator until use.

Figure 4.5.   Dialyzed *Gonometa rufobrunnae* and *Gonometa postica* silk fibroin solutions

4.4   Preparation of silk fibroin nanofibres

4.4.1   Electrospinning parameters

SF nanofibres were prepared using *Gonometa* fibroin via electrospinning. The electrospinning setup included a power supply, syringe pump, syringe with needle tip and the aluminium foil collector (Figure 4.6).

Water, formic acid (FA) and trifluoroacetic acid (TFA) were studied as electrospinning solvents. The electrospinning solutions were prepared by dissolving FD-RSF or RD-RSF powders in the solvent under constant stirring at room temperature until a homogeneous solution was obtained. Each RSF solution was electrospun at ambient temperature through a gauge 20 stainless steel needle fitted on a 3 mL disposable syringe at a flow rate controlled by a syringe pump (New Era, NE 1000). RSF concentrations of 10-40 % (w/v) were investigated. Applied voltages from 10-25 kV and flow rates between 0.05-0.80 mL min^{-1} were studied. Tip to collector distance was varied from 7 to 20 cm.

4.4.2   Post treatment of silk fibroin matrices

Methanol, ethanol, propanol, acetone and chloroform were used to assess solvent-induced β-sheet crystallization of fibroin. Electrospun nanofibres were immersed in each of the above mentioned solvents for 15 min. Nanofibres were also treated with water vapour by placing them in a desiccator containing saturated sodium sulphate decahydrate solution for 16 h. The nanofibres were then vacuum dried in a dessicator at room temperature for 24 h prior to analysis.
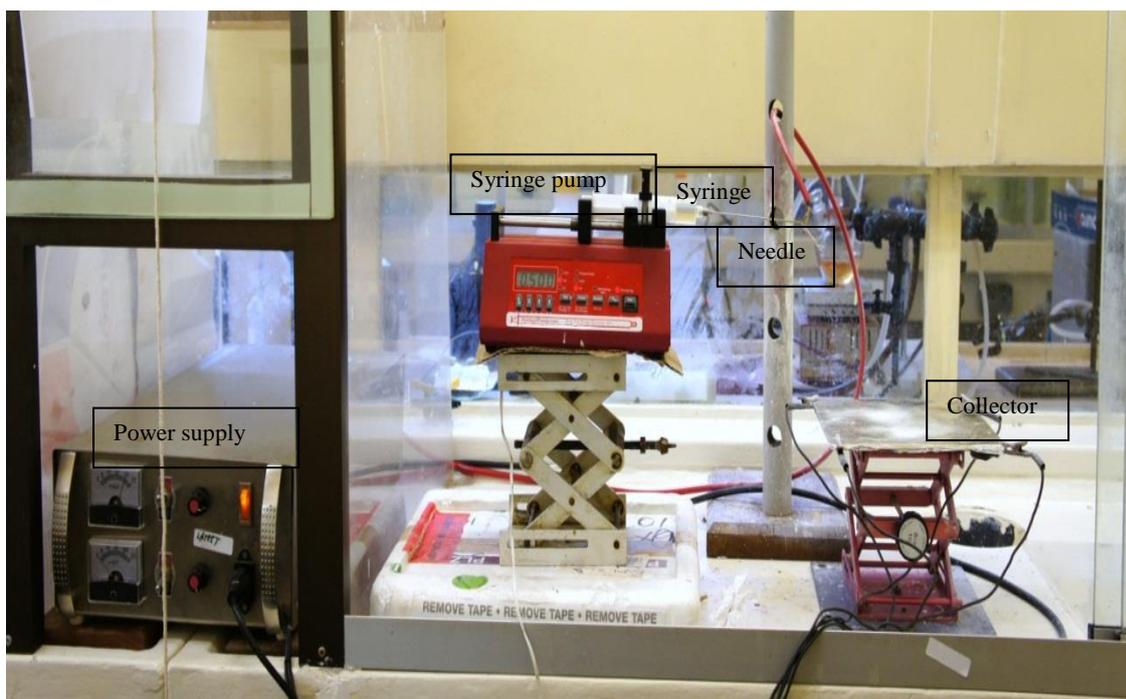
Figure 4.6.   Equipment and setup used for electrospinning

4.5   Adsorption and release of resveratrol on silk nanofibres

4.5.1   Adsorption studies

Resveratrol solutions (10-50 ppm) used for the adsorption studies were freshly prepared by dissolving resveratrol in ethanol. Fibroin nanofibre samples (6-8 mg) were immersed in 5 mL of the resveratrol solutions. The resveratrol uptake of the nanofibres was determined by measuring the change in solution concentration after immersion. Aliquots of 70 μL were drawn at different time intervals between 0-2 h to determine rate of adsorption. The resveratrol was measured using an Agilent 7100 capillary electrophoresis system (Waldbronn, Germany) with a diode array detector (DAD) (Figure 4.7). 30 mM phosphate buffer at pH 8.0 was used for the separation and detection was at 285 nm. The influence of time, temperature, initial resveratrol concentration and shaking on the adsorption of

47

resveratrol onto the silk nanofibres was examined. The resveratrol loaded nanofibres were dried under vacuum and stored in a dark cupboard until further analysis.

4.5.2   Release studies

For the release studies, the resveratrol loaded nanofibres were incubated in tubes containing 5 mL of phosphate buffered saline (PBS) at pH 7.4. The suspensions were gently shaken in a thermostated water bath maintained at 37 ℃. Samples of 100 µL released solution were taken at predetermined intervals and the same amount of fresh PBS solution was added to replace the extracted aliquot. The extracted aliquot was then dried using a rotavapor and reconstituted in ethanol. A standard addition method was used to quantify the released resveratrol.

4.6   Characterization studies

4.6.1   Micellar electrokinetic chromatographic (MEKC) analysis of fibroin

4.6.1.1   Instrumentation

An Agilent 7100 capillary electrophoresis system equipped with a DAD detector was used for separation and quantification of amino acids (Figure 4.7). The optimum wavelength for detection was 210 nm. Instrument control, data collection and processing were achieved using Agilent Chemstation revision B.04.01 (DE, Germany).

Uncoated fused silica capillaries (Agilent, Germany) with 50 µm id, 63.5 cm total length and 55.0 cm effective length were used. Buffer pH was adjusted using a Metrohm 827 pH meter (Hersau, Switzerland)

Figure 4.7.   Agilent 7100 Capillary electrophoresis system used in the study

4.6.1.2 Separation conditions

Buffers used for the study were prepared by weighing out the appropriate amounts of each component and dissolving in UHP water. A MEKC separation was developed using the surfactant SDS in phosphate and borate buffers. Influence of pH, temperature and applied voltage on the separation was investigated. All new capillaries were conditioned by rinsing with methanol for 5 min, followed by a 10 min rinse with 1 M NaOH and ultra-high purity water respectively. The capillaries were then conditioned with the running buffer. To ensure reproducible migration times and peak areas, capillaries were rinsed between runs with buffer for 15 min. The capillary was rinsed with water for 10 min at the end of each working day. Samples were pressure injected at 50 mbar for 2 sec.

All rinsing solutions, background electrolytes and samples were filtered through 0.45 µm PVDF filters. Buffers were stored at 4 °C and the pH checked regularly throughout the experiments.

4.6.1.3   Hydrolysis of fibroin

For each silkworm species, five replicates of 5 mg of fibroin were accurately weighed into acid-washed reaction vials. One mL of 6 M HCl was added to each vial and thoroughly mixed using a vortex mixer. The vials were deaerated by purging with nitrogen for about two minutes and were immediately tightly capped. Hydrolysis was carried out in an oven at 110 °C for 24 h after which the hydrolysates were cooled to room temperature. Hydrolysates were then filtered through a 0.45 µm PVDF membrane filter to remove any solid impurities.

4.6.1.4   Preparation of calibration standards

The calibration curve was prepared using six concentration levels of amino acid standards covering a concentration range of 0.005 mg mL^{-1} to 0.05 mg mL^{-1}. These calibration standards were prepared from a stock solution of 0.1 mg mL^{-1} prepared by dissolving amino acids in UHP water and a few drops of 0.1 M NaOH added to facilitate dissolution.

4.6.1.5   Derivatization of amino acids with phenylisothiocyanate (PITC)

Derivatization was done for detection of the amino acids using UV detection. The reagent phenylisothiocyanate (PITC) used in the study reacts with free amino acids under basic conditions to produce phenylthiocarbamyl (PTC) amino acid derivatives [284] as shown in Figure 4.8.
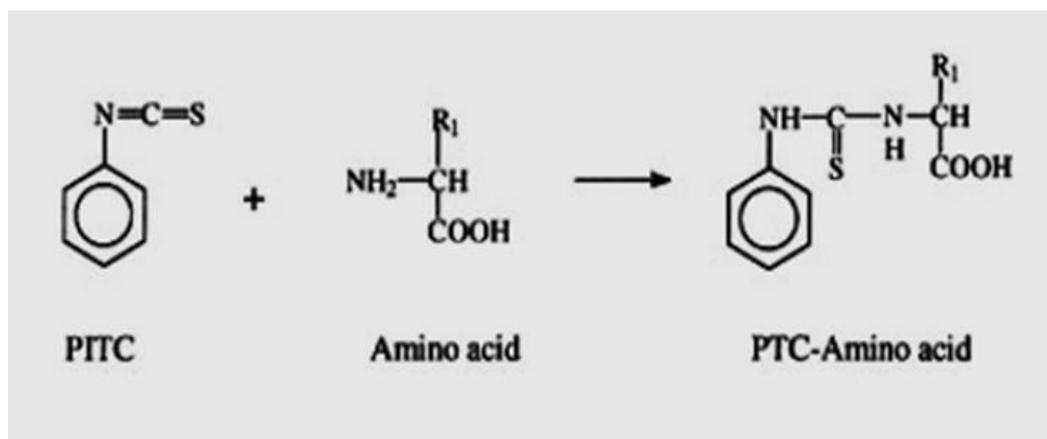
Figure 4.8. Derivatization reaction of PITC with amino acids

An appropriate volume of the calibration standard solution for each concentration level was pipetted into a vial and dried under vacuum for 30-60 min. 20 µL of re-drying solution which consisted of methanol:water:triethylamine (2:2:1, v/v/v), was added to each vial and then dried under vacuum for 30 min. Derivatization then proceeded by adding 30 µL of the derivatizing reagent consisting of methanol:water:triethylamine:PITC (7:1:1:1, v/v/v/v) to each vial. After vortexing for 30 sec, the vials were tightly closed and incubated at room temperature for 30 min. The amino acid-phenylthiocarbamyl (PTC) derivatives were then dried in vacuo using a SpeedVac (Thermo Fisher, USA). Fibroin samples were derivatized according to the procedure described above except that 50 µL aliquots of sample and 100 µL of reagents were used at each stage. The re-drying process was done twice for the samples. PTC-amino acids were stored at -20 °C and were re-constituted in the running buffer just before analysis.

4.6.2 Validation procedures

The MEKC method was validated for linearity, limit of detection (LOD), limit of quantification (LOQ), recovery and precision. Precision was evaluated by assessing injection

and method repeatability (intra-day repeatability) as well as intermediate precision (inter day precision). Statistical evaluation parameters were calculated using the data analysis tool in Microsoft Excel.

4.6.3   Scanning Electron Microscopy

Undegummed, degummed and electrospun nanofibres were examined using scanning electron microscopy (SEM). Images were obtained using a TESCAN Vega VG1760481J scanning electron microscope (Brno, Czech Republic). Nanofibre samples were prepared by cutting an aluminium sheet covered with electrospun fibres and fixing it onto the copper stubs used in the analysis. Degummed and undegummed fibres were fixed onto the copper stubs using adherent tape. Each specimen was gold-coated prior to analysis at 20 kV. Diameters of the electrospun fibres were also estimated by randomly measuring 25 fibres from different SEM images.

4.6.4   FTIR spectroscopy

Fourier transform infrared (FTIR) spectra for the degummed and undegummed silk fibres were obtained from a Perkin Elmer spectrometer (Massachusetts, USA) with an ATR attachment spectrometer. Spectra were acquired in transmittance mode with 32 scans at a resolution of 2 cm^{-1} over the 4000-600 cm^{-1} spectral region. FTIR analysis for the RSF powders and nanofibres was done using a Perkin Elmer RX1 spectrometer (Massachusetts, USA) with a Miracle^{TM} ATR attachment. Spectra were acquired in transmittance mode with 32 scans at a resolution of 2 cm^{-1} over the 4000-600 cm^{-1} spectral region.

4.6.5   FT-Raman spectroscopy

The morphology of silk fibres was examined using a Bruker MultiRAM FT-Raman spectrometer (Ettlingen, Germany) with a germanium detector. Silk samples were mounted

vertically in front of a mirror and the spectra were accumulated from 512 scans at a 4 cm^{-1} resolution using 0.45 W laser power.

4.6.6 X-ray diffraction

Diffraction curves were recorded using a PANalytical X'pert Pro X-ray diffractometer (Almelo, Netherlands) with Cu (Kα) radiation (λ = 1.54 Å) from 1° to 70° with a scan step size 0.02626° (2θ). Voltage and current of the X-ray source were 45 kV and 40 mA, respectively.

4.6.7 Thermal Analysis

Thermogravimetric analysis (TGA) of the silk fibres and nanofibres were studied using a TA Instruments TGA Q500 (DE, USA). Samples (10-15 mg) were loaded into a platinum crucible. The samples were heated under nitrogen from 25 to 1000 °C at a heating rate of 10 °C min^{-1}.

For differential scanning calorimetry (DSC), a TA Instruments DSC Q2000 (DE, USA) calorimeter was used with a scanning rate of 10 °C min^{-1} (between 25 and 450 °C) and nitrogen and air gas flow rate of 50 mL min^{-1}. Approximately 4.5 mg samples were used for the analysis.

4.6.8 Mechanical properties

The silk fibres were kept in the lab under atmospheric condition of 20 ± 1 °C and relative humidity of 65 ± 2% for at least 24 h before testing. The conditioned samples were then tested for bundle strength, tenacity and fibre fineness. The fibres were carefully combed with a fine comb, and then fibre bundles were prepared. The bundle tensile test was carried out on the Instron Tensile Tester (Model 4411) at 0.01 mm gauge length using the Pressley method (ASTM 3060:1974). Ten bundles were tested per sample with bundles being carefully

assembled to ensure continuous and parallel fibres in the test area. The bundles were weighed and the linear density (Tex) of the fibre bundles was calculated using a gravimetric method. The fibre diameter was estimated by measurement of mean fibre diameter per sample using an Optical Fibre Diameter Analyser (OFDA). The cross-section of one sample was examined with Image analyser (Olympus CX31 Image analyser) at 400X magnification.

4.6.9 Degradability

The mass loss of the nanofibres, following immersion in water and PBS at pH 7.4 for 24 h, was measured. Degradability was calculated as a percentage by comparing the mass of the nanofibres before and after immersion.

4.6.10 Cytotoxicity studies

The cytotoxic effects of the nanofibres were tested by Sulforhodamine B (SRB) assay on the WI38 cell line. The WI-38 cell line - normal Human Fetal Lung Fibroblast from ECACC was routinely maintained as a monolayer cell culture at 37 ℃, 5% CO_2, 95% air and 100% relative humidity in EMEM containing 10% fetal bovine serum, 2 mM L-glutamine and 50 µg/ml gentamicin.

For screening experiments, the cells (21-50 passages) were inoculated in 96-well microtiter plates at plating densities of 10 000 cells/well and were incubated for 24 h. After 24 h the cells were treated with different masses of the samples in DMSO. Cells without addition of samples served as control. The blank contained complete medium without cells. Etoposide was used as a standard. The plates were incubated for 48 h after addition of the samples. Viable cells were fixed to the bottom of each well with cold 50% trichloroacetic acid, washed, dried and dyed by SRB. Unbound dye was removed and protein-bound dye was extracted with 10 mM Tris base for optical density determination at the wavelength 540 nm

using a multiwell spectrophotometer. Data analysis was performed using GraphPad Prism software. 50% of cell growth inhibition (IC50) was determined by non-linear regression.

4.6.11   Antibacterial activity

The antibacterial properties of the nanofibres were tested using the disc diffusion method. Gram negative *Escherichia coli (E. coli)* and gram positive *Staphylococcus aureus* (*S. aureus*) bacteria were used for the tests. The tests were carried out for resveratrol solutions at different concentrations and on SF nanofibres with and without resveratrol. The resveratrol solutions (2 μL) were impregnated into sterile filter paper discs. The resveratrol-paper discs samples and nanofibre samples were applied to the surface of the agar plate containing the microorganism to be tested. The effectiveness of the samples against the studied bacteria was assessed by the growth inhibition zones. The zones of inhibition are observed as clear areas surrounding the disc due to the diffusion of the antimicrobials into the plate.

4.6.12   Antioxidant activity

The radical scavenging activity was determined using DPPH (2,2-diphenyl-1 -picrylhydrazyl hydrate) assay. Briefly, the stable free radical DPPH was dissolved in methanol to give a 100 μM solution. Different masses of the nanofibre samples were immersed in DMSO in 96 well plates and then treated with DPPH solution. The mixtures were shaken vigorously and kept in the dark for 30 min at room temperature. Change in absorbance was measured spectrophotometrically at 540 nm. Each concentration of nanofibre samples was assayed in triplicate wells. DPPH + DMSO without addition of sample served as control. The blank contained methanol + DMSO and gallic acid was used as a standard. Radical scavenging activity was calculated by the following formula:

% Radical scavenging = [(A DPPH$_{Control}$ - ADPPH$_{Test}$)/ A DPPH$_{Control}$] × 100

4.6.13 Anticancer activity

The growth inhibitory effects of the samples were tested in the 3-cell line panel consisting of TK10 (renal), UACC62 (melanoma) and MCF7 (breast) cancer cells by Sulforhodamine B (SRB) assay. The human cell lines TK10, UACC62 and MCF7 was obtained from the Drug Evaluation Branch (NCI) in the framework a collaborative research program between the Council of Science and Industrial Research (CSIR) and NCI. Cell lines were routinely maintained as a monolayer cell culture at 37 ºC, 5% CO_2, 95% air and 100% relative humidity in RPMI containing 5% fetal bovine serum, 2 mM L-glutamine and 50 µg/ml gentamicin.

For the screening experiment, cells (3-19 passages) were inoculated in 96-well microtiter plates at plating densities of 7-10 000 cells/well and were incubated for 24 h. After 24 h, one plate was fixed with TCA to represent a measurement of the cell population for each cell line at the time of sample addition (T_0). The other plates with cells were treated with different masses of the nanofibres in DMSO. Cells without the nanofibres served as control. The blank contained medium without cells. Etoposide was used as a reference standard. The plates were then incubated for 48 h after addition of the nanofibres. Viable cells were fixed to the bottom of each well with cold 50% trichloroacetic acid, washed, dried and dyed by SRB. Unbound dye was removed and protein-bound dye was extracted with 10 mM Tris base for optical density determination at the wavelength 540 nm using a multiwell spectrophotometer. Optical density measurements were used to calculate the net percentage cell growth.

CHAPTER FIVE

CHEMICAL AND PHYSICAL PROPERTIES OF SILK FIBROIN

5.1 Introduction

This chapter presents results on the chemical and physical characteristics of the studied African silk fibroins. Comparison was done with *B. mori* fibroin because of its extensive use as a model for investigating and correlating the chemical and physical properties of silk proteins. Reference to other wild silkworm species is made where appropriate. Part of this work has been published in International Journal of Biological Macromolecules [71].

5.2 Development of MEKC separation for PTC-modified amino acids

Our previous study focused on developing a MEKC method with borate and/or phosphate buffers using the anionic sodium dodecyl sulphate (SDS) as a surfactant. The best separation achieved baseline resolution of thirteen amino acids in sericin derived from *Gonometa rufrobrunnae* [285]. The current work aimed to improve the previous method with an attempt to resolve all eighteen amino acids found in silk fibroin. Parameters evaluated were those that play a critical role in MEKC separations such as concentration of SDS, buffer type, concentration and pH.

It should be noted peak identification was not done during the preliminary method development studies (Figures 5.1 and 5.2). The detail of peak identity is therefore given when the best separating conditions using for the borate-SDS and phosphate-SDS buffers were used.

5.2.1 MEKC with borate buffer

When developing a MEKC separation, optimization of separation of components in CZE mode is often the starting point. Using borate, 20 mM buffer at pH 9.0 showed improved resolution of the amino acids (Fig 5.1a) with 14 peaks observed compared to the 11 peaks seen using 10 mM borate (Fig 5.1b). Further increase in the borate concentration did not yield better results; therefore this 20 mM concentration was used in developing the MEKC method.

The concentration of SDS was varied from 20 mM to 120 mM in the 20 mM borate buffer at pH 9.0. The critical micelle concentration (CMC), which is the minimum concentration above which micelles are formed, of SDS is around 8 mM and varies with presence of different additives such as organic solvents and salts [286]. Concentrations above 10mM were therefore investigated. There was no significant improvement in separation when 20 mM concentration of SDS was added to the running buffer (results not shown). However, as the SDS concentration was increased, significant improvement in separation of the analytes was observed.

Figure 5.2 shows electropherograms where 20 mM/60 mM borate-SDS and 20 mM/100 mM borate-SDS buffers both at pH 9.0 were used. In both systems, 17 peaks were separated, although using 20 mM/100 mM borate-SDS buffer resulted in better resolution with a total of 9 being baseline resolved as compared to 7 with 20 mM/60 mM borate-SDS buffer. Increasing the SDS concentration resulted in increased partitioning of the amino acids between the buffer and the pseudo-stationary phase thereby improving resolution. Higher SDS concentrations also result in longer run times as micelles tend to move slowly towards the detector because of their counter mobility towards the anode. Increasing the SDS concentration resulted in increased partitioning of the amino acids between the buffer and the pseudo-stationary phase thereby improving resolution. Higher SDS concentrations also result

in longer run times as micelles tend to move slowly towards the detector because of their counter mobility towards the anode. Also, with more micelles, there are additional chromatographic interactions between the pseudo-stationary phase and the analytes which also contributes to longer run times.
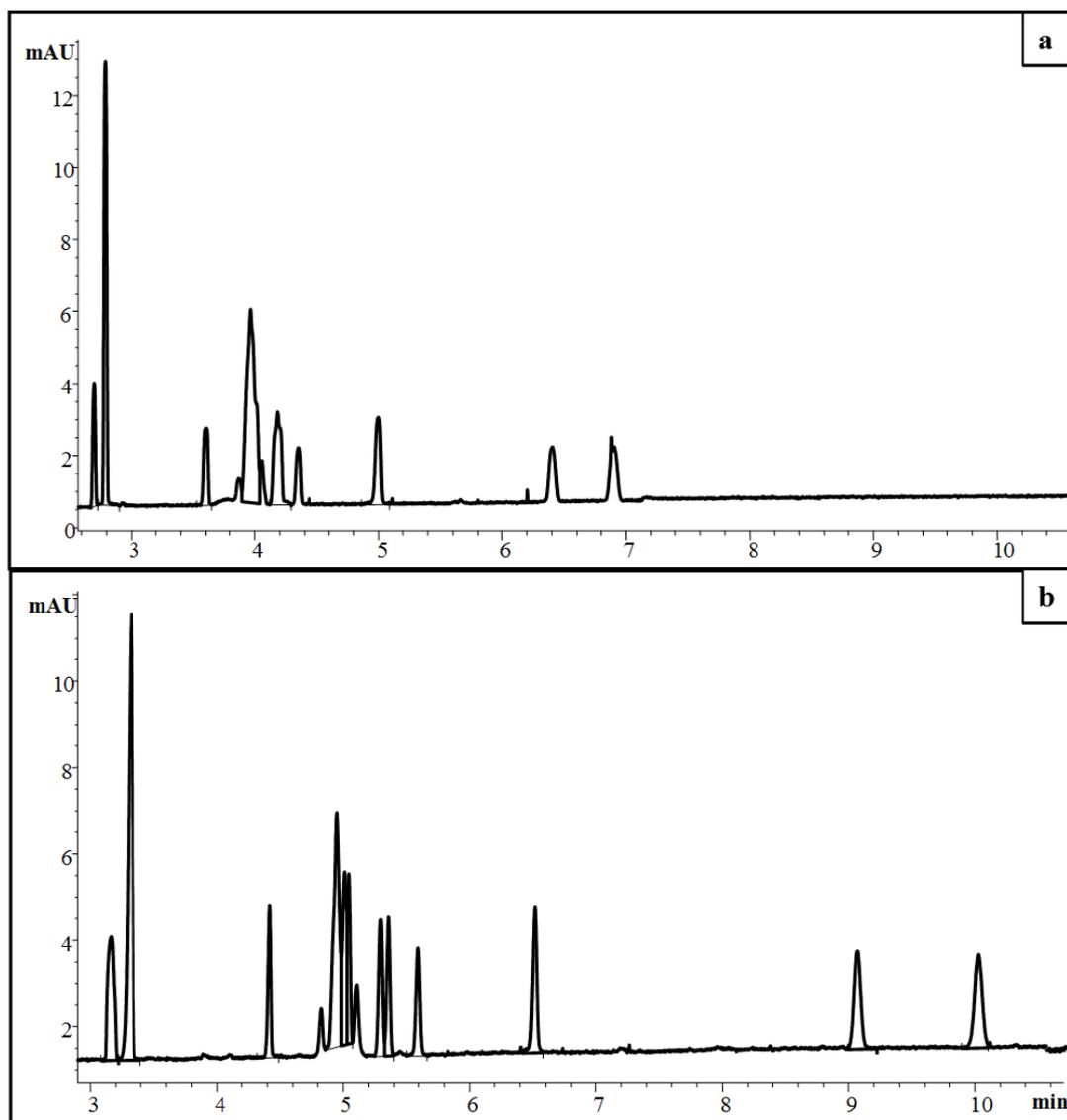
Figure 5.1.   CZE of 20 PTC-amino acids using a) 10 mM borate buffer, pH 9.0 and b) 20 mM borate buffer, pH 9.0. Conditions: Capillary, 40 cm effective length (total 48.5 cm) x 50 μm i.d; voltage +20 kV, pressure injection (50 mb for 2 sec); temperature 25 °C; UV-Vis detection at 210 nm (peaks not identified)
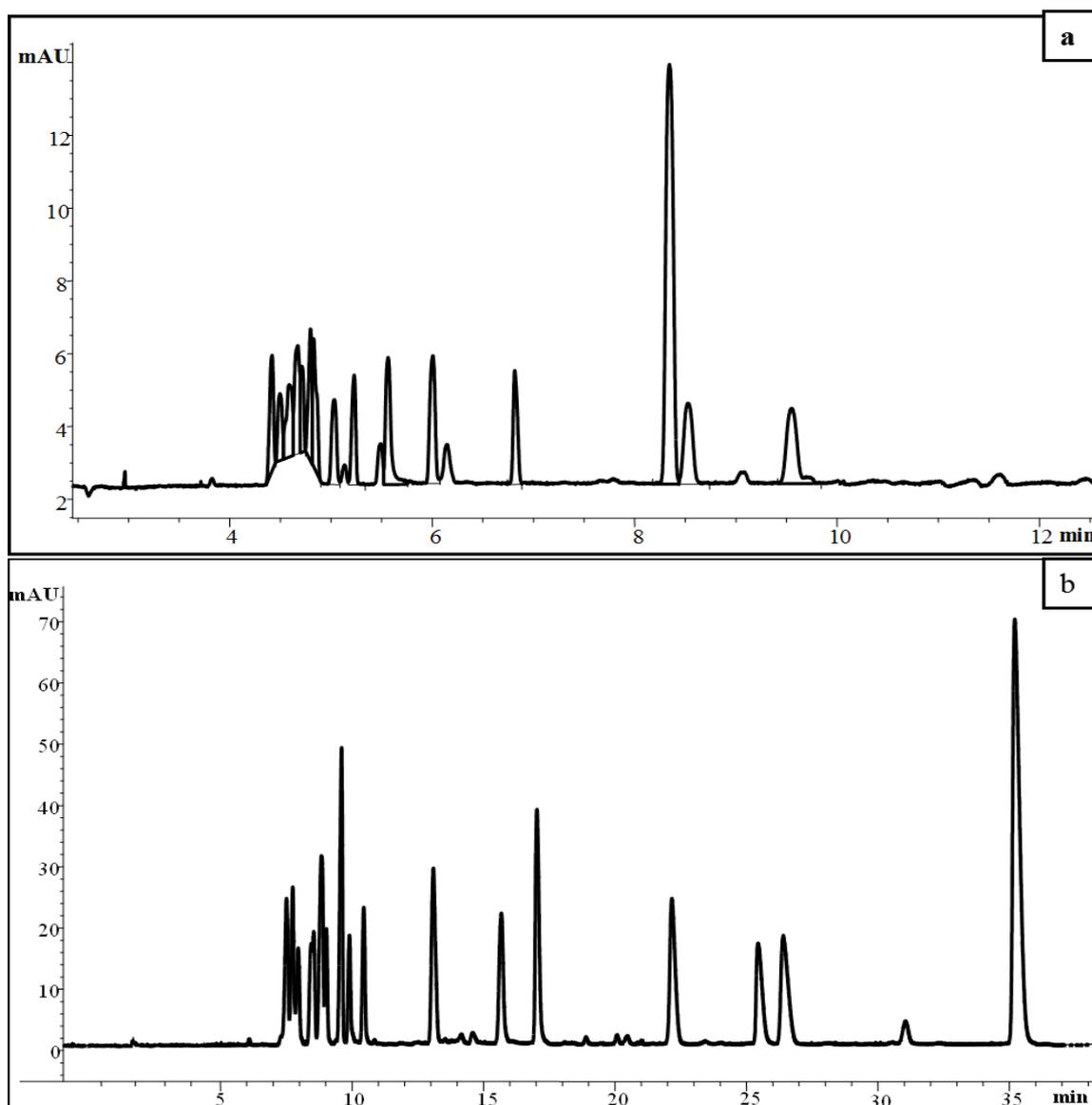
Figure 5.2. MEKC of 20 PTC-amino acids using a) 20 mM/60 mM borate SDS buffer pH 9.0 and

b) 20 mM/100 mM borate SDS buffer pH 9.0. Conditions: as in Figure 5.1 (peaks not identified)

Better separation was achieved using 20 mM/120 mM borate SDS buffer (Figure 5.3). Under

these conditions, 19 peaks were observed with 14 being baseline resolved. Of the resolved

peaks, 11 were identified as amino acids and the remaining ones, including the largest peak

around 34.9 min, were due to excess PITC reagent and its by-products.
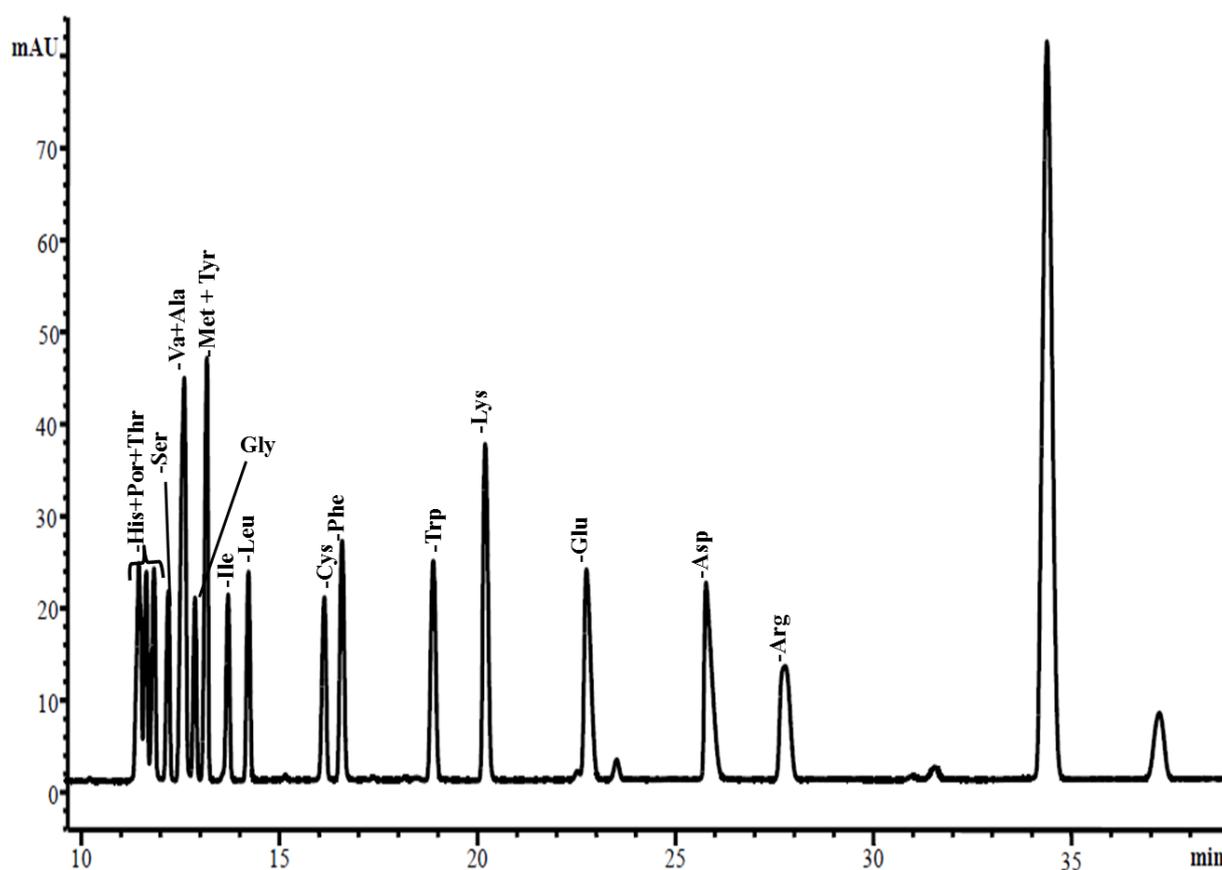
Figure 5.3. MEKC of PTC-amino acids using 20 mM/120 mM borate SDS buffer, pH 9.0. Conditions: as in Figure 5.1

Coelution was observed for some amino acids which can be correlated to their properties. For example, the coeluting pairs of valine + alanine have similar pKa values (see Table 2.4) and therefore close isoelectric values (5.96 and 6.00 respectively). In addition they have similar structures that do not interact much with SDS micelles hence they present a challenge to separate. Higher concentrations of SDS did not afford any significant improvement in resolving coeluting peaks and had a significant increase in run times (>50 min). Since no further improvement could be realized with borate buffer, MEKC using phosphate buffer system was investigated.

5.2.2 MEKC with phosphate buffer

Phosphate buffer provides an alternative operating pH range from borate buffer thereby manipulating the electrical charge on the different analytes. It therefore offers different separation conditions for the amino acids. Conditions for the phosphate–SDS buffer system were adapted from Zahou *et al.* [287] and optimized to achieve the best separation for quantification of the amino acids. In their study, resolution of 18 amino acids was achieved within 15 min using 29 mM phosphate buffer (pH 7.4) containing 168.3 mM SDS. In this study, separation for most of the amino acids was achieved using a 32 mM phosphate buffer with 172 mM SDS at pH 6.70 where 17 PTC-amino acid derivatives were baseline resolved with the exception of cystine (Cys) and the internal standard norleucine (Nleu) which were not included in those analyzed by Zahou *et al*.

In previous work [285], mixed buffer systems have been found to improve resolution of some coeluting amino acids. Incorporation of 0.5 mM concentration of borate into the phosphate-SDS buffer improved the resolution between Cys and Nleu. Resolution of the 19 amino acid standards was thus achieved within 20 min using an optimum buffer system consisting of 32 mM/0.5 mM phosphate-borate buffer at pH 6.70 with 172 mM using an applied voltage of +26 kV. The optimum temperature for the separation was 27 °C where the resolution of closely co-eluting tyrosine and alanine as well as glycine and valine was also improved (Figure 5.4).
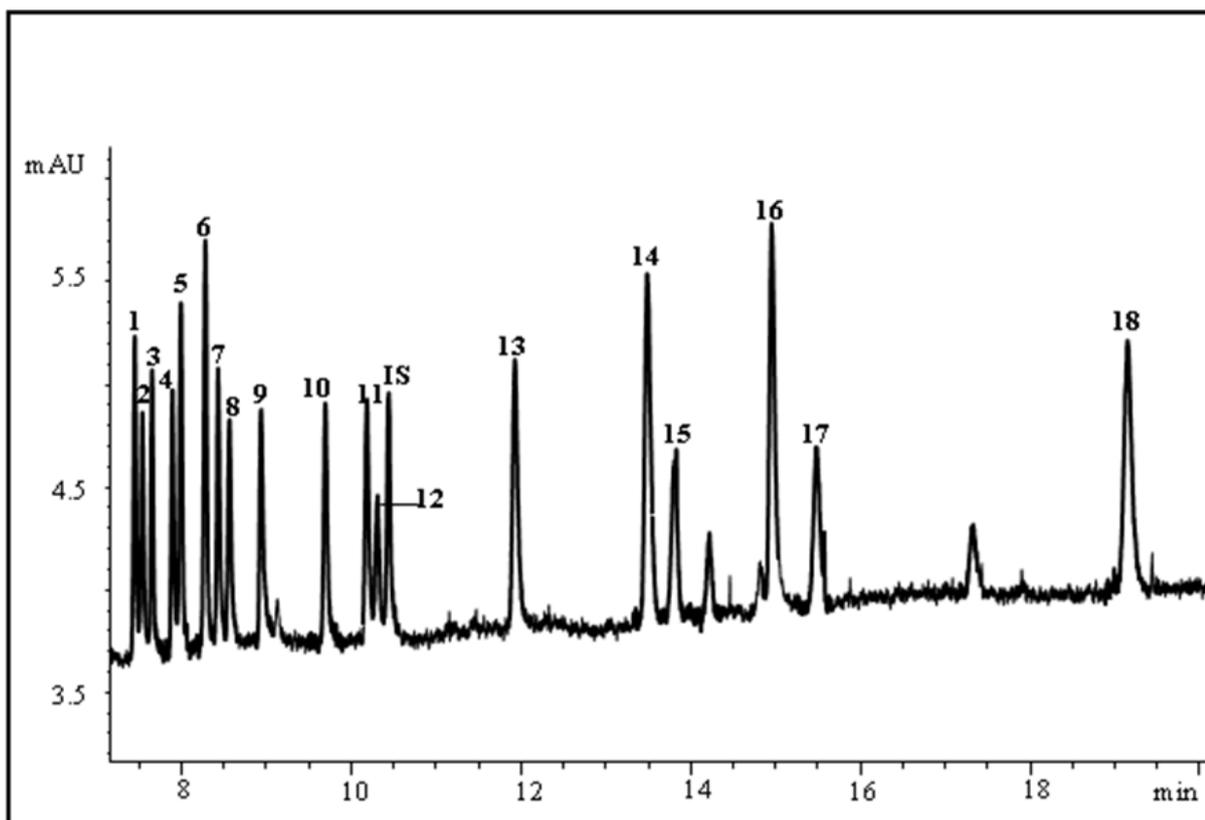
Figure 5.4. MEKC of PTC-amino acids at 0.005 mg mL^{-1} concentration using 32 mM phosphate /0.5 mM borate /172 mM SDS buffer, pH 6.70. Conditions: Capillary, 55 cm effective length (total 63.5 cm) x 50 μm i.d; voltage +26 kV, temperature 27 °C; UV-Vis detection at 210 nm. Peak i.d: 1 = proline, 2 = threonine, 3 = serine, 4 = tyrosine, 5 = alanine, 6 = glycine, 7 = valine, 8 = methionine, 9 = histidine, 10 = isoleucine, 11 = leucine, 12 = cysteine, 13 = phenylalanine, 14 = tryptophan, 15 = glutamic acid, 16 = lysine, 17 = aspartic acid, 18 = arganine, IS = internal standard (norleucine)

5.3   Method Validation

5.3.1. Linearity

An external standard calibration approach was used for quantitation of the amino acids. Six concentration levels with five replicates were used to determine linearity. Detector responses of the amino acid analytes were normalized against the response of the internal standard Nleu to give peak area ratios or corrected peak area ratios. Corrected peak areas (peak area of

analyte divided by migration time of the analyte) are often used in CE to compensate for differential migration of analytes through the detector as well as migration time drifts thereby minimizing quantitative bias [288]. Calibration curves plotted using both uncorrected peak area ratios and corrected peak area ratios showed significant linearity (Table 5.1). The linearity was assessed using the F-test at 95% confidence level where large F values indicate significant linearity of the calibration curve when using ANOVA. Better correlation coefficients (0.9979 to 0.9999) were obtained using corrected peak areas as compared to those with uncorrected peak areas (0.9850 to 0.9997). Therefore, calibration curves used for quantification purposes were plotted using corrected peak area ratios. The significance of the error of regression was evaluated using the F-test where the standard deviation of ten replicate samples was compared to the standard error of regression of the calibration curve for the analyte. Calculated values indicated that the regression residuals observed are attributable to random error rather than systematic error at 95% confidence level. Overall, our calibration curves could be used to reliably quantify the analytes of interest.

5.3.2   Limit of Detection (LOD) and Limit of Quantification (LOQ)

In this study no suitable blank was available for determination of limit of detection and limit of quantification. Both the LOD and LOQ of the method were therefore determined from regression statistical analysis according to ISO11843 method. The parameters were calculated as follows:

$$LOD = \frac{3s_{y/x}}{b} \text{ and } LOQ = \frac{10s_{y/x}}{b}$$

where $s_{y/x}$ is the standard error of regression and b is the slope of the curve. The values obtained were in the range of 0.6-5.1 mg L^{-1} and 2.0-17.1 mg L^{-1} for LOD and LOQ respectively (Table 5.2).

5.3.3. Precision

Intra-day and inter-day variability was measured to assess precision and all results are shown in Table 5.2. Injection repeatability was assessed by injecting one standard (0.04 mg mL^{-1}) ten times and calculating RSDs of corrected peak area ratios and migration times. Injection repeatability RSDs values averaged 0.83 % and 3.16 % for migration time and peak area respectively. For method repeatability ten replicate standards at 0.03 mg mL^{-1} were analyzed and RSDs of peak area and migration time were calculated. Maximum values obtained were 2.8 % and 6.3 % for migration time and peak area respectively.

Intermediate precision was done by injecting standards at 0.01, 0.02 and 0.04 mg mL^{-1} on different days over a period of three weeks. RSD values observed at the three concentration levels were less than 3.2 % and 8.2 % for migration time and peak area respectively. Generally, RSD values were larger for the slow migrating analytes compared to the fast migrating ones. Precision results showed that MEKC method has good repeatability and is reliable for quantification of the analytes of interest.

Table 5.1.   Linearity, regression, LOD, LOQ data for of PTC- amino acids using the developed MEKC method

Peak number	Amino acid	Correlation coefficients, r		[a]F value						[b]$S_{y/x}$
		Uncorrected peak area	Corrected peak area	Uncorrected peak area	Corrected peak area	intercept	slope	LOD mgL^{-1}	LOQ mg L^{-1}	
1	Proline	0.9994	0.9999	4886	44428	0.355	1.36	0.7	2.2	0.3
2	Threonine	0.9997	0.9999	8364	45139	0.285	1.17	0.8	2.2	0.3
3	Serine	0.9989	0.9997	2401	10485	0.743	1.20	1.3	4.5	0.5
4	Tyrosine	0.9994	0.9998	4183	14225	0.599	1.10	1.2	3.8	0.4
5	Alanine	0.999	0.9999	12235	42367	0.328	1.70	0.7	2.2	0.4
6	Glycine	0.9994	0.9999	4249	53877	-0.117	2.04	0.6	2.0	0.4
7	Valine	0.9997	0.9998	8359	13030	0.495	1.25	1.2	4.0	0.5
8	Methionine	0.9991	0.9997	3035	8965	0.427	1.20	1.5	4.8	0.6
9	Histidine	0.9986	0.9998	1722	12596	-0.102	1.38	1.2	4.1	0.6
10	Isoleucine	0.9984	0.9996	1659	7016	-0.018	1.23	1.6	5.5	0.7
11	Leucine	0.9989	0.9999	2408	41729	-0.012	1.22	0.7	2.2	0.3
12	Cysteine	0.9997	0.9997	7384	10327	0.142	1.29	1.6	5.3	0.7
13	Phenylalanine	0.9940	0.9979	412	1204	-0.584	1.51	2.0	6.6	2.0
14	Tryptophan	0.9850	0.9998	257	13779	0.142	1.95	0.9	2.9	0.6
15	Glutamic acid	0.9987	0.9999	2001	32919	-0.053	0.925	0.8	2.5	0.2
16	Lysine	0.9924	0.9979	329	1199	-3.53	2.47	4.0	13.2	2.3
17	Aspartic acid	0.9993	0.9996	3707	6594	0.048	0.961	2.3	7.5	0.7
18	Arginine	0.9965	0.9991	716	2182	2.120	0.926	5.1	17.1	1.6

[a]F statistic value from F-test using ANOVA

[b] $S_{y/x}$ represents standard error of regression

Table 5.2. Intra and inter-day precision data for PTC-amino acids using the developed MEKC method

Amino acid	Injection repeatability (intra-day) n=10		Method repeatability (intra-day) n=10		Inter day repeatability n=7					
					0.01 mg mL^{-1}		0.02 mg mL^{-1}		0.04 mg mL^{-1}	
	Migration time (min), RSD (%)	Corrected peak area, RSD (%)	Migration time (min), RSD (%)	Corrected peak area, RSD (%)	Migration time (min), RSD (%)	Corrected peak area, RSD (%)	Migration time (min), RSD (%)	Corrected peak area, RSD (%)	Migration time (min), RSD (%)	Corrected peak area, RSD (%)
Proline	0.6	3.3	1.0	4.4	1.6	6.8	1.6	3.6	1.2	2.7
Threonine	0.7	3.8	1.1	4.0	1.6	5.7	1.7	3.7	1.5	4.4
Serine	0.7	2.4	1.0	3.9	1.6	4.5	2.1	4.4	2.6	3.5
Tyrosine	0.7	1.9	1.1	4.4	1.7	4.4	1.9	4.0	1.8	6.1
Alanine	0.7	2.7	1.1	3.0	1.7	3.6	1.5	3.0	1.9	3.7
Glycine	0.7	3.0	0.7	3.1	1.7	3.3	1.8	4.1	2.5	5.4
Valine	0.7	3.6	1.2	4.4	1.6	7.1	1.8	5.3	1.4	3.7
Methionine	0.7	4.3	1.2	3.2	1.8	5.7	1.7	5.4	1.4	3.6
Histidine	0.8	3.2	1.5	4.2	2.0	4.2	1.8	4.6	1.7	3.2
Isoleucine	0.7	1.7	1.4	3.3	1.8	2.2	2.1	3.0	2.7	4.7
Leucine	0.7	3.0	1.5	5.5	1.8	5.9	2.3	4.5	2.8	5.0
Cysteine	0.7	3.3	1.6	3.8	2.1	6.1	2.3	6.5	1.9	3.5
Phenylalanine	0.8	2.5	2.0	4.6	2.0	6.3	2.4	5.1	1.9	3.2
Tryptophan	1.0	2.8	1.9	5.5	2.3	7.3	2.7	3.9	2.3	2.0
Glutamic acid	1.1	4.2	1.6	4.5	2.2	4.2	2.5	6.3	2.4	4.6
Lysine	1.0	3.4	2.0	5.8	2.2	7.5	2.9	7.2	3.1	5.3
Aspartic acid	1.3	3.2	2.0	5.8	1.8	4.2	2.1	4.2	2.8	3.7
Arginine	1.5	4.6	2.8	6.3	2.5	6.9	3.1	8.2	2.9	7.4
Average	**0.8**	**3.2**	**1.5**	**4.4**	**1.9**	**5.4**	**2.1**	**4.8**	**2.2**	**4.2**

5.4   Quantification of amino acids in fibroin samples

The validated method was applied for the separation and quantification of amino acids in fibroin samples from the silkworm species (Figure 5.5). Some of the peaks in the electrophoregram exhibited tailing, possibly due to sample matrix effects which cause changes in ionic strength of the injected sample plug and the running buffer. The unidentified peaks seen in the electrophoregrams are by- products of PITC as determined during the method development. The mass of amino acids recovered as a ratio of total mass of fibroin hydrolyzed was 70-80 % for all species analyzed. Acid hydrolysis can be a major contributor to variation of amino acid quantification due to complete or partial destruction of some amino acids. Some reports indicate that serine, threonine and methionine can be partially destroyed during hydrolysis. Tryptophan is completely destroyed during the process therefore only seventeen of the reported eighteen amino acids were identified and quantified in the studied SF. It has also been reported that some peptide linkages, particularly those between amino acids possessing bulky side chains such as Ile-Ile, Val-Val, Ile-Val, Val-Ile, undergo slow and/or incomplete hydrolysis due to steric hindrance [289]. The side chains of asparagine and glutamine are deaminated resulting in aspartic and glutamic acid. Therefore the % quantity reported for the acids is inclusive of the amides that may be present in the fibroin.

Table 5.3 shows the quantification and precision data for amino acids in fibroin protein from the species investigated. Repeatability of peak areas was generally better for amino acids present at higher concentrations in the fibroin such as glycine and alanine than for those present in low concentrations such as methionine, cysteine and isoleucine. Consistent with reports from other studies, the fibroins were mostly composed of glycine, alanine, and serine, which amounted to at least 70% in all the species studied. These three amino acids are the main components of the characteristic primary structure which makes up the β-sheet structure in the crystalline region of fibroin [290, 291]. Their nonpolar nature therefore renders fibroin

68

mainly hydrophobic. *A. panda* had the highest composition of these three amino acids with glycine and alanine alone contributing almost 85 % of the total amino acids. In contrast, Kebede *et al.* reported glycine and alanine of *A. panda* amounted to only 62 % [72]. Their study however only reported a few of the amino acids found in fibroin. Our results are however very similar to those reported for other *Anaphe* silks [292].
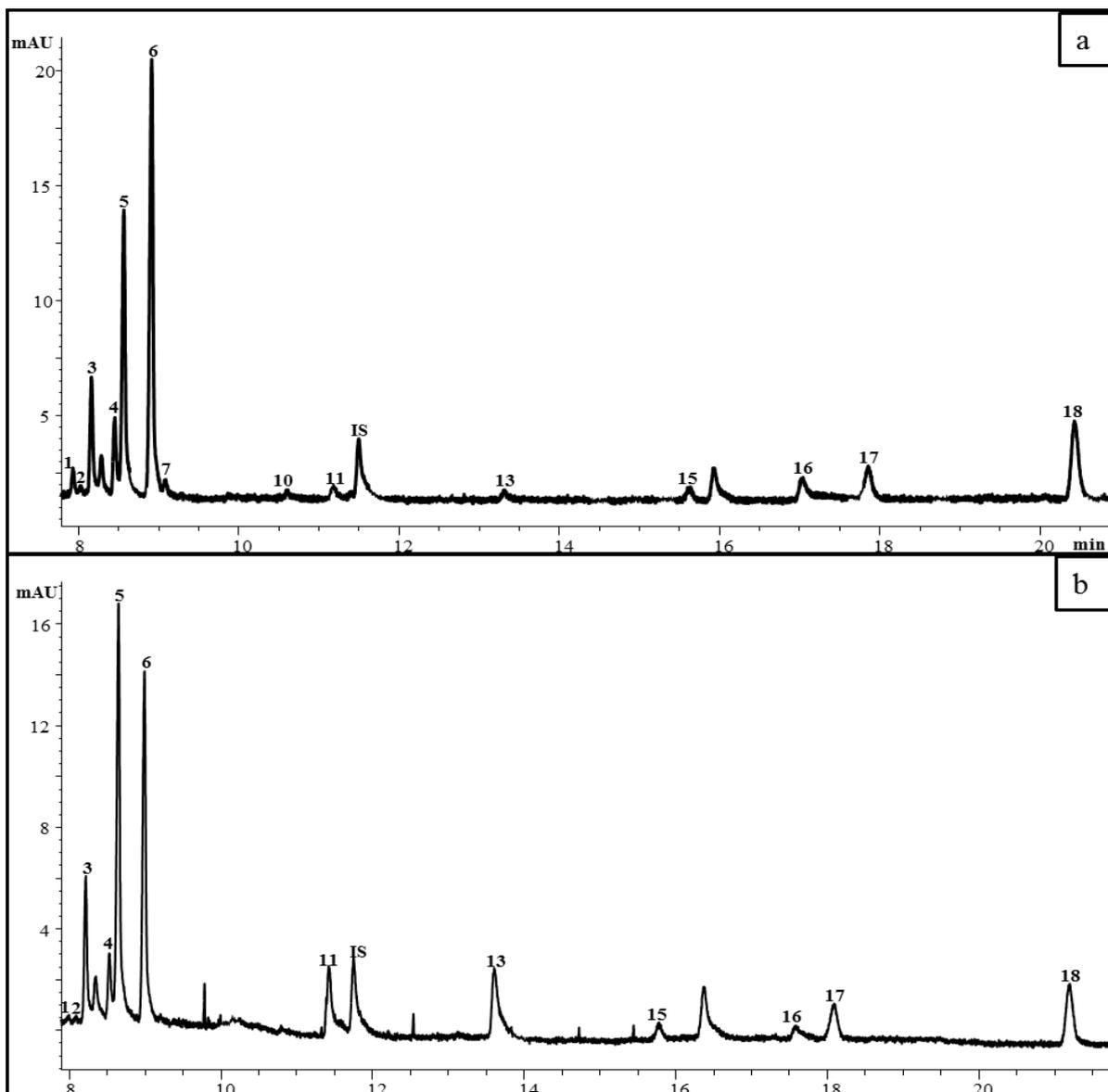
Figure 5.5. MEKC separation of amino acids in a) *G. postica* and b) *A. mimosae* silk fibroin hydrolysates using 32 mM phosphate /0.5 mM borate /172 mM SDS buffer, pH 6.70. Conditions and peak i.d as in Figure 5.4

Table 5.3A.   Amino acid composition of fibroin protein from the silkworm species as determined by the developed MEKC method

n=5	*G. rufobrunnae* (Botswana)		*G. rufobrunnae* (Zimbabwe)		*A. mimosae* (Kenya)		*A. mimosae* (Swaziland)	
	% ± SD	RSD	% ± SD	RSD	% ± SD	RSD	% ± SD	RSD
Non-polar								
Glycine	33.2 ± 1.5	4.0	35.1 ± 1.7	4.8	24.4 ± 1.9	3.9	23.9 ± 1.6	4.1
Alanine	26.0 ± 1.5	4.3	28.4 ± 1.3	5.1	36.1 ± 1.2	4.7	36.4 ± 1.6	4.3
Proline	2.3 ± 0.2	7.7	2.4 ± 0.2	6.3	0.2 ± 0.1	11.8	0.4 ± 0.1	12.5
Valine	1.4 ± 0.2	9.1	1.6 ± 0.1	8.1	0.8 ± 0.1	12.3	0.7 ± 0.1	11.7
Leucine	1.2 ± 0.2	8.4	1.4 ± 0.2	7.7	5.5 ± 0.4	5.9	6.2 ± 0.3	5.1
Isoleucine	0.7 ± 0.1	13.7	0.8 ± 0.1	13.1	0.2	19.7	0.2	19.3
Methionine	0.3 ± 0.1	18.2	0.3 ± 0.1	17.1	-		-	
Polar								
Serine	13.1 ± 0.5	4.6	13.4 ± 0.4	5.4	10.4 ± 0.4	4.9	10.1 ± 0.3	6.1
Threonine	0.7 ± 0.1	11.4	0.8 ± 0.1	11.9	0.3 ± 0.1	14.7	0.4 ± 0.1	14.0
Cysteine	0.1	18.9	0.1	19.2	detected		detected	
Acidic								
Aspartic acid	3.0 ± 0.1	6.8	2.6 ± 0.1	8.7	4.0 ± 0.2	7.1	3.8 ± 0.2	7.7
Glutamic acid	1.1 ± 0.1	9.0	0.9 ± 0.1	9.4	1.4 ± 0.2	9.5	1.0 ± 0.2	10.1
Basic								
Arganine	6.5 ± 0.2	4.6	5.4 ± 0.2	5.0	4.8 ± 0.2	17.1	5.1 ± 0.2	17.1
Lysine	0.9 ± 0.1	8.9	1.0 ± 0.1	10.1	1.0 ± 0.2	12.2	0.8 ± 0.1	12.2
Histidine	0.3	16.1	0.3 ± 0.1	14.9	0.2 ± 0.1	18.3	0.3 ± 0.1	18.3
Aromatic								
Tyrosine	9.1 ± 0.4	6.7	10.9 ± 0.5	5.3	6.8 ± 0.2	7.2	6.6 ± 0.3	7.2
Phenylalanine	0.7 ± 0.1	11.5	0.7 ± 0.1	12.1	3.9 ± 0.3	8.9	4.1 ± 0.3	8.9
Tryptophan	-		-		-		-	
Gly/Ala ratio	**1.27**		**1.24**		**0.68**		**0.65**	
[a]LC/SC ratio	**0.38**		**0.30**		**0.41**		**0.42**	

[a]LC, long chain amino acids and SC, short chain amino acids.

Table 5.3B.   Amino acid composition of fibroin protein from the silkworm species as determined by the developed MEKC method

n=5	*G. postica*		*E. bahuniae*		*B. mori*		*A. panda*	
	% ± SD	RSD	% ± SD	RSD	% ± SD	RSD	% ± SD	RSD
Non-polar								
Glycine	36.9 ± 1.2	4.3	28.2 ± 1.1	3.4	44.9 ± 1.6	4.0	28.9 ± 0.9	4.1
Alanine	28.1 ± 1.0	4.1	40.3 ± 1.9	3.7	29.2 ± 1.1	4.6	54.3 ± 1.7	3.4
Proline	2.5 ± 0.2	7.6	0.8 ± 0.1	9.4	0.5 ± 0.1	10.8	1.6 ± 0.2	7.3
Valine	1.6 ± 0.2	8.1	0.6 ± 0.1	12.1	2.4 ± 0.2	7.8	0.3 ± 0.1	15.5
Leucine	1.5 ± 0.2	8.3	1.2 ± 0.1	8.9	0.7 ± 0.1	11.7	0.3 ± 0.1	15.0
Isoleucine	0.8 ± 0.1	11.2	0.3 ± 0.1	16.8	0.4 ± 0.1	15.9	0.2	19.1
Methionine	0.3 ± 0.1	14.5	-		0.2	18.8		-
Polar								
Serine	12.1 ± 0.3	4.6	9.6 ± 0.3	5.5	9.6 ± 0.4	5.8	4.2 ± 0.2	5.0
Threonine	0.9 ± 0.1	11.4	0.6 ± 0.1	12.7	0.3 ± 0.1	15.0	0.2	18.5
Cysteine	0.1	18.9	detected		0.1	19.1	detected	
Acidic								
Aspartic acid	4.2 ± 0.2	6.8	3.2 ± 0.2	6.6	0.3 ± 0.1	12.1	2.9 ± 0.2	8.2
Glutamic acid	1.2 ± 0.1	9.0	1.1 ± 0.1	8.4	0.6 ± 0.1	11.3	0.5 ± 0.1	13.3
Basic								
Arganine	6.5 ± 0.3	5.6	4.9 ± 0.3	6.7	0.2	17.1	2.9 ± 0.2	6.6
Lysine	1.1 ± 0.1	7.9	0.6 ± 0.1	12.3	0.6 ± 0.1	12.2	0.3 ± 0.1	14.6
Histidine	0.2	17.1	0.3 ± 0.1	13.3	0.2	18.3	0.4 ± 0.1	13.8
Aromatic								
Tyrosine	8.3 ± 0.3	6.5	7.8 ±0.4	6.1	9.6 ± 0.3	6.6	2.9 ± 0.2	8.4
Phenylalanine	0.8 ± 0.1	11	0.6 ±0.1	11.5	0.7 ± 0.1	11.7	0.2	18.7
Tryptophan	-		-		-		-	
Gly/Ala ratio	**1.31**		**0.69**		**1.54**		**0.53**	
[a]LC/SC ratio	**0.30**		**0.28**		**0.19**		**0.14**	

[a]LC, long chain amino acids and SC, short chain amino acids.

The ratio of glycine to alanine (Gly/Ala ratio) in fibroin is important in defining the crystalline arrangement of silks. *Gonometa* fibroin had a higher glycine than alanine content resulting in a Gly/Ala ratio greater than 1, similar to *B. mori* fibroin. However, because the glycine content in *B. mori* fibroin (44.9 %) was higher than in the *Gonometa* fibroin (~36 %), the Gly/Ala ratio differed significantly suggesting a distinction in the primary structure and organization of residues in the two species. Our result for the Gly/Ala ratio for *G. rufobrunnea* (1.27) is different to that reported by Freddi *et al.* (1.51) [34]. This was because the alanine content reported in the two studies differed greatly though the reason for the discrepancy was unclear. However, statistical analysis showed there was no significant difference between the two studies for the results of the remaining amino acids. In contrast to *Gonometa* and *B. mori* fibroin, *A. mimosae* and *E. bahuniae* fibroin had more alanine than glycine, resulting in a Gly/Ala ratio less than 1. This is similar to reports from several Asian silks belonging to their *Saturniidae* family [292]. *A. panda* (*Thaumetopoeidae* family) also showed a higher alanine content but due to the greater amount of glycine present, it exhibited a different Gly/Ala ratio to *A. mimosae* and *E. bahuniae* fibroin.

The LC/SC (long chain/ short chain) ratio provides insight on the relative degrees of crystallinity in fibroin by comparing amino acids making up the crystalline region (glycine, alanine and serine) and amorphous region (the rest of the amino acids) [293]. Long chain amino acids are often bulky and considered β-sheet breakers as they disturb the close packing of adjacent fibroin molecules. A high content of these amino acids (higher LC/SC ratio) therefore implies less structural regularity and a greater occurrence of less ordered regions. Higher LC/SC ratio calculated for *Gonometa* and *Saturniidae* fibroin suggests a lower order and more amorphous content compared to the *B. mori* silk with a lower LC/SC ratio (Table 5.3). Most of the bulky and polar amino acids such as arginine and aspartic acid were more

abundant in *Gonometa* fibroin than the other silks. Amongst the *Saturniidae* fibroin, *E. bahuniae* had larger amounts of leucine and phenylalanine than *A. mimosae* fibroin resulting in *E. bahuniae* having a significantly higher LC/SC ratio. *A. mimosae* composition in this respect is similar to that reported for *D. japonica* [292] whilst that of *E. bahuniae* is more comparable to the *Antheraea* silks [292]. *A. panda* fibroin exhibited the lowest ratio indicating a greater degree of structural order than the other silks in this study.

Serine and tyrosine, which are mostly part of the crystalline region, also attained fairly high concentrations in the fibroins. With the exception of *A. panda* fibroin, serine and tyrosine content ranged from about 7 to 13.5 % and 6.5-11 % respectively. *A. panda* fibroin had much smaller quantities of serine (~4.2 %) and tyrosine (~2.9 %). Serine plays an important role in stabilization of the protein structure by providing hydrogen bonds to neighbouring backbone N–H and C=O groups [294]. Tyrosine is also considered as a β-sheet favouring amino acid as it participates in hydrogen bonding and in aromatic- aromatic interactions within the silk [295].

The quantity of the polar and non-polar amino acids in the amorphous region gives an indication of the potential reactivity of the fibroin. Polar amino acids possess amino, carboxyl, and hydroxyl groups that are available for functional modifications whilst the non-polar amino acids do not provide these binding sites. When found within the protein structure, the polar groups form hydrogen bonds amongst themselves and are therefore not readily available for additional chemical interactions. Most of these polar groups are however found on the outer surfaces of proteins and are therefore available to take part in several chemical reactions [296, 297]. The presence of these amino acids in the fibroin therefore has an influential role in determining the chemical and physical properties of the protein. The *Gonometa* and *Saturniidae* fibroins showed a significantly higher content of polar amino acids compared to *B mori*. It can be inferred that these African silks have greater potential for

opportunities in blending or reacting with other materials. Though *A. panda* fibroin had much smaller quantities of polar amino acids than the other African fibroins, they were more than those found in *B. mori* SF.

The polar amino acids were mostly evenly distributed between the acidic and basic amino acids. Basic amino acids have been of more interest to biomedical researchers as it has been shown that they play a key role in cell attachment and growth when fibroin was used as a substrate for cell and tissue growth [145]. Arganine is also part of the tripeptide sequence (arginine-glycine-aspartic acid) that has also been identified as promoting cell attachment [145]. Results of this work thus suggest that fibroin from the African silkworm species, in particular, *Gonometa* fibroin, has prospective use in cell and/or tissue culture, possibly performing better than *B. mori* fibroin.

Not much variation was noted between the amino acid compositions of the same species sampled from different areas (Table 5.3A). It was thus assumed that the small differences would not have a great impact on their physical properties and therefore results reported represent the particular species.

5.5   Cocoon and fibre properties

Cocoon constructs, including some in this study [298, 299] have shown great diversity depending mostly on the species, environment and function of the cocoon. As seen in Figure 4.2 (experimental section), cocoons from the different silkworm species showed differences in size, colour and architecture. *Gonometa* cocoons had a similar oval shape and were light grey to light brown in colour. *Saturniidae* cocoons showed more variance with *A. mimosae* cocoons having unique perforations and a shiny silver colour whereas *E. bahuniae* cocoons had a light brown colour. Similar to reports in literature [48], *A. panda* silkworms had unique constructs with a large brown cocoon which enclosed as many as 60 smaller light yellow

cocoons. The cocoons from the wild species were much tougher than those of *B. mori*. As a consequence, harsher degumming conditions were required than those for *B. mori* cocoons. Wild silkworm cocoons tend to be more resilient in order to withstand the harsh environmental conditions they are exposed to in their natural habitats such as extreme heat or cold [58]. SEM images of the cocoons showed that the silk fibres from *G. rufobrunnae, G. postica*, *A. panda*, *A. mimosae* and *E. bahuniae* were heavily cemented with sericin making a compact structure (Figure 5.6). *B. mori* cocoons had less sericin coating than the other cocoons with individual fibres visible. It has been reported that the amount of sericin produced and its extent of binding the fibres is greatly determined by the biology and habitat of the insects [299]. A white deposit observed on the surface of *Gonometa* and *A. mimosae* cocoons has been previously ascribed to calcium oxalate from silkworm excretions [293, 298]. A recent comprehensive study on cocoons from various silkworm species suggests that the calcium oxalate may have a structural function in the cocoon construct, though further investigations are needed in this respect [299].

Complete sericin removal is very important for quantitative analysis of the amino acids in the fibroin as well as determination of some physical properties of the fibroin. SEM examination of the degummed cocoons showed individual silk fibres with a clean surface free from sericin indicating proper degumming (Figure 5.7). Further examination of the fibres showed they had considerable variability in shape and size. Diameters ranging from 18-33 μm were observed for *G. postica* and 13-24 μm for *G. rufobrunnae*, similar to those for *E. bahuniae* (16-25 μm). Fibres from *A. mimosae* cocoons were the largest in diameter ranging from 33-46 μm. *A. panda* fibres were very fine and had diameters around 9-13 μm, similar to *B. mori* fibres (7 to12 μm). Though silk fibre diameter has not been a point of discussion in technological applications, it is an important characteristic in the textile industry influencing properties such as abrasion resistance, softness and stiffness [300].
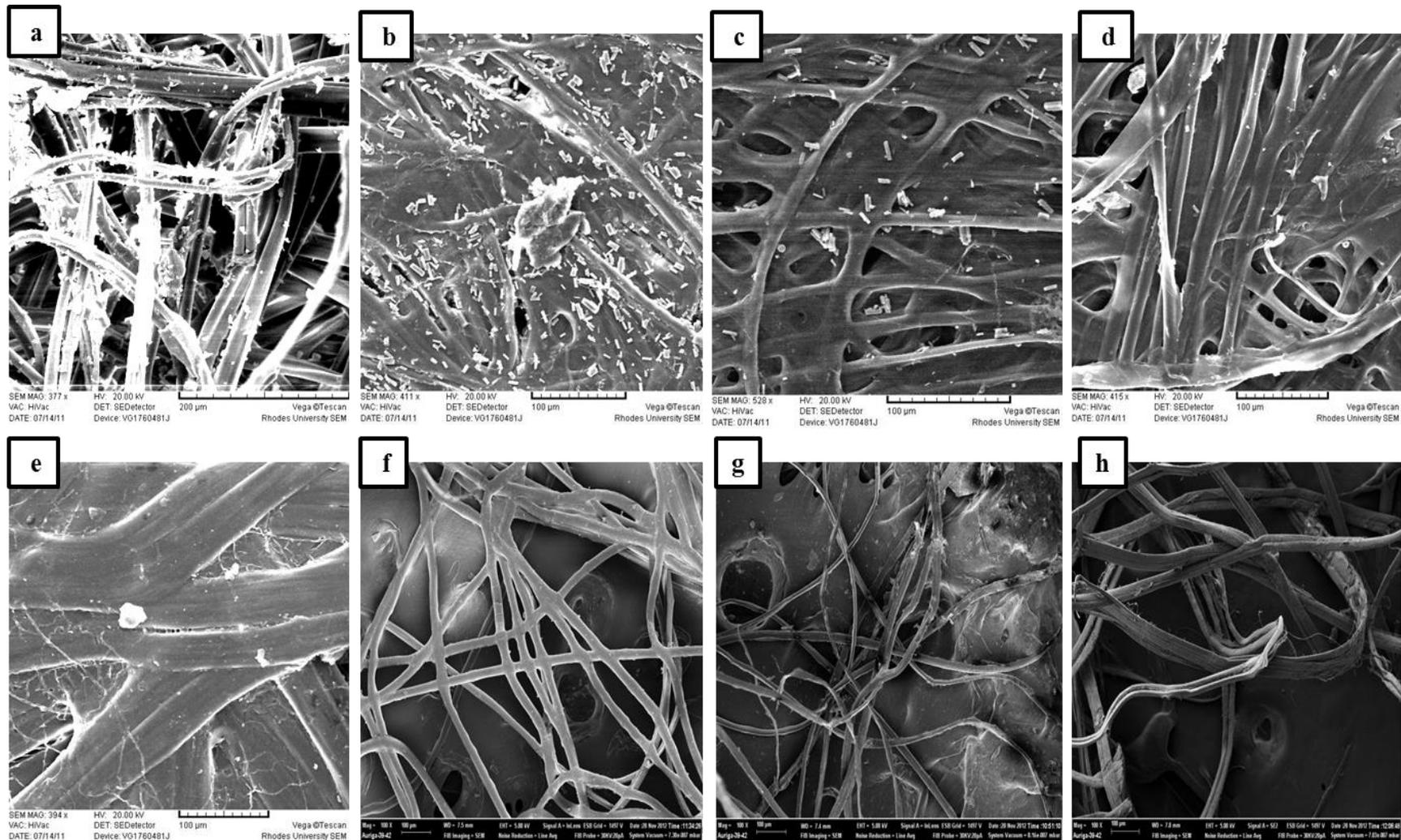
Figure 5.6. SEM images of a) *B. mori*, b) *G. rufobrunnae* (Bots) c) G. *rufobrunnae* (Zim) d) *G. postica*, e) *A. mimosae*, f) *A. panda* (outer), g) *A. panda* (inner) and h) *E. bahuniae* undegummed silk fibres
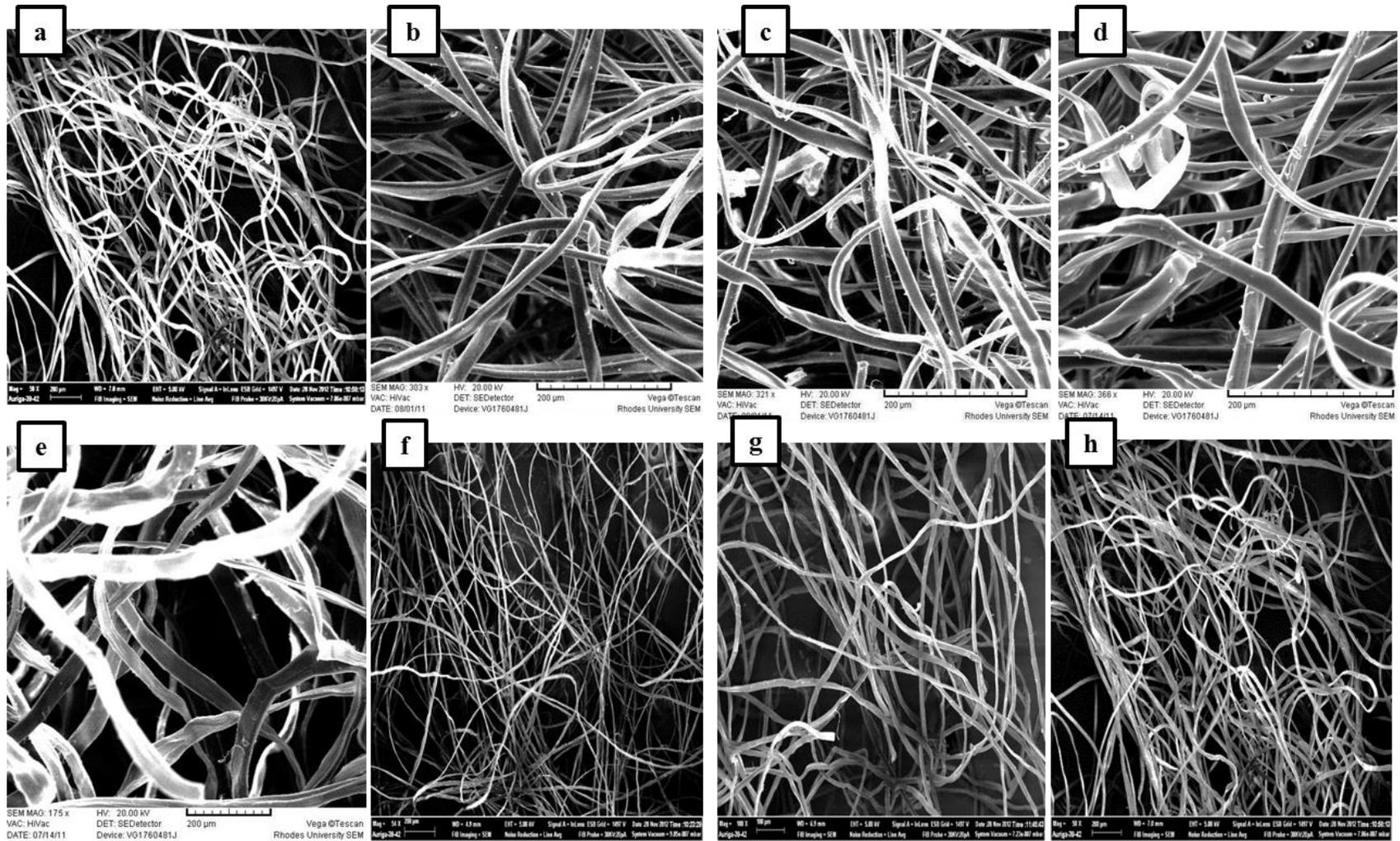
Figure 5.7.   SEM images: a) *B. mori*, b) *G. rufobrunnae* (Zim) c) *G. rufobrunnae* (Bots) d) *G. postica*, e) *A. mimosae*, f) *A. panda* (outer), g) *A. panda* (inner) and h) *E. bahuniae* degummed silk fibres

Various cross sectional shapes, mostly round, oblong, triangular and elliptical were observed in the fibroins as exemplified by *G. postica* fibres (Figure 5.8).
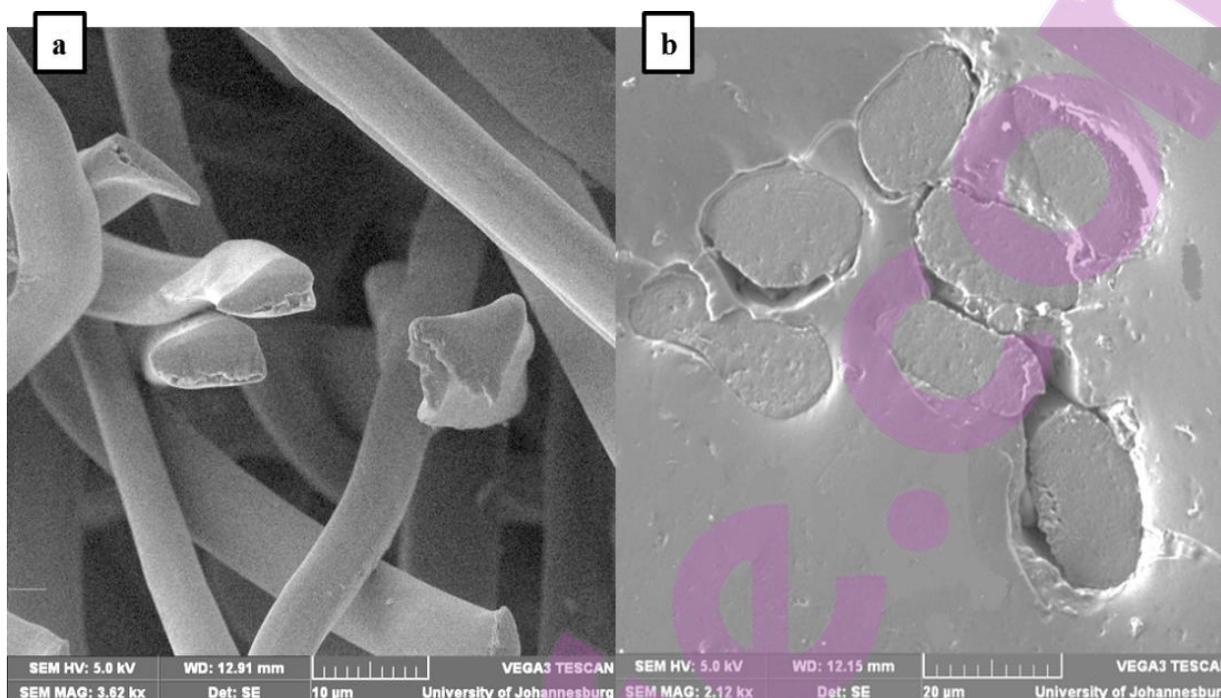
Figure 5.8. Cross sectional images of *G. postica* a) bundle fibres and b) fibres embedded in resin.

5.6 FTIR and Raman Spectroscopy

Infrared (IR) spectroscopy studies can provide useful data regarding the secondary structure of proteins. The technique takes advantage of groups of atoms that exhibit characteristic vibrational bands irrespective of their parent molecule [301]. This makes it possible to analyze various protein conformations depending on the position and intensity of the observed peaks. SF exists mainly in the three previously described conformations; namely random coil, α-helix and β-sheet. Using FTIR, the characteristic absorption bands for random coil are around 1647 cm^{-1} (amide I), 1541 cm^{-1} and 660 cm^{-1} (amide V), α-helix absorption peaks around 1655 cm^{-1} (amide I), 1546 cm^{-1} (amide II), 1270 cm^{-1} (amide III), 625 cm^{-1}

(amide V), and β-sheet absorption around 1630 cm^{-1} (amide I), 1520 cm^{-1} (amide II), 1240 cm^{-1} (amide III), 965 cm^{-1} (amide IV) and 695 cm^{-1} (amide V) [128].

The FTIR spectra of fibroin from all the silk species in the study showed the strongest peaks around 1514 and 1622 cm^{-1}, which are attributed to the β-sheet structure (Figure 5.9).
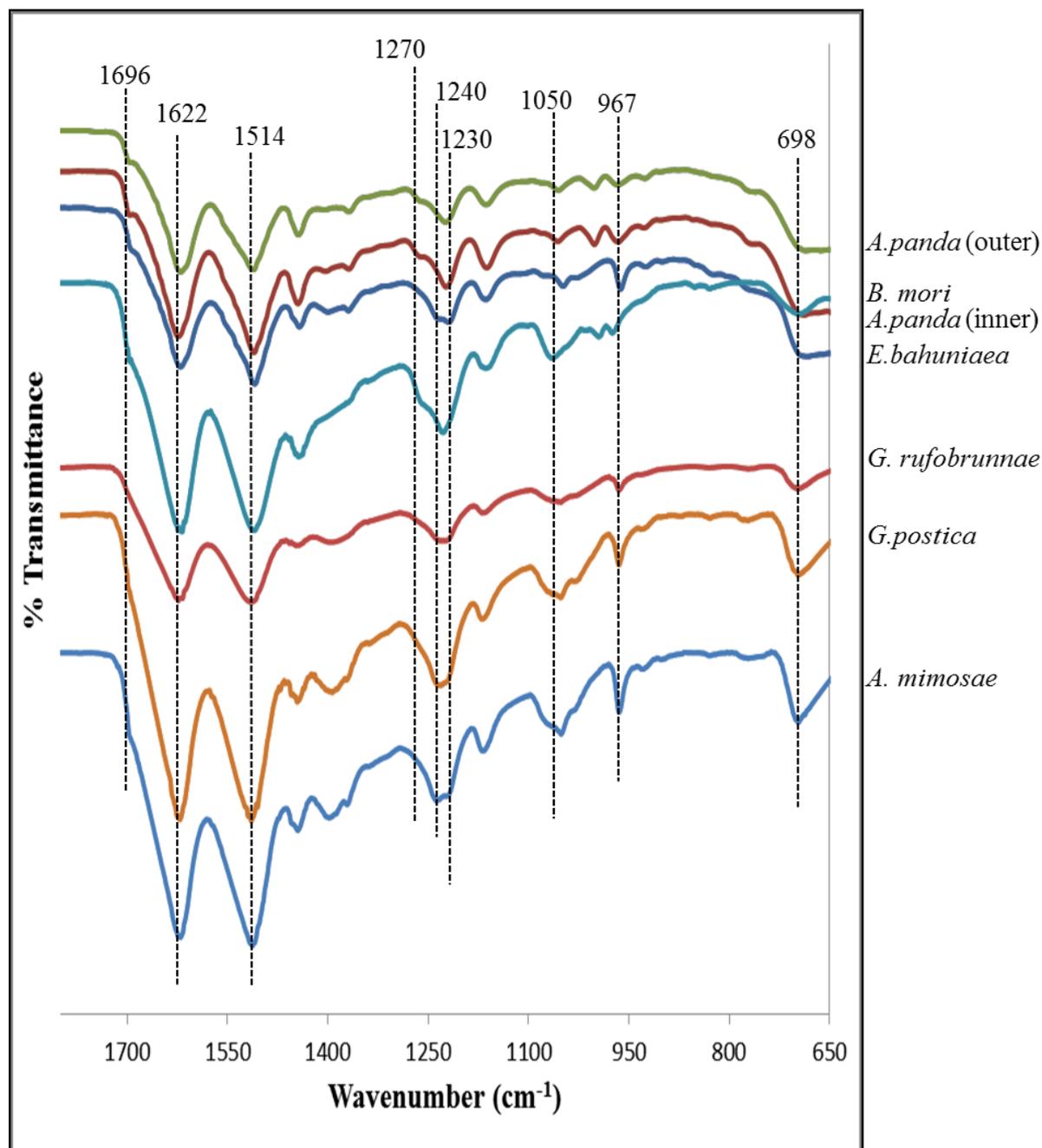
Figure 5.9.   FTIR spectra of silk fibroin from different silkworm species

Less prominent peaks seen at 698 and 1240 cm^{-1} are also indicative of β-sheet structure. Recently, it was deduced that a peak around 1050 cm^{-1} is characteristic of glycine-alanine (poly-Gly-Ala) sequences in the fibroin structure [302]. A peak was noted around this region, with varied intensity, for all the silk fibroins. These linkages have never been reported for the *Saturniidae* species and therefore cannot be attributed to the poly-Gly-Ala polypeptides until further conclusive research has been done. A shoulder peak at 1270 cm^{-1} (α-helical structure) was seen in the spectra for *B. mori* and *A. panda* fibroin but was not clear in the spectra for the other silks. Another shoulder peak was present around 1696 cm^{-1} in the fibroin spectra with the exception of those of the *Gonometa* fibroins. The peak is attributed to β-turn conformation of the hairpin-folded antiparallel β-sheet structure [303, 304]. Further analysis of the spectra showed a peak around 967 cm^{-1} for the *Gonometa*, *A mimosae*, *A. panda* and *E. bahuniae* fibres attributed to β-sheet crystallinity relating to alanine-alanine (poly-Ala) linkages [293]. A small peak noted around 972 cm^{-1} in the *B. mori* fibroin spectra could not be attributed to the poly-Ala linkages as they have not been previously reported for this species. Similar to results on the amino acid analysis, the spectra for the *A. panda* inner and outer silks were almost identical. *G. postica* also showed similar spectra to that of *G. rufobrunnae*. The *Saturniidae* silks (*A. mimosae* and *E. bahuniae*) exhibited very similar molecular conformation to reports for other Asian silks from the same family [305, 306].

Overall, the results show that the silk fibroin from the species examined in this study is mainly of β-sheet structure with some α-helix structure also existing. The *Saturniidae* and *Gonometa* silks showed similarities and were different from *B. mori* fibroin. Interestingly, *A. panda* showed a very similar structure to *B. mori* fibroin.

Raman spectroscopy was also utilized as an additional technique in analyzing the silk structure. As seen in Figure 5.10, the Raman spectra of all the silk fibroins showed strong peaks around 1666 cm^{-1} and 1090 cm^{-1} which is evidence of β-sheet crystallinity [307, 308].

A peak at 904 cm^{-1} associated with poly-Ala sequences [308] was observed in the fibroin spectra with the exception of *B. mori* fibroin thus confirming the absence of poly-alanine linkages in *B. mori* SF. Other peaks seen have been attributed in literature to various structures. A peak seen around 1225-1230 cm^{-1} in the fibroins has been ascribed to β-sheet structures [205, 309].
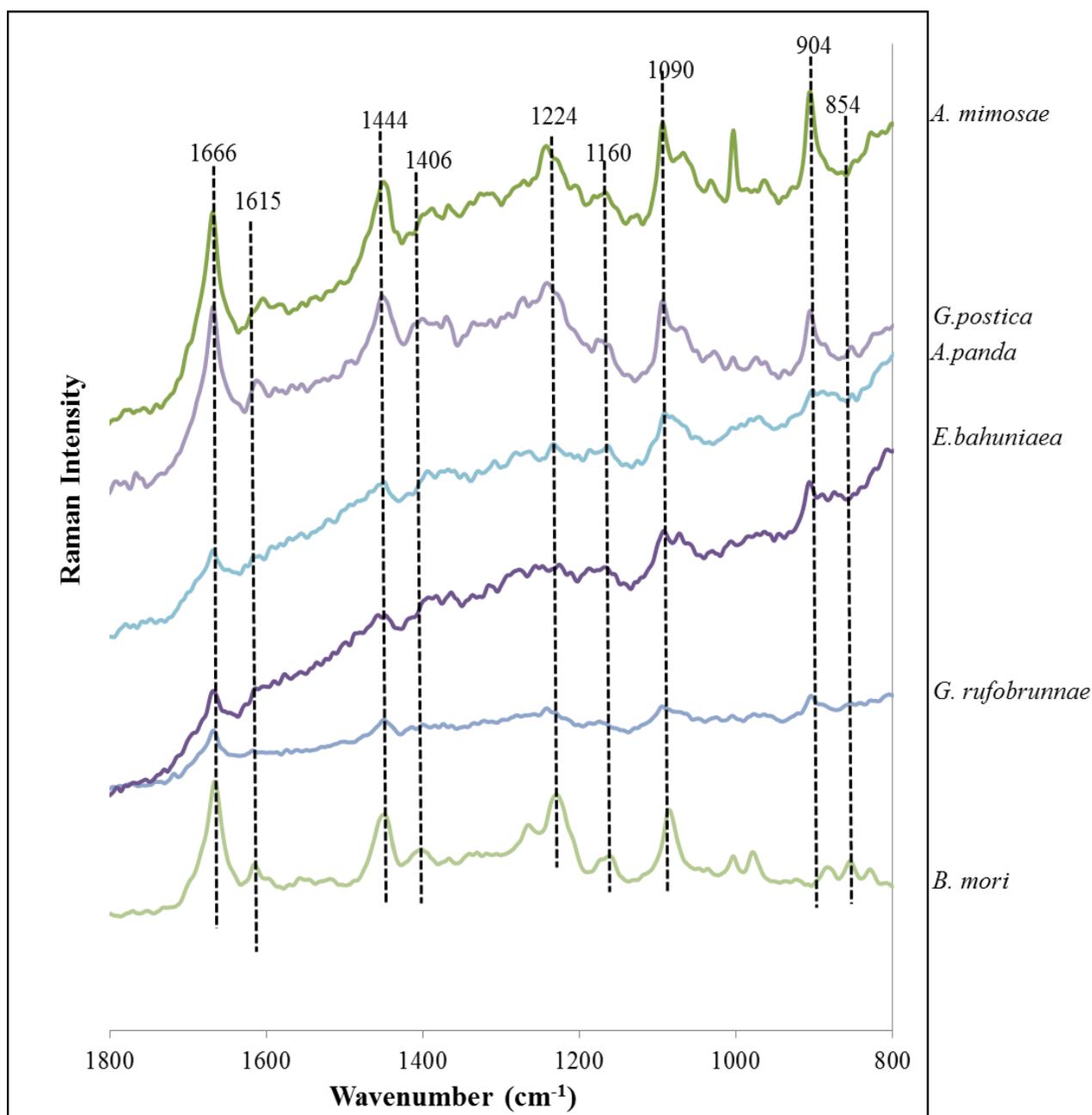
Figure 5.10.   FT-Raman spectra of silk fibroin from different silkworm species

Minor peaks around this region were observed for the other silk species. Additional bands at about 1615 cm^{-1} as well as 854 cm^{-1} have been assigned to the side chains of the amino acids phenylalanine and tyrosine respectively [308, 310]. The data provided by FTIR and Raman spectroscopy highlights how the proportions of the amino acids determine the primary structure and hence the secondary structure of the different fibroins. In the *Gonometa* fibroin, the glycine content is lower than in *B. mori* fibroin though their alanine content is very similar. This may possibly promote alanine-alanine linkages in the *Gonometa* fibroin in addition to glycine-alanine linkages. *A. panda, A. mimosae,* and *E. bahuniae* have higher alanine than glycine content which promotes primary sequences with alanine-alanine linkages. It can be assumed that the lower amount of glycine in the *Saturniidae* and *A. panda* fibroin (less than 30 % in all), is insufficient to promote significant poly-Gly-Ala linkages, unlike that for *Gonometa* and *B. mori* fibroin (more than 35 %).

5.7   XRD analysis

XRD is useful in examining the structure of crystalline and semi-crystalline polymers and was used to study the silk fibroin in this work. X-ray diffraction studies were conducted to elucidate the physical structure by identifying the positions of the diffraction peaks. Peaks were observed for all the fibroins examined (Figure 5.11). The peaks for *E. bahuniae* and *A. panda* were not as intense as the other fibroins, but are clearly visible in the insert on Figure 5.12. All the fibroins exhibited peaks around 20.5º and 24.5º corresponding to crystalline spacings of 4.35 Å and 3.62 Å respectively. These peaks are evidence of the β-sheet crystalline structure of the fibroin [90, 128]. There have also been reports suggesting that the above mentioned peaks are indicative of a concurrence of an amorphous matrix with a β–sheet crystalline structure [311]. The African fibroins exhibited additional peaks around 17º, 16.5º and 15.5º for *Gonometa*, *Saturniidae* and *A. panda* respectively. These peaks were absent in the *B. mori* fibroin.
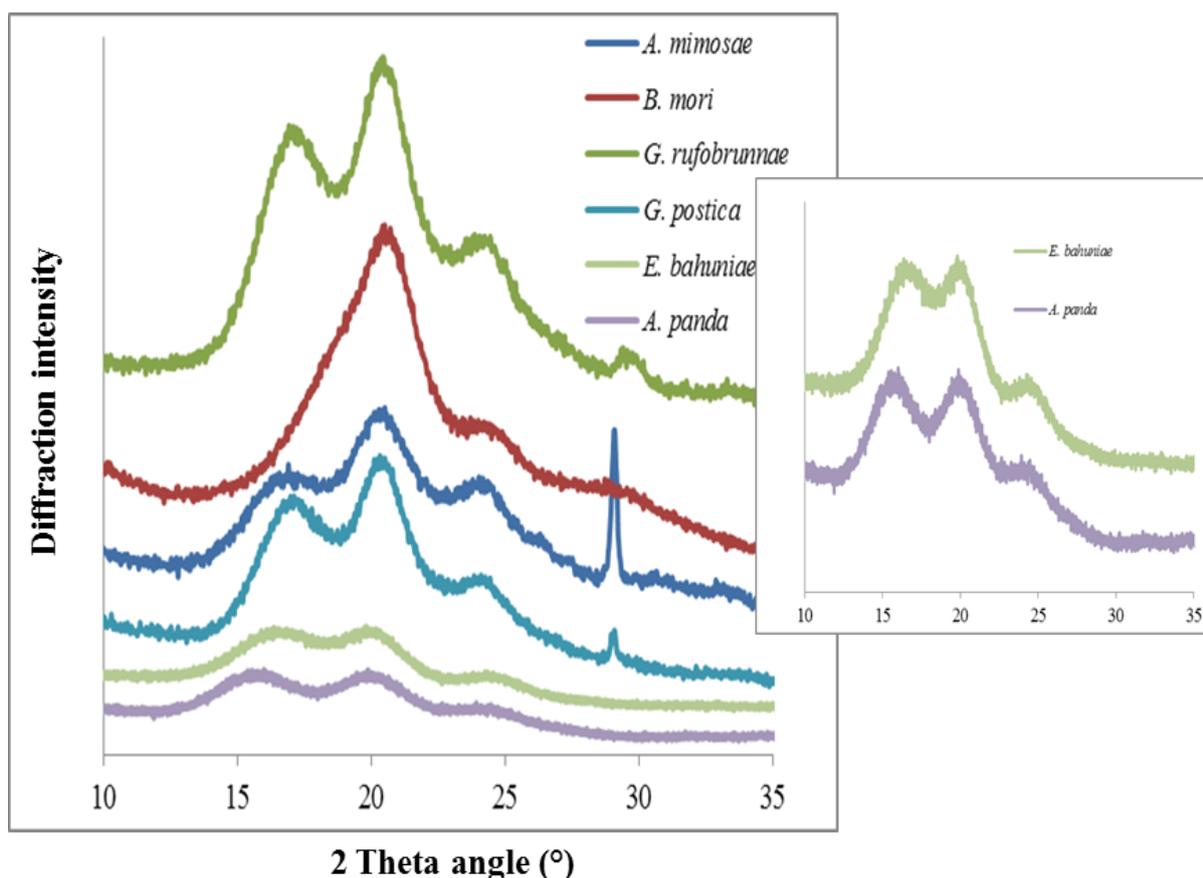
Figure 5.11. XRD analysis of silk fibroin from different silkworm species

Earlier research by Warwicker attributed different peaks seen in diffractograms to varying dimensions of the unit cell of the crystallites in the different fibroins [312]. The size of the crystallites are dependent on the amino acids making up the crystalline components, which further highlights the impact of amino acid composition on the structure of the fibroins. The XRD data therefore provides further evidence of a distinct difference in the crystalline structure of the wild African fibroins and *B. mori* fibroin.

Results for *A. mimosae* and *E. bahuniae* are in agreement with those reported for other species belonging to the *Saturniidae* family, which are mainly composed of alanine-alanine sequences [293]. The data of the African fibroins, though similar, also suggest there are

differences amongst them. Study using advanced X-ray techniques (for instance synchrotron based) can be used to further elucidate differences in crystalline structure of the fibroins. Quantitative determination of the different phases (crystalline and amorphous) could also prove useful in examining differences noted for the fibroins. This however could not be done in this study due to an absence of suitable standards for the different phases.

5.8 Thermal Analysis

Thermal properties of the silks were examined using TGA and DSC techniques. Thermogravimetric (TG) curves of the silk fibroins are shown in Fig 5.12. An initial weight loss occurred below 100 °C which is widely attributed to loss of water. The fibres showed thermal stability up to about 200 °C after which they showed initial stages of decomposition. The thermograms were then characterized by rapid mass loss with over half of the fibroin mass degraded at 400 °C. Differential weight loss (DTG) curves provided a clearer depiction of the degradation steps as they directly relate to specific thermal decomposition stages (Figure 5.13). Unlike *B. mori* fibroin, fibroins from the African silkworm species were characterized by several degradation steps. A small degradation peak at 230 °C seen for *Gonometa* and *Saturniidae* fibres is associated to the loss of low molecular weight gases (H_2O, CO_2, NH_3), resulting from the breakdown of side chain groups of amino acid residues as well as from cleavage of peptide bonds in the amorphous region of the silk [313, 314]. The main peaks of degradation between 350 °C and 375 °C are associated with mass loss due to the permanent decomposition of the fibroin molecules. The *Gonometa* and *Saturniidae* fibres showed very similar degradation patterns with maximum decomposition occurring around 375 ° C for the fibres. *A. pernyi* and other silks belonging to the *Saturniidae* family have also been found to undergo a number of decomposition steps attributed to their crystalline structure and amino acid composition [314]. *A. panda* exhibited its maximum degradation around 360 °C, the lowest amongst the African fibres. The main degradation peak was

around 350 °C for the *B. mori*, which therefore implies the African wild silk fibres are relatively thermally more stable. No assignment has been previously given to the peaks seen above 400 °C but they may possibly represent further decomposition of the silk fibroin structure. However, TGA combined with FTIR can give more insight into the specific structural degradation of the fibroin at the different stages of heating.
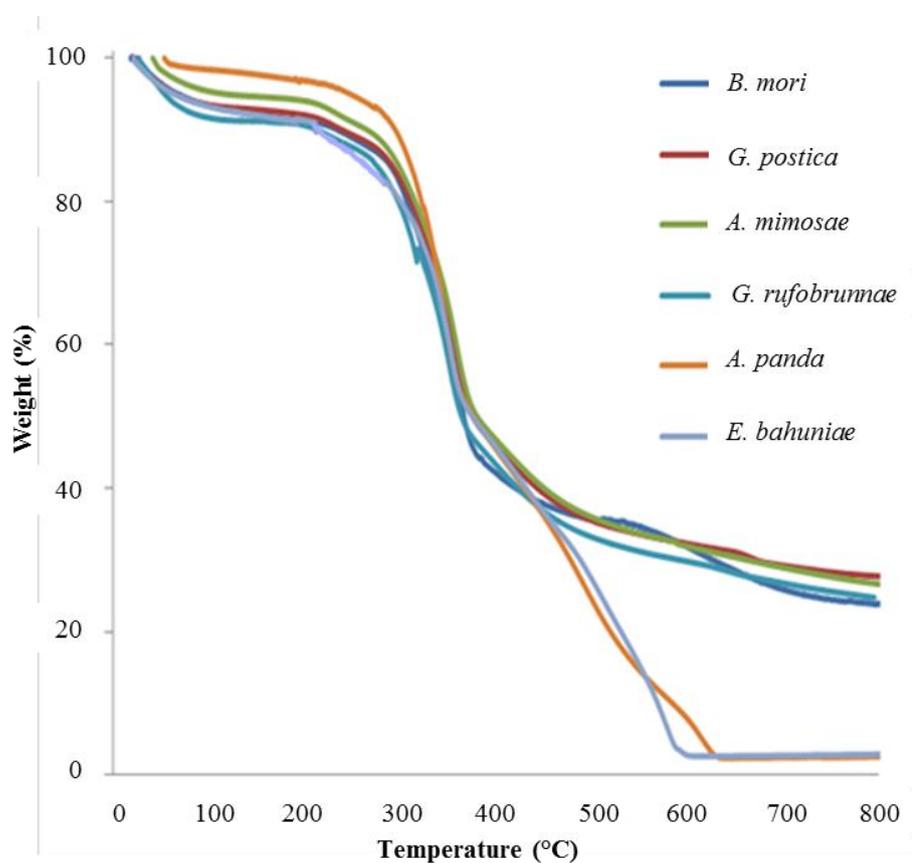
Figure 5.12. TGA curves for the silk fibroins

DSC curves of the fibroins (Fig 5.14) showed an endotherm below 100 °C which is due to absorption of heat for removing water. In addition to this dehydration endotherm, *B. mori* fibroin showed one other main peak around 320 °C. Similarly, *A. panda* also showed one major peak around 365 °C. The peaks found between 320 and 365 °C represent the degradation of the β -sheet structures of the protein. This data, similar to TGA results, shows

B. mori fibroin is less thermally stable than the African fibroins. This may be due to the higher thermal stability of poly-Ala β-sheets [315] which are present in the African fibroins.
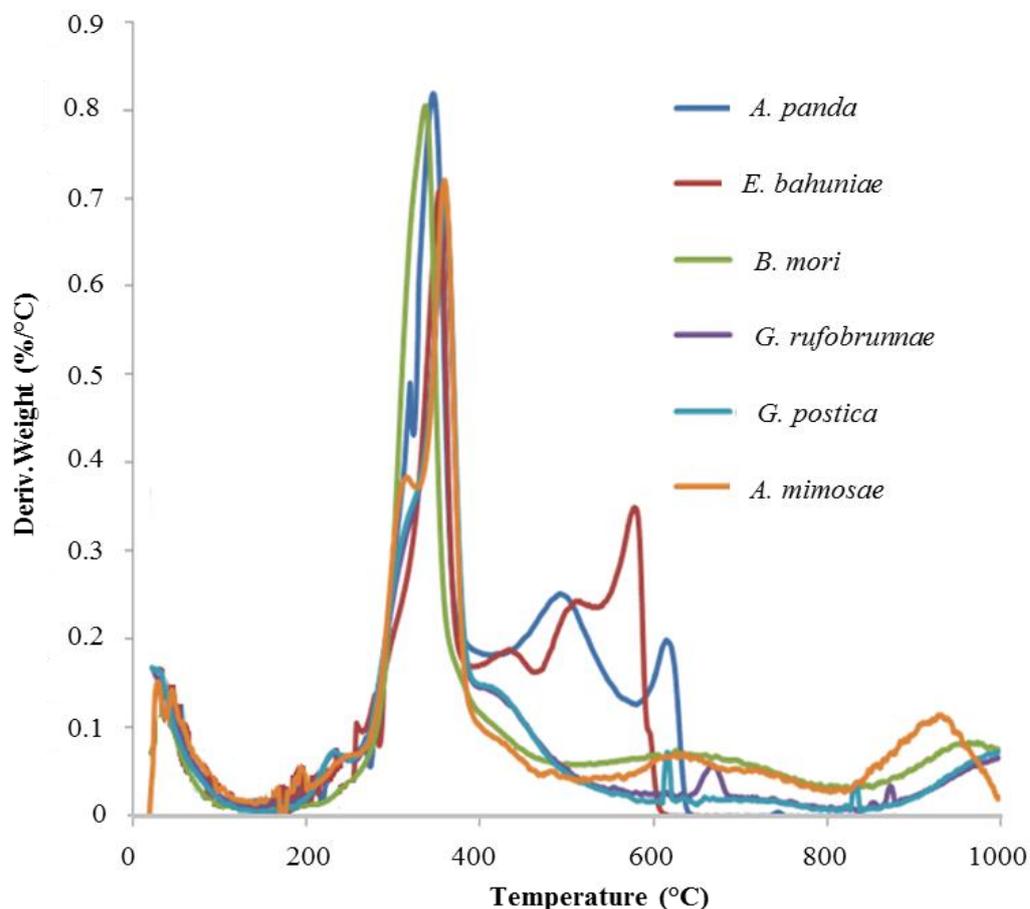
Figure 5.13. DTG curves for the silk fibroins

With the exception of *B. mori* and *A. panda*, the rest of the fibroins exhibited another significant peak around 228 °C which is attributed to the strong molecular motion and rearrangement within the α-helix crystals in the amorphous region [293]. DSC and TGA results however vary with regards to *A. panda* fibroin. TGA shows it to be slightly less stable than the other African fibroins whilst DSC results show the main decomposition endotherm at a higher temperature than the other fibroins.
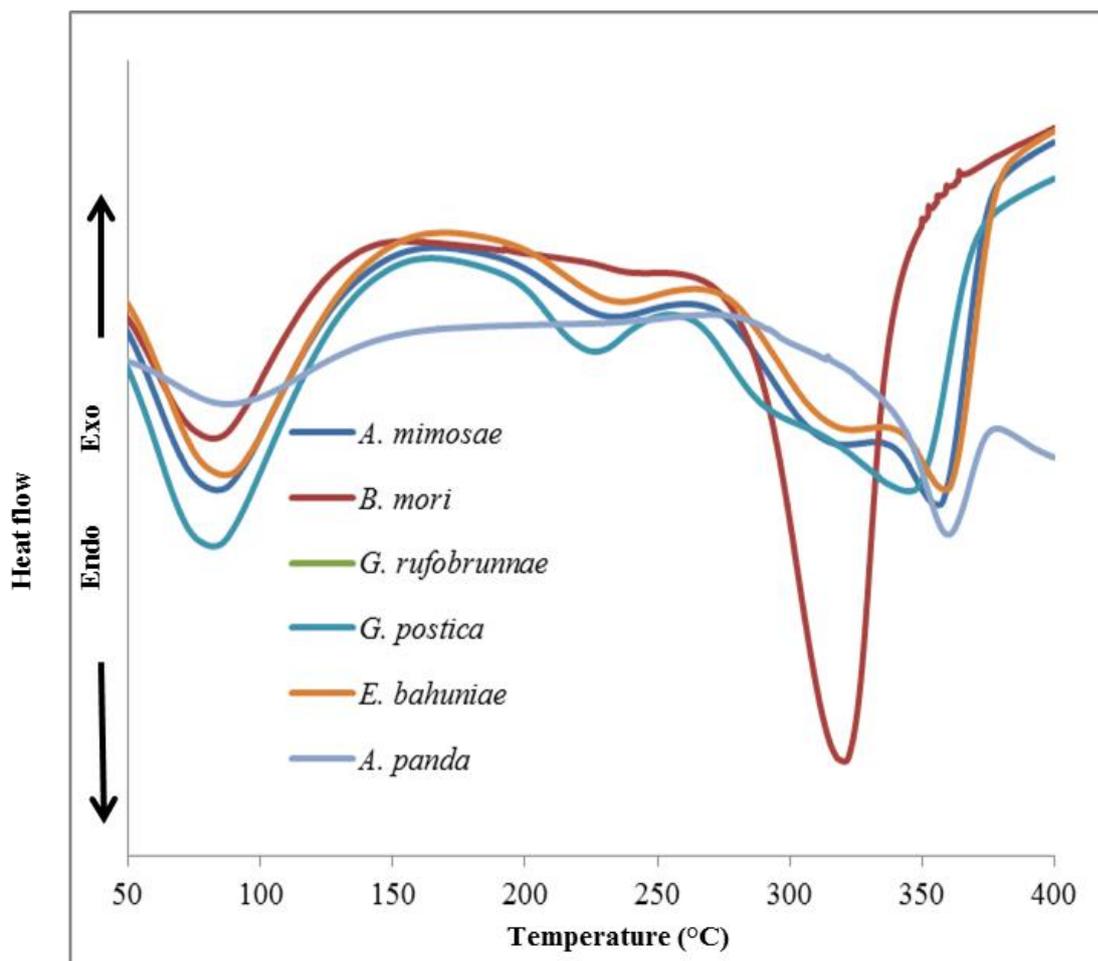
Figure 5.14. DSC curves for the silk fibroins

5.9 Mechanical properties

The quality of the silk fibres can be assessed by examining mechanical properties such as tensile strength, tenacity, Young's modulus and toughness. Table 5.4 shows the results of the measurements of tenacity and tensile extension done for fibres from the different species. The diameters for all the silks were determined using optical imaging as exemplified in Figure 5.15. Tenacity measures the strength of a fibre or yarn by determining the point at which it breaks; the higher the fibre tenacity, the higher the strength of the fibre. *B. mori* silk showed

the highest tenacity of all the fibres tested. Amongst the African silks, *A. panda* had the highest tenacity followed by *G. rufobrunnae*, *G. postica*, *A. mimosae* and *E. bahuniae*.

Figure 5.15.   Optical image for cross section of *A. panda* silk fibres

The mechanical performance of fibroin is governed to a large extent by its chemical structure, particularly the amino acid composition and sequence.

The larger amount of bulky amino acids in their structure hinder close packing of fibroin chains which enables formation of strong hydrogen bonds between the chains. *A. panda* consists mostly of glycine (28.9 %) alanine (54.3 %) and serine (4.2 %) and a small percentage of amino acids with bulky side groups. This suggests an extensive crystalline

region and less amorphous content than the other African silks hence it exhibited the highest tenacity amongst the African silk fibres.

The strength at break of *E. bahuniae* and *A. mimosae* fibroin was about half that of *B. mori*. Literature however suggests that poly-alanine β-sheets (predominant in *E. bahuniae* and *A. mimosae* fibroin) exhibit a higher tensile strength than the poly-Gly-Ala β-sheets (predominant in *B. mori* fibroin) due to a higher binding energy [316]. The authors indicated that in poly-Ala rich segments, hydrophobic interactions interlock adjacent chains into stable antiparallel β-sheets, whereas in the poly Gly-Ala rich segments, the glycine residues are not capable of forming the same types of hydrophobic interactions hypothesized for an alanine residue [316]. This ultimately results in less stable β-sheets in poly Gly-Ala regions due to fewer chain interactions.

Table 5.4. Mechanical properties of the silk fibroins

Properties	*E. bahuniae*	*G. rufobrunnae*	*B. mori*	*A. mimosae*	*A. panda*	*G. postica*
Mean Tenacity @ Max.Load (cN/tex)	12.08	15.89	32.11	12.11	24.69	15.1
CV%	18.7	30.3	23.9	16.39	16.43	20.3
Mean Tensile extension@ max. Load (mm)	0.73	1.04	0.62	0.79	0.72	1.08
CV%	18.4	34.3	29.5	29.62	40.8	7.17
Mean fibre diameter (μm)	14.8	14.7	12.1	27.0	11.9	16.2
CV%	30.9	31.7	26.9	43.7	31.9	34.4

It has also been noted that mechanical properties such as tenacity are also related to the finess of the silk fibres. A general rule established from work done by Meredith [317] is that the finer the silk, the higher the tenacity and the lower the breaking extension. This is somewhat reflected in the results obtained in this work, more so for the tensile extension.

G. postica and *G. rufobrunnae* silks had the highest extension values of all the silks. When silks are stretched, deformation begins in the amorphous regions, therefore the proportion of the amorphous region and the interaction of the chains in this region will strongly determine the resistance to extension. Under tensile load, the semi-amorphous regions unravel first owing to breaking of hydrogen bonds, which accounts for the high level of extensibility observed in silk [318]. The presence of more bulky amino acids in the amorphous region also allows the SF chains to flow easier, conferring elasticity and better extension of the fibre [319]. *Gonometa* fibroin is comprised of a more extensive amorphous region than the other silks which may explain their higher extension. *E. bahuniae* and *A. mimosae* fibroins had comparable extension to *A. panda* fibroin and slightly higher extension than *B. mori* fibroin. Data obtained in this work is in reasonable agreement with some other published data for degummed fibres. Kushal and Murugesh determined that because the non-mulberry silks contain more amino acid residues with bulky side groups they exhibit higher extensibility [319]. Teshome *et al.* revealed that the African wild silk fibres belonging to the *Saturniidae* silks showed larger extensibility when compared with the *Thaumetopoeidae* [36]. They also reported that the African wild silk fibres had a lesser breaking elongation than *B. mori*, which is contrary to our results.

One of the factors that may significantly contribute to variances in mechanical properties is the degumming process. Some of the fibres from the wild silks show some damage (Figure 5.16), possibly due to the intensive degumming procedure as reported by other researchers

[320]. It was also noted that the cocoons consisted of several different layers and some of the fibres could be more easily pulled out in some layers compared to others.
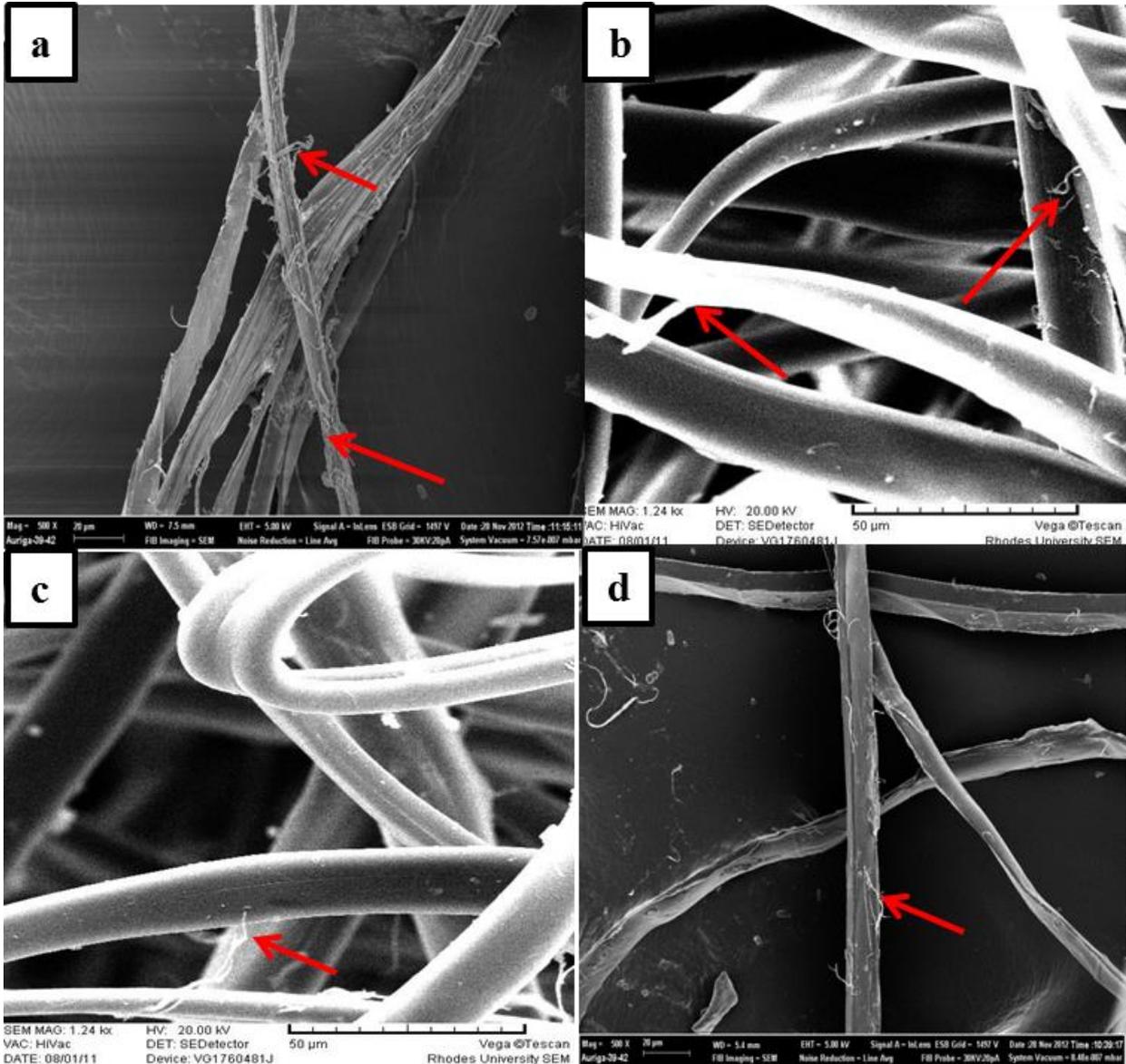
Figure 5.16. SEM images of damage done to silk fibres from a) *A. panda* (inner), b) *G. postica* c) *G. rufobrunnae* and d) *A. panda* (outer) during degumming

This suggests the extent of cementing the fibroin with sericin differs which may result in some of the fibres being exposed to the degumming solution for too long leading to the damage observed. This damage has proven to be detrimental to the mechanical properties of

the silk [321, 322] and affects its performance as a textile material. However, for use as biomaterials, the fibroin is processed by first dissolving degummed silk; thus the inherent mechanical properties of the silk fibres are lost and any damage caused by the removal of sericin is not detrimental.

CHAPTER SIX

FABRICATION AND CHARACTERIZATION OF ELECTROSPUN SILK NANOFIBRES

6.1   Introduction

This chapter covers the processing of silk fibroin into regenerated silk (RSF) as well as fabrication and characterization of *Gonometa* silk fibroin nanofibres. Part of this work has been published in the Journal of Macromolecular Research [323].

6.2   Dissolution of degummed silk fibroin

Dissolution of fibroin is a necessary step in preparing RSF from silk fibres prior to processing into morphologies for biotechnological applications such as sponges, films and nanofibres. Commonly used concentrated salt solutions achieve dissolution by binding with polar residues in the fibroin causing disruption of van der Waals forces and hydrogen bonds in fibroin molecules [324]. Although several solvent systems have been found effective for dissolution of fibroin from other species, there has been no information on the dissolution of the African fibroins prior to our work [323]. Recently, Teshome and co-workers also made a contribution in this regard [325]. This section thus gives a detailed account of our findings on the ability of several solvent systems to dissolve the fibroin from some African silkworm species. The studies also provide further insight on the chemical nature of the fibroins as their dissolution involves interaction of solvent ions with functional groups present within the fibroin structure.

6.2.1 Effect of different aqueous salts and concentration

Results obtained on the solubility of the fibroins in various aqueous salts at different concentrations are presented in Table 6.1. *G. postica* and *G. rufobrunnae* fibroin dissolved easily in 9.5 M $Ca(NO_3)_2$ producing solutions of approximately 22 % (w/v) after 5 h dissolution. *A. mimosae*, *A. panda* and *E. bahuniea* fibroin showed the lowest solubility in $Ca(NO_3)_2$ with less than 3% of the fibroin dissolving.

Table 6.1.   Dissolution of silk fibroins in aqueous salt solutions

	$Ca(NO_3)_2$			$CaCl_2$	LiBr			LiCl
	5 M	7 M	9.5M	Up to saturated solution	5 M	7 M	9.5 M	Up to 9.5M
G. postica	×	++	+++*	×	×	++	+++	×
G. rufobrunnae	×	++	+++	×	×	++	+++	×
A. mimosae	×	×	+	×	×	×	+	×
A. panda	×	×	+	×	×	×	+	×
E. bahuniaea	×	×	+	×	×	×	+	×
B. mori	+	++	+++	+	+	++	+++	+

*: +++ = Very soluble, ++ = Soluble, += Slightly soluble, × = Insoluble

Gonometa fibroin also dissolved easily in 9.5 M LiBr whilst *A. mimosae*, *A. panda* and *E. bahuniae* fibroin were again practically insoluble with less than 2 % dissolving. None of the African fibroins were solubilized using $CaCl_2$ and LiCl solutions. In stark contrast to the African fibroins, *B. mori* fibroin dissolved in all salt solutions investigated, though solubility in $CaCl_2$ and LiCl solutions was relatively low (< 5 % w/v). For the salts that solubilized the African fibroins, the dissolution process was slower than that observed for *B. mori* fibroin. The effect of different concentrations of the salts was also examined. As expected, lower

concentration of the salt solutions resulted in lower solubility of the fibroin from all the species. Only *B. mori* and *Gonometa* fibroin dissolved in 7 M salt solutions.

There was no dissolution of any of the fibroins when 5 M solutions of the salts were used (Table 6.1). The results suggest that there are several factors affecting solubility of the fibroin. Firstly, there is evidence the solubility of fibroin is highly dependent on the type of salt ions available for the process. The ionic strength of salts has been highlighted as a key parameter in protein solubility. Ions with high charge density, such as Ca^{2+} and Mg^{2+}, are strongly hydrated and tend to increase protein solubility by interacting more with amide moieties in proteins than less hydrated cations (Li^+, K^+). Studies have further established that the dissolution process is more dependent on the anions, possibly because of their larger size compared to cations [326, 327]. Nucleophilic attack by the anions on the abundant electrophilic centres (hydroxy, amide, amino groups) in the fibroin results in the disruption of the hydrogen bonded chain networks. Br^- and NO_3^- are more nucleophilic than Cl^- and would thus have better protein solubilizing power. This possibly explains why the fibroins dissolved more in LiBr and $Ca(NO_3)_2$ but not in LiCl and $CaCl_2$ solutions.

Secondly, the variation observed in solubility can be attributed to differences in their structure as influenced by their amino acid compositions. The amorphous region of fibroin is the one that is open to interactions with other compounds and/or solvents that can cause changes in structure, and studies have shown that silk dissolution starts in this region [328]. The larger proportion of polar groups in the *Gonometa* and *Saturniidae* silks could result in increased networking of fibroin molecules through hydrogen bonding, possibly creating a stronger amorphous structure than the other fibroins. It would thus be expected that the *Gonometa* fibroin would show the least solubility with multiple bonds requiring disruption. Results however do not reflect this as *Gonometa* fibroin was the most soluble of the African fibroins. On the other hand, a larger amount of polar groups would provide multiple sites for

interaction with salt molecules causing dissolution to proceed faster than in fibroin with less polar groups.

This assumption, again, fails to address the stark differences between the *Gonometa* and *Saturniidae* fibroin as well as the easier dissolution of *B. mori* fibroin. A more plausible explanation can be found in the crystalline structures of the different silks. In terms of the β-sheet forming residues, *B. mori* fibroin has (Gly-Ala)$_n$ units, *Gonometa* SF has (Gly-Ala)$_n$ and (Ala-Ala)$_n$ units and *A. mimosae*, *A. panda* and *E. bahuniae* are composed of (Ala-Ala)$_n$ repeats. Packing of (Ala-Ala)$_n$ beta sheets is more compact than (Gly-Ala)$_n$ [316] which may hinder penetration of water and solvent ions for dissolution of the fibroin. Thus, the order of dissolution observed was *B. mori* fibroin being the most soluble and *A. mimosae*, *A. panda* and *E. bahuniea* being the least soluble. This suggests that the crystalline composition is the major determining factor in its solubility and further investigations are required to fully understand the process as this would greatly assist in dissolution of the more resistant fibroins. Results of percentage dissolution are not directly comparable with the report by Teshome *et al.* because of difference in the conditions of the studies. Both studies are however in agreement that LiBr was a very good solvent for *B. mori* and *G. postica* fibroin and less effective for *A. mimosae*, *A. panda* and *E. bahuniea* fibroin. Also, CaCl$_2$ proved to be a poor solvent for dissolution of the African silk fibroins.

6.2.2 Effect of organic ternary mixtures

Some researchers have reported enhanced dissolution of fibroin by adding organic solvents such as methanol and ethanol to salt solvents [329]. The organic component and the salt ions act cooperatively to dissolve the fibroin. As the salt ions break down hydrogen bonds between the β-sheets, the organic component (methanol/ethanol) penetrates the hydrophobic regions of fibroin and makes the molecules hydrophilic thereby enhancing dissolution [330].

Table 6.2.　　　Dissolution of fibroins in ternary solvent systems

	Ca(NO$_3$)$_2$.4H$_2$O /MeOH (3:1)	CaCl$_2$/EtOH/H$_2$O (1:2:8)	LiBr/H$_2$O/EtOH	LiCl/ H$_2$O/EtOH
G. postica	++	×	++	×
G. rufobrunnae	++	×	++	×
A. mimosae	+	×	+	×
A. panda	+	×	+	×
E. bahuniae	+	×	+	×
B. mori	+++	+++	+++	+

*: +++ = Very soluble, ++ = Soluble, += Slightly soluble, × = Insoluble

Under the same experimental conditions used for the aqueous salt solutions, there was a decrease in solubility for both *Gonometa* fibroins from 22 % (w/v) in aqueous salts to $\approx$ 10 % (w/v) in the salt-organic solvent mixtures (Table 6.2). No improvement in dissolution was observed for the fibroins when methanol and ethanol were added to CaCl$_2$ and LiCl salt solutions. Although the lower solubility was not fully understood, it could possibly be explained by the fact that water miscible organic solvents have been found to lower the dielectric constant of salt solutions. When the dielectric constant is reduced, charge-dipole and dipole-dipole interactions are thus promoted resulting in reduced protein solubility [331]. The interaction of ternary organic solvents with fibroin has been described by some researchers. In a study by Perez-Rigueiro *et al.* [332], the authors explained the important role water plays in swelling the amorphous region and disrupting inter- and intra-molecular hydrogen links in the protein. Incorporation of organic solvents such as methanol and ethanol, which are desiccants, to the aqueous salts can increase protein-protein hydrogen bonding reducing the solubilizing power of the solvent mixture [332].

The behaviour of *B. mori* fibroin in the ternary solvents was unlike that of the African silks. *B. mori* fibroin dissolution was enhanced with the addition of the organic solvents with the fibroin dissolving almost immediately when added into the solvent. From these results, we concluded that it is possible that the increased quantity of polar groups (mostly in the amorphous region that dissolves first) *Gonometa* fibroin, may explain the difference in solubility compared to *B. mori*. Because of the large amount of polar amino acids, the enhancement of hydrogen bonding network would reduce the dissolution of the fibroin as we observed in our work. Overall, these results highlight the complexity of the dissolution of fibroin, the process influenced by the structure of the silk and interactions between the protein molecules, water and the salt ions. The extent of the amorphous region appears not to influence dissolution as much as the composition of the crystalline regions when using aqueous salt solutions as we see that *B. mori* and *A. panda* fibroin showed dissimilarity in solubility despite both having a smaller and comparable amorphous region. We can therefore assume that the type of linkages in the crystalline region may have an impact on the solubility shown by the trend in dissolution of the fibroins.

6.3   Electrospinning of RSF

Due to poor dissolution of *A. mimosae*, *A. panda* and *E. bahuniea* in the solvents utilized in this study, it was impractical to carry out electrospinning experiments due to the little amounts of regenerated fibroin obtained. We therefore report results on the electrospinning of only *Gonometa* SF as it dissolved quantitatively in the solvents available in this study.

The process of electrospinning requires optimization of several parameters for defect free nanofibres to be produced. Several authors have highlighted, through systematic investigations, the significance of various electrospinning parameters in fabricating nanofibres [333-335]. Solution concentration, voltage, flow rate and spinning distance were

investigated in electrospinning *Gonometa* SF. Both freeze dried (FD-RSF) and rotavapor dried (RD-RSF) solutions were used in the study.

6.3.1   Selection of electrospinning solvent

Polymers can be soluble in many solvents but each solvent influences electrospinnability depending on its properties. The choice of electrospinning solvent is therefore critical for optimal production of nanofibres. A good solvent allows SF chain extension to form significant chain entanglements that result in a lower concentration for electrospinning [336]. Water, formic acid and trifluoroacetic acid are some of the solvents that have been useful in electrospinning SF [208, 212] and were used in assessing electrospinnability of *Gonometa* SF. Despite the numerous reports of successful electrospinning of SF in water, bead free fibres could not be formed from the *Gonometa* aqueous RSF solutions (Figure 6.1a). Increasing the concentration of RSF resulted in a thick gel being formed which could not flow through the capillary. Highly concentrated solutions of aqueous SF can quickly aggregate via hydrogen bonds to form the water insoluble silk II structure [337]. Figure 6.1b & 6.1c show fibres electrospun from 25 % (w/v) FD-RSF solutions in FA and TFA. Though both solvents produced beaded fibres, TFA solution produced the most promising fibres with fewer beads. The differences noted between the two solvents may be due to different solvent properties combined with the behaviour of fibroin in solution with each solvent. Jeong *et al.* examined the electrospinnability of fibroin in various solvents and concluded that different solvents produce fibres with different morphologies as a result of their solvent properties such as surface tension and conductivity [336]. Zhou *et al.* in their work also reported that TFA was a better solvent than FA for electrospinning cellulose acetate due to its higher conductivity and lower boiling point as highlighted in Table 6.3 [338]. Considering the results obtained, TFA was used as the electrospinning solvent for further experiments.

Table 6.3.   Solution properties of formic acid and trifluoroacetic acid

	Conductivity (S·m^{-1})	Boiling point (°C)	Surface tension (dyn/cm)
Trifluoroacetic acid	2.6 x 10^5	72.4	13.63
Formic acid	6.4 x 10^{-5}	100.8	37.67

6.3.2   Effect of concentration on electrospinning of FD-RSF and RD-RSF

Solution concentration has been reported to be a major determining factor in electrospinning of polymers. A critical polymer concentration, which allows sufficient polymer chain entanglements, has to be exceeded in order for electrospinning of beadless fibres [339]. Below this critical concentration, the polymer solution fragments into droplets before reaching the collector when voltage is applied [18]. The electrospinnability of both freeze dried (FD-RSF) and rotavapor dried (RD-RSF) was evaluated, as well as quality of resultant nanofibres.

Results showed that there was a difference in the electrospinnable concentration of both FD-RSF and RD-RSF powders. No fibres were formed when low concentrations of RSF (15 % w/v and below) were electrospun. It is probable that SF chain entanglements were insufficient to prevent the breakup of the electrically driven jet into droplets. Using FD-RSF, increasing solution concentration to 30 % (w/v) resulted in the formation of nanofibres with a mixture of beaded and smooth fibres (Figure 6.2b). Although not quantitatively measured, there was a visible increase in the viscosity of the RSF solutions with increase in concentration. Smooth fibres (without beads) were produced at 40 % (w/v) (Figure 6.2c). The diameters of electrospun fibres collected for both *Gonometa* species at 40 % (w/v) were between 400-1000 nm. At higher concentrations, the solution was too thick to flow through the needle; therefore electrospinning was not possible.

Figure 6.3 shows the morphology of fibres that were electrospun from RD-RSF powders at 27-35 % (w/v) RSF concentrations. The minimum electrospinning concentration at which smooth fibres could be formed from RD-RSF powders was 27 % (w/v). Nanofibres with diameters ranging from 300 to 760 nm were obtained at this concentration. As the concentration was increased, the nanofibre diameters increased with diameters of 540-1200 nm produced at 30 % w/v and 1-2.5 µm at 35 % w/v. This clearly shows that nanofibre diameter is directly related to the polymer solution concentration; the higher the concentration of polymer solution, the larger the nanofibre diameters. The differences in the spinnable concentrations of FD-RSF and RD-RSF could be attributed to conformational changes in the RD-RSF during drying with methanol. Though freezing procedures such as freeze drying have been found to induce a certain degree of crystallinity in RSF, addition of organic solvents does so to a greater extent [340]. While methanol was primarily used to ensure complete removal of water during drying of the RSF, it also probably affected the secondary structure of the RSF as it is one of the solvents commonly used in crystallizing water soluble silk [305]. There were no definitive differences in the electrospinnability, morphology or diameter of the nanofibres from *Gonometa postica* and *Gonometa rufobrunnae* species.

6.3.3   Effect of applied voltage

Figure 6.4 shows SEM images of nanofibres spun at different voltages with other parameter fixed. At an applied voltage below 10 kV, only droplets collected on the aluminium foil collector possibly because the electrostatic force could not overcome the surface tension of the solution. Stable jets and fibres were formed when the applied voltage was greater than 10 kV. However applied voltages above 15 kV resulted in split jets and the fibres formed also showed some defects that included beading.
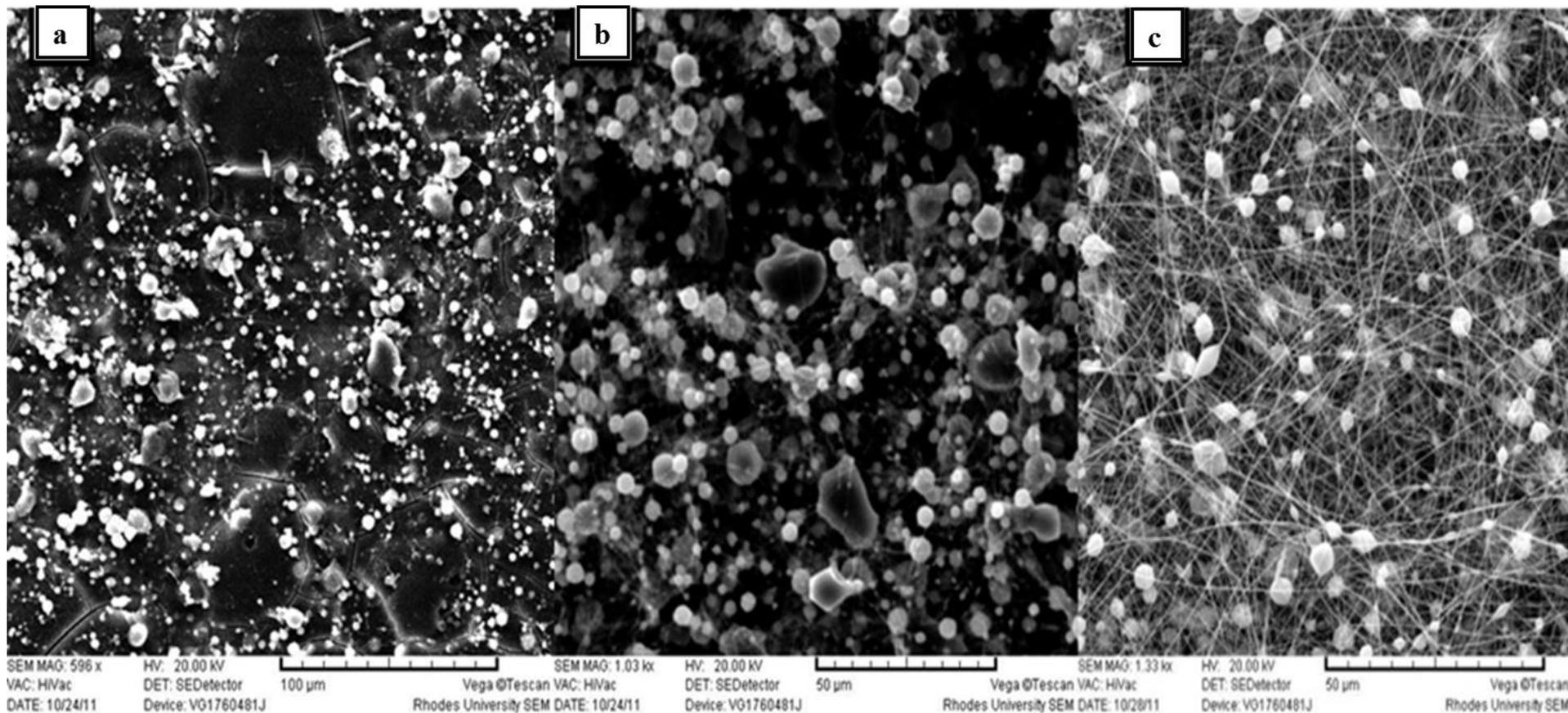
Figure 6.1. SEM images of electrospun fibres using FD-RSF a) 40% in water, b) 25% in FA and c) 25% in TFA
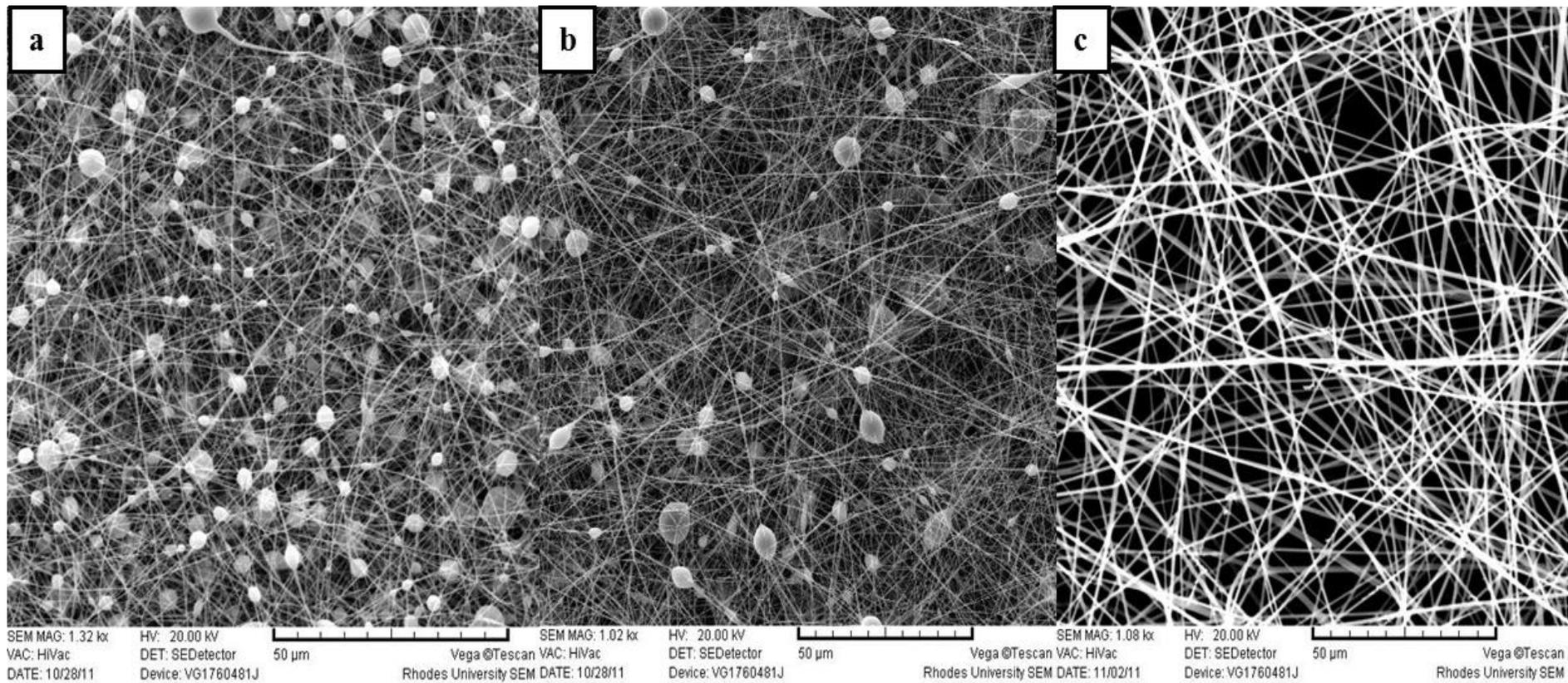
Figure 6.2.   SEM images of electrospun fibres at a) 20%, b) 30% and c) 40% FD-RSF in TFA
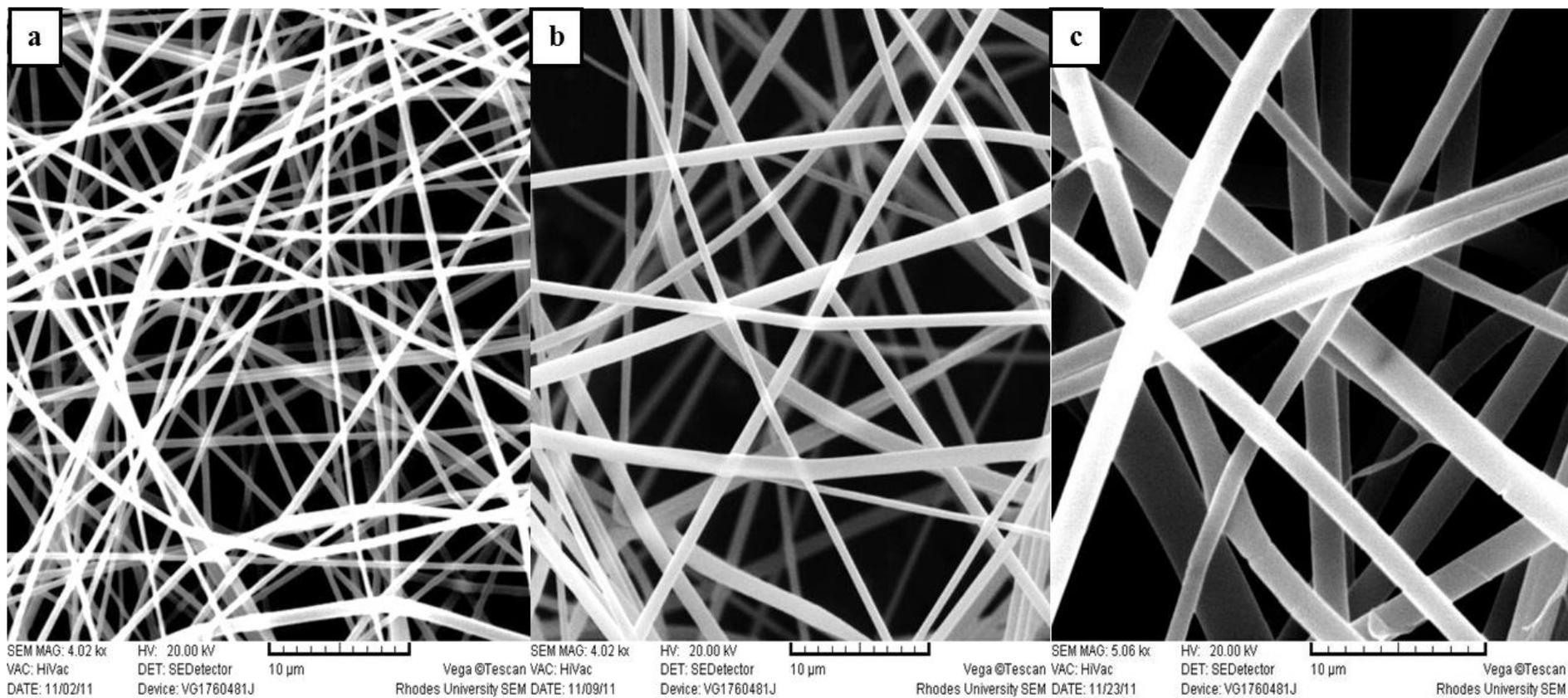
Figure 6.3. SEM images of electrospun fibres at a) 27%, b) 30% and c) 35% RD-RSF in TFA

6.3.4 Effect of tip to collector distance

When the nanofibre jet has a short distance to travel to the collector, there is little time for the solvent to evaporate, which promotes formation of flat shaped fibres. The distance also influences the electric field strength which determines whether electrospinning or electrospraying occurs [341]. When tip to collector distance was set at 7 cm, the nanofibres appeared wet and were beaded probably due to insufficient time for the complete evaporation of the solvent and elongation of the nanofibres (Figure 6.5a). As the distance was increased to 10 cm, there was no adhesion of the fibres or beading indicating that there was sufficient time for solvent to evaporate (Figure 6.5b). At a distance of 13 cm, the nanofibres collected had a smaller fibre diameter than those at 10 cm but were frayed and at times not continuous (Figure 6.5c). The longer distance afforded more time for elongation of the nanofibres hence the finer diameters observed. This was however accompanied by defects on the nanofibres indicating that the distance was too long.

6.3.5 Effect of polymer flow rate

It is critical that the solution fed to the needle tip balance with that which is drawn from the tip for formation of continuous nanofibres [342]. This maintains the Taylor cone at the capillary tip and prevents beading of the nanofibres. Flow rates of 0.05-0.08 mL/h allowed for a stable cone to be formed at the needle tip and continuous fibres were formed. Higher flow rates (above 0.1 mL/h) resulted in nanofibres with slightly larger fibre diameters. Above 0.3 mL/h, beaded fibres were produced as the RSF solution collected at the needle tip, probably due to delivery rate of solution to the capillary tip exceeding the rate at which the solution was removed from the tip by electric forces. It was also noted that the flow rate of the RSF solution depended on the concentration of the RSF solution.
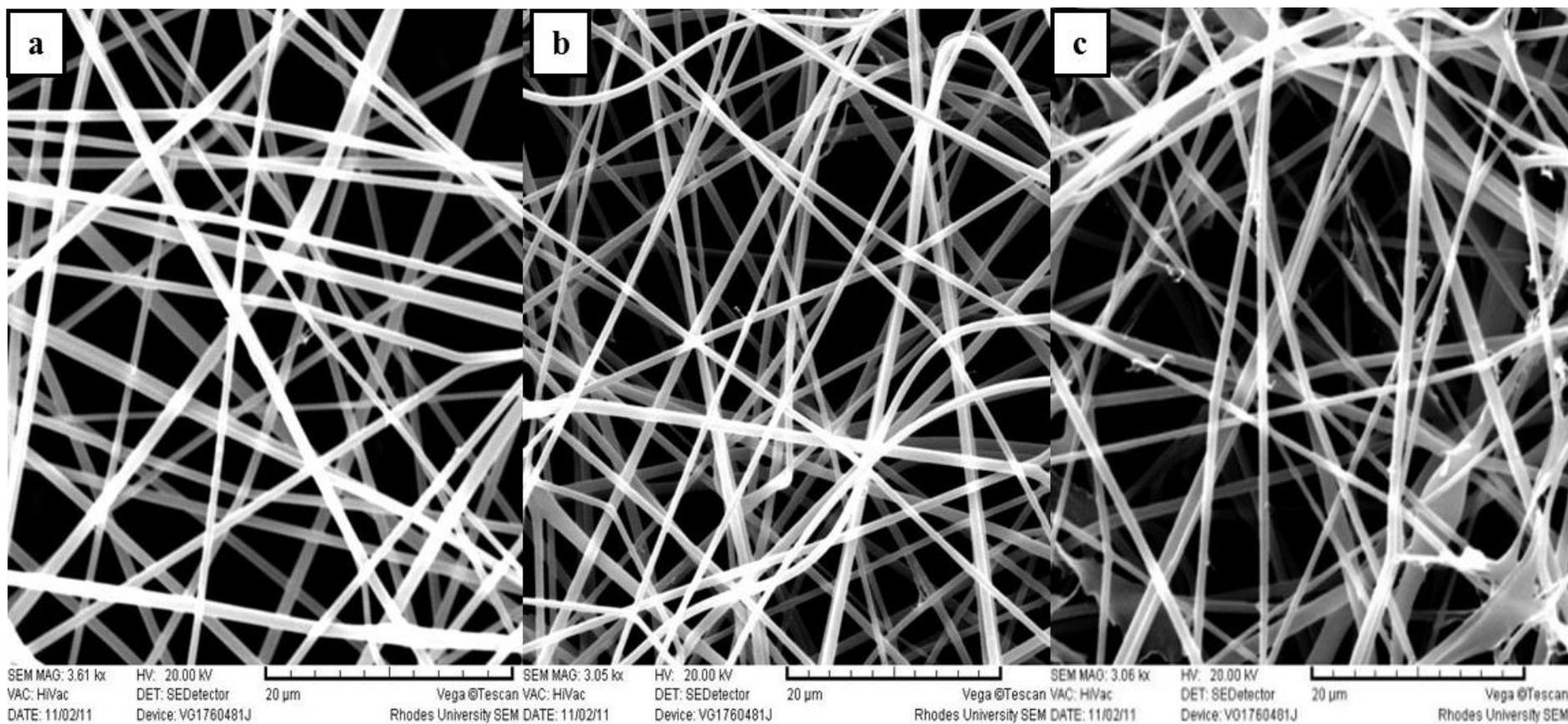
Figure 6.4.   Electrospun nanofibres from 40% (w/v) solution of fibroin in TFA, flow 0.05 mL/h, distance 10 cm at (a) 10 kV, (b) 15 kV, and (c) 20 kV
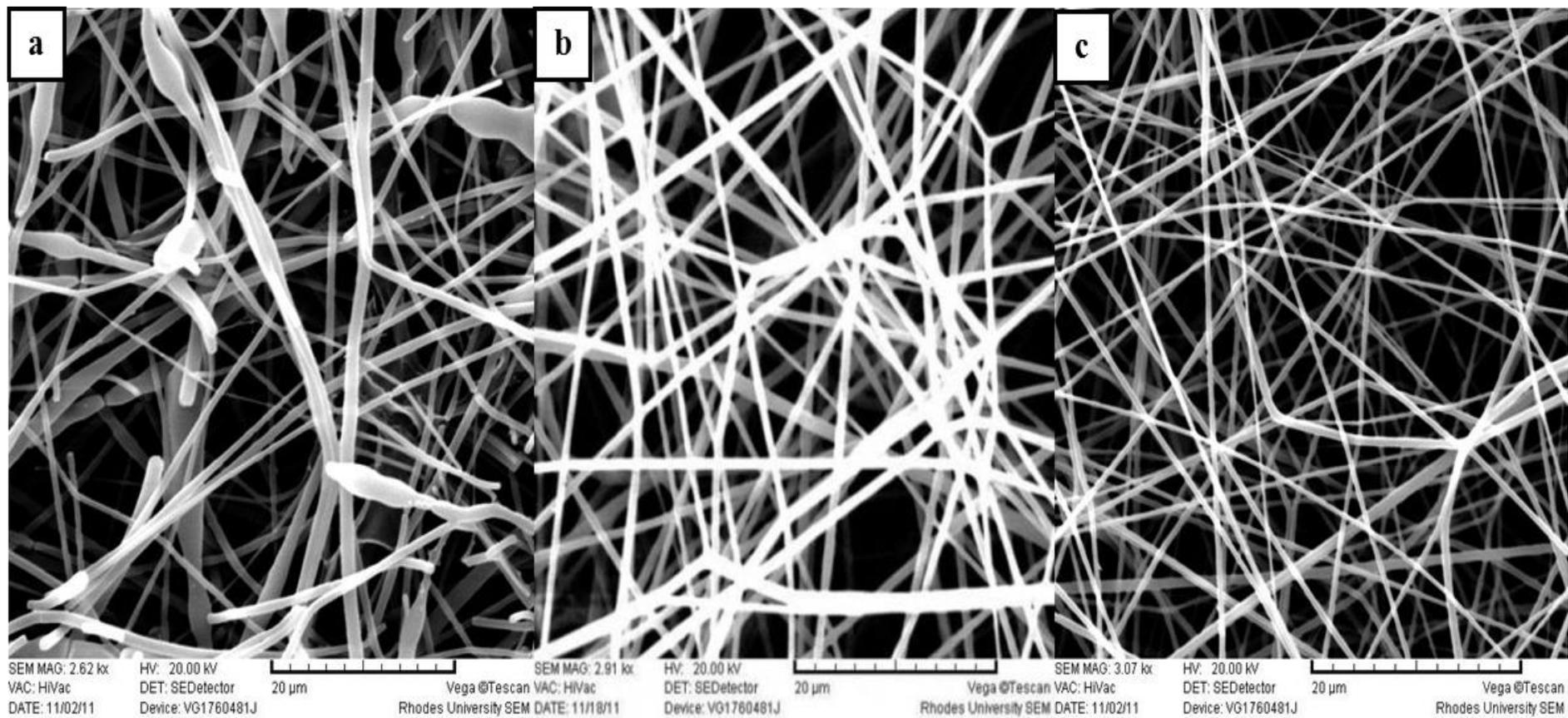
Figure 6.5. Electrospun nanofibres from 40% solution of fibroin in TFA, flow 0.05 mL/h, distance at 15 kV at (a) 7 cm, (b) 10 cm, and (c) 13 cm

A lot of adhesion and beading of nanofibres was observed when high flow rates and low concentration RSF solutions were used. However, with high concentrations of RSF solutions, higher flow rates could be realized without having a significant effect on the morphology and diameter of the nanofibres. The optimum conditions for electrospinning *Gonometa* RSF were found to be 0.05 mL/h flow rate, 10 cm tip to collector distance and an applied voltage of 15 kV. Figure 6.6 shows the pictures of the SF nanofibre mats collected for further analysis.
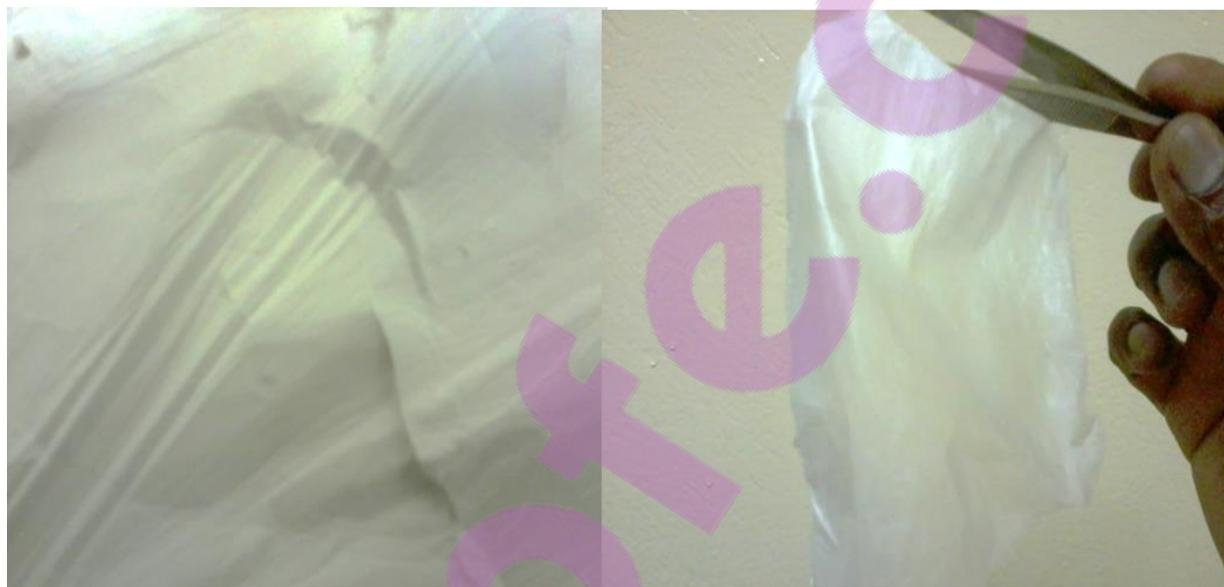
Figure 6.6.   Photographs of *Gonometa* SF electrospun nanofibres

6.4   FTIR spectroscopy

FTIR analysis was used to examine any structural transformation of SF during the various processing stages to produce the nanofibres. Using this technique, some band overlaps have been noted for the random coil and α-helix structure in the amide I and amide II region [343, 344]. Peaks that were observed in these regions were described as either of the structures.

The main secondary conformation in degummed silk is β-sheet as evidenced by peaks at 970 cm^{-1}, 1522 cm^{-1} and 1628 cm^{-1} (Figure 6.7). The presence of random coil/α-helix structure

was confirmed by the peak at 1240 cm^{-1}. On examination of spectra for FD-RSF and RD-RSF, similar peaks to those seen for the degummed silk fibre were observed. This suggests that the main silk structure was essentially preserved after processing into the RSF powders. However, the peak broadness seen around 1650 cm^{-1} for both powders, indicative of random coil/α-helix structure, points to the possibility of a change in fibroin structure during processing. Despite the differences in their electrospinnable concentrations, there were no remarkable differences in conformational peaks observed in the spectra for RD-RSF and FD-RSF.
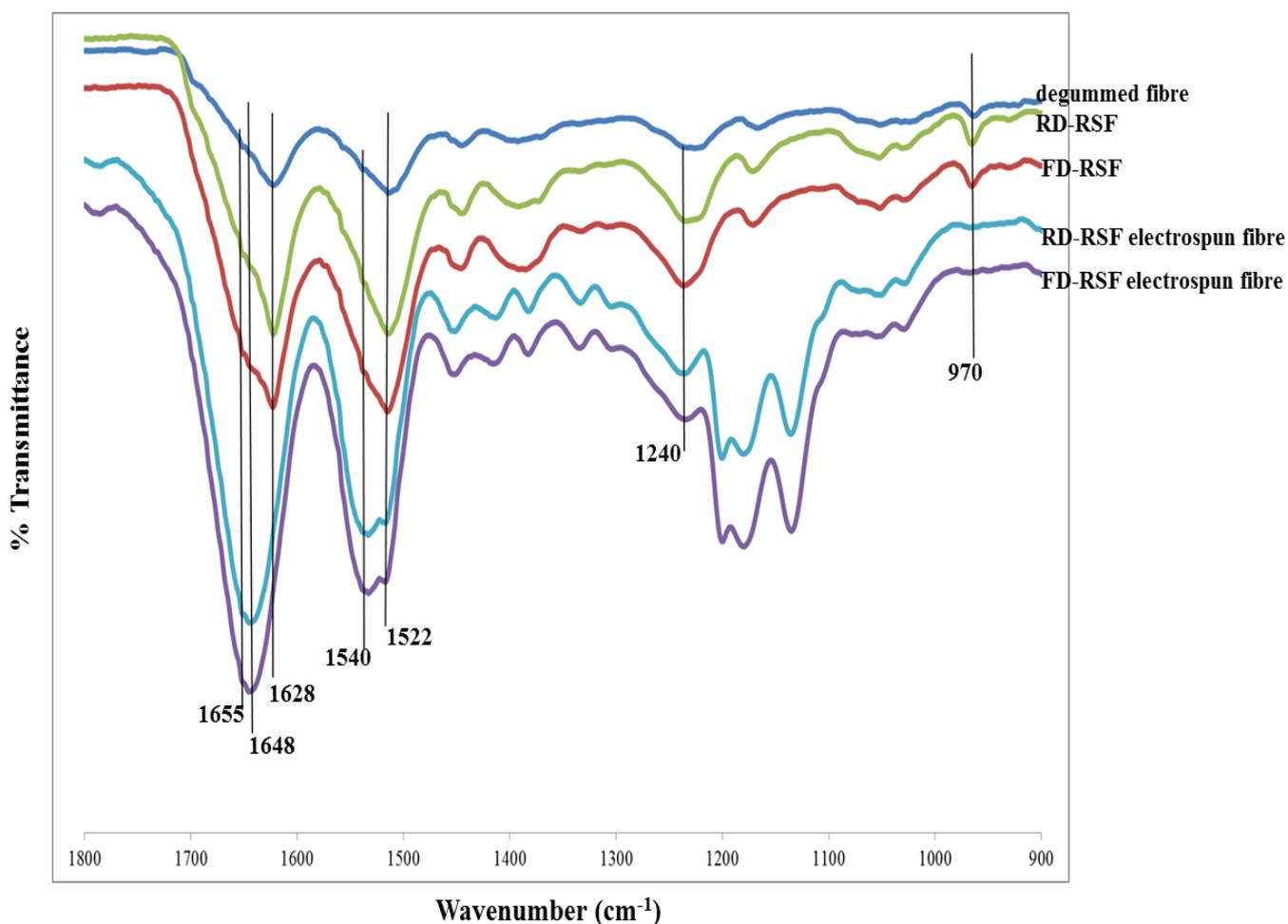
Figure 6.7.   FTIR spectra for the various silk fibroin formats

It was however concluded from XRD analysis that RD-RSF has a more abundant crystalline structure than FD-RSF powders (Figure 6.8) as seen by the reduction in the intensity of the observed peaks. This suggests increased disorder in the FD-RSF than RD-RSF. The crystallinity could however not be quantified due to the absence of a suitable standard for the analysis. SF nanofibres showed a major change in conformation when compared to the degummed silk and RSF powders (Figure 6.7).
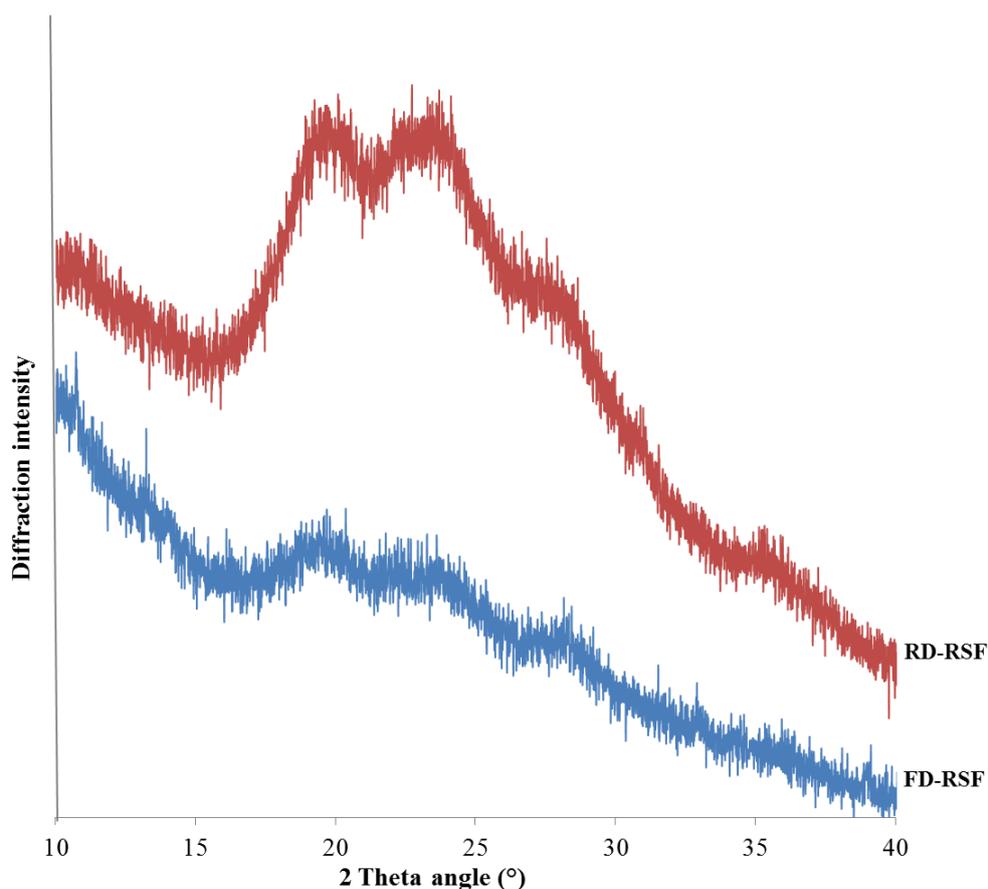
Figure 6.8.   X-ray diffractograms for RD-RSF and FD-RSF

Peaks at 970 cm^{-1} and 1628 cm^{-1} relating to β-sheet crystallinity were absent in the spectra for the electrospun fibres. The nanofibres exhibited strong peaks at 1648 cm^{-1}, 1540 cm^{-1} and 1240 cm^{-1} indicating that their secondary structure was mainly random coil/α-helical. The presence of a shoulder peak at 1522 cm^{-1} implies that there is some β-sheet crystallinity

110

present in the electrospun fibres. Overall, these results suggest that processes involved in the preparation of RSF powders and electrospinning result in secondary structure changes of silk fibroin. These changes, however, appear to be more prominent during the electrospinning process as seen by the significant degradation of the silk β-sheet structure and increase of random coil/α-helical structure in the nanofibres.

6.5   Post treatment of RSF nanofibres

The nanofibres electrospun from FD-RSF dissolved instantly in aqueous or aqueous-organic mixtures, whilst those from RD-RSF maintained their integrity for just over 72 h. Water solubility of SF nanofibres is indicative of structural degradation which results in poor mechanical strength. This hampers the use of SF nanofibres in applications where mechanical and structural integrity is a requirement such as in vascular grafts or as support for cells and tissues. There is therefore often a need for post treatment of the nanofibres to restore their structural integrity. Immersion and vapour treatments using polar organic solvents are the most frequently used techniques to induce β-sheet crystallinity in SF matrices [305, 213]. These solvents act by penetrating the amorphous region generating a hydrophobic environment which causes aggregation of the hydrophobic chains. Rearrangement within the hydrogen bonding network then results in the formation of the water stable silk II structure [345, 346].

Methanol, ethanol, propanol, acetone and chloroform were investigated as solvents to induce this transition. In this study, nanofibre mats were immersed for 15 minutes in each solvent to ensure maximum crystallization though some reports have revealed that as little as three minutes is sufficient to make silk matrices insoluble in water [238]. Water vapour treatment, which has been described as an effective yet a mild alternative to induce water insolubility in SF [213], was also used. FTIR spectroscopy was used to confirm secondary structure

transition in the nanofibres after post-treatment with the various solvents. Generally, the solvent treatment resulted in an increase in β-sheet content with a simultaneous reduction of silk I structures evidenced by shifting of conformational peaks in the various amide band regions (Figure 6.9). The peak in the amide I region shifted from 1648 cm^{-1} for untreated nanofibres to 1628 cm^{-1} in the spectra for the nanofibres treated with methanol, isopropanol, ethanol and water vapour.
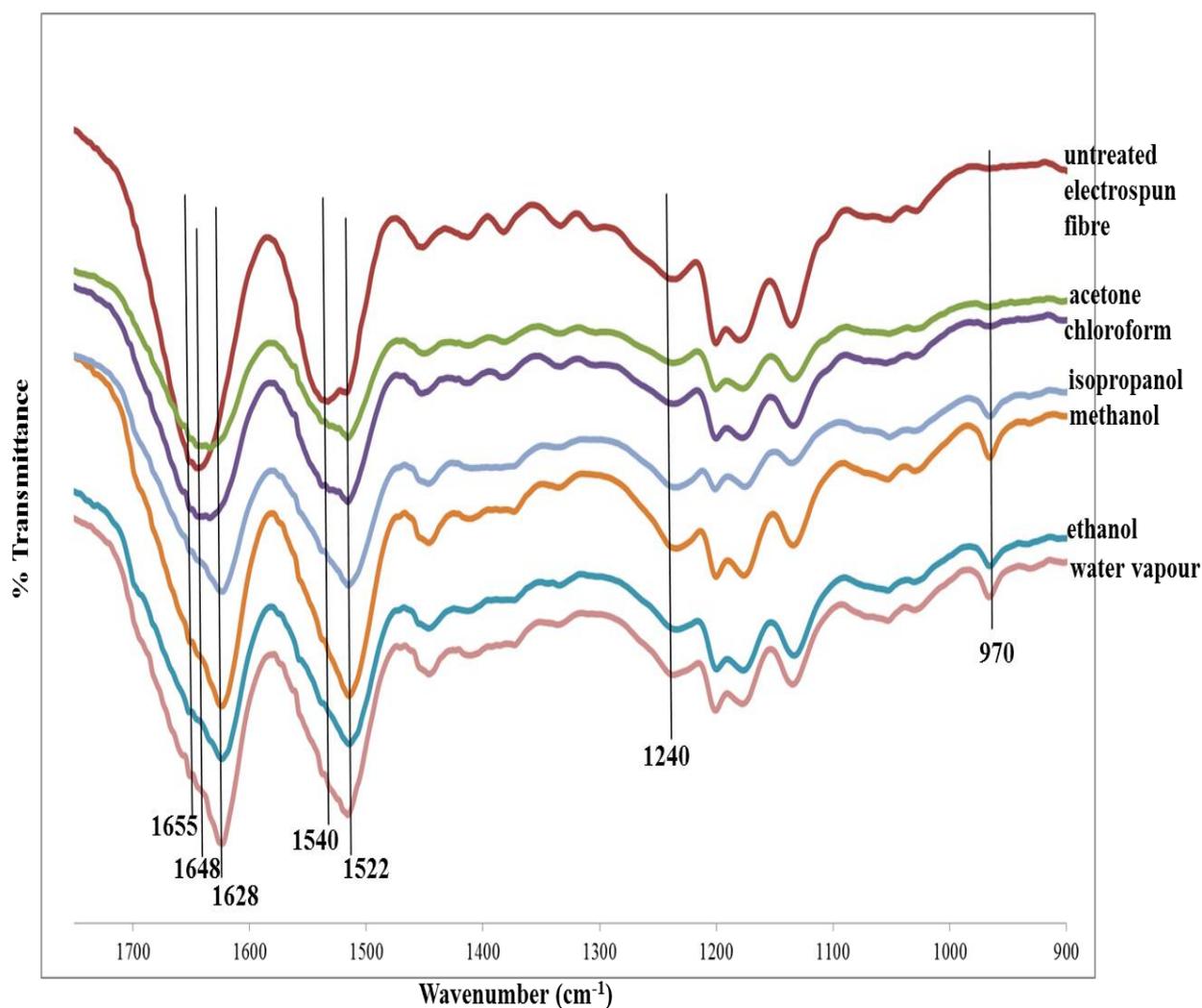
Figure 6.9.   FTIR spectra of untreated and solvent treated SF nanofibres

In the amide III region, the peak at 1540 cm^{-1} disappeared and only the one at 1522 cm^{-1} was observed, also showing the successful transition from random coil and/or α-helix to β-sheet conformation. Reappearance of the peak at 970 cm^{-1}, which is also seen in the spectra for the degummed silk fibre, also indicates the increase in β-sheet content.

The spectra for chloroform and acetone treated nanofibres were slightly different from those observed for the nanofibres treated with the other solvents. They showed broad peak between 1636 cm^{-1} and 1655 cm^{-1} indicative of a significant presence of random coil conformation /α-helix conformation. Structural transition to β-sheet structure was evident in that the peak at 1540 cm^{-1} was less intense whilst the peak at 1522 cm^{-1} is more intense when compared to spectra for the untreated nanofibres. The peak at 970 cm^{-1} was also seen in the spectra for chloroform and acetone treated nanofibres, though it was weaker than that seen in the spectra for nanofibres treated with the alcohols and water vapour. This implies that the transition using chloroform and acetone is small with some molecular regions remaining in α-helix and random coil conformation.

It is thus clear that under the conditions used in this work, acetone and chloroform can facilitate secondary structure transition to β-sheet crystallinity to a different extent than the alcohols and water vapour. This highlights that crystallinity of SF nanofibres can be tailored to suit various applications by utilizing different annealing solvents. It is important to note that the structural changes in SF caused by the electrospinning process did not result in complete degradation of its structure as it could still rearrange into a similar structure to that seen in the degummed fibre upon solvent treatment.

In addition to structural change, post treatment also serves as a method of removing excess electrospinning reagents. TFA is highly toxic to cells and any residue in the nanofibres could

result in cell death making the nanofibres unsuitable for tissue engineering applications. Chen *et. al* reported that TFA in SF-chitosan nanofibres forms salts with protonated amino groups and exhibit three FTIR peaks in the region from 720 to 840 cm^{-1}[218]. In their work, these peaks disappeared after treatment of the nanofibres with ammonia/ethanol solution, which indicated the complete removal of the TFA. The TFA salt peaks were not evident in our results thus suggesting the absence of any TFA in the nanofibres produced. However, there were new peaks seen in the spectral region between 1100 and 1210 cm^{-1}after electrospinning where characteristic peaks of TFA are also found. If these peaks were indicative of TFA it would imply a significant amount of 'free' TFA would be present in the nanofibres. This is unlikely though as it would significantly impact the cytotoxicity results for the nanofibres considering the toxicity of TFA to cells. This toxicity was not observed for the cytotoxicity tests (Section 6.11) and it is therefore highly unlikely that these new peaks are attributable to excess TFA. Further research is therefore needed to identify the source and identity of the new peaks.

6.6   Morphology of the treated nanofibres

To further characterize the treated nanofibres, SEM imaging was used to view the effect of the different solvents on the fibre morphology. Generally, the solvents caused an alteration of fibre shape and a reduction of inter-fibre pores (Figure 6.10) when compared to the untreated electrospun fibres (Figure 6.3). Nanofibres treated with methanol were heavily fused and very brittle as evidenced by 'cracks' in the nanofibre mats (Figure 6.10d). This has been previously observed by other researchers and is attributed to a high crystalline content in methanol treated nanofibres [213]. Brittleness usually results in poor mechanical properties. Similar observations, in terms of reduction in the inter-fibre pores and brittleness, were seen with propanol and acetone treated nanofibres (Figure 6.10 a & c). Less brittle fibres were

observed with ethanol treatment compared to the other alcohols and also showed less reduction in the inter fibre pores (Figure 6.10 e). Chloroform treated nanofibres were almost completely degraded with individual fibres not evident in the SEM images (Figure 6.10b). FD-RSF and RD-RSF nanofibres did not show any major differences after treatment with all the solvents except with water vapour. The nanofibres prepared from FD-RSF were swollen and fused together, showing degradation of individual fibres (Figure 6.10f). In contrast, nanofibres from RD-RSF mostly maintained the circular shape of the untreated nanofibres and a smaller reduction of inter fibre pores (Figure 6.10g), most similar to ethanol treated fibres. Porosity is an important property for a tissue supporting scaffold, providing passage of nutrients to the growing cells and room for cell migration and proliferation.

From the results, we can conclude that water vapour and ethanol are better solvents in maintaining the morphology and inter-fibre porosity of SF nanofibre mats.
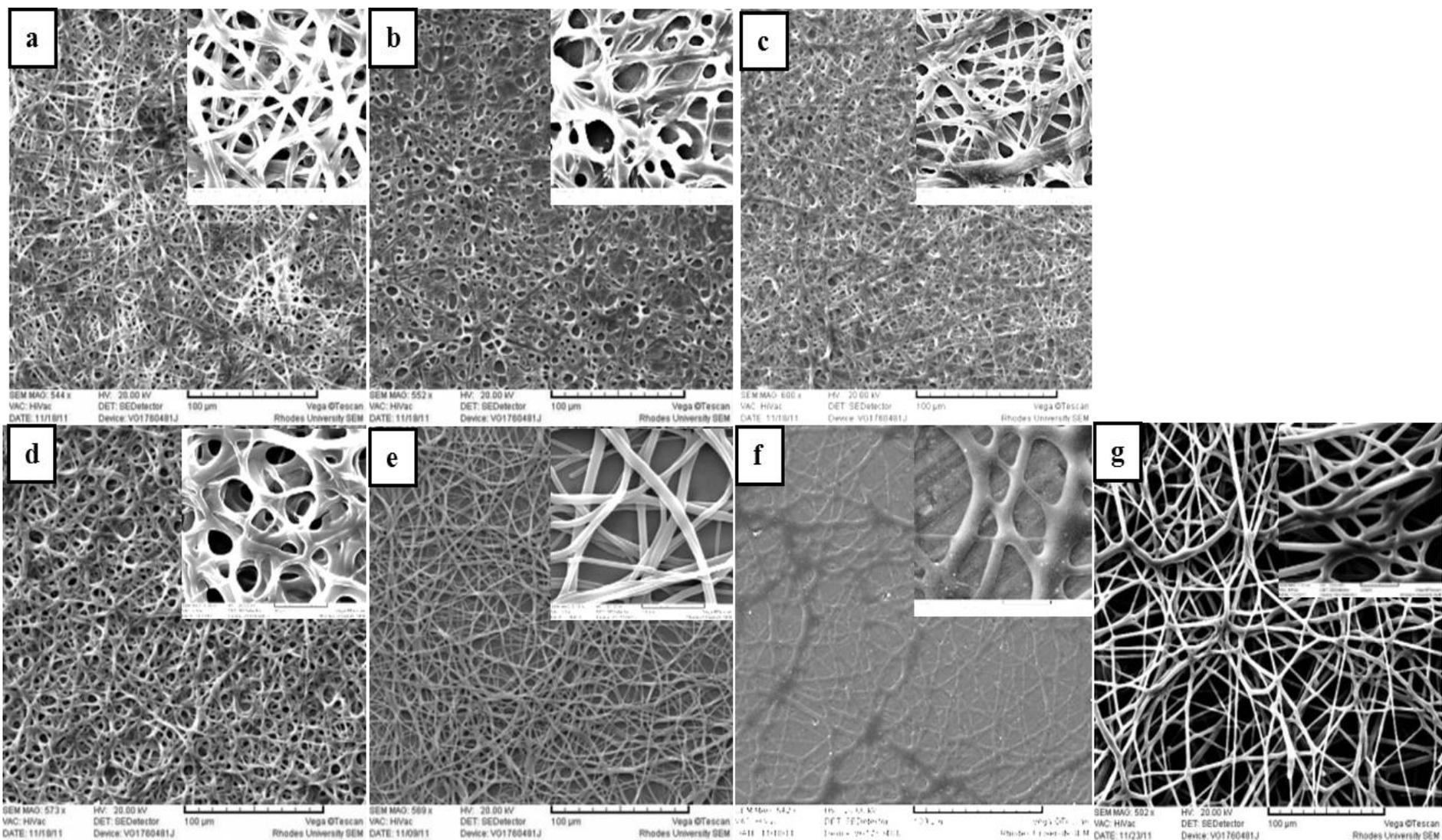
Figure 6.10. SEM micrographs of SF nanofibres treated with a) acetone, b) chloroform, c) isopropanol, d) methanol, e) ethanol, f), water vapour (FD-RSF), and g) water vapour (RD-RSF)

6.7   Water solubility of SF nanofibres pre- and post- solvent treatment

After solvent treatment, there was a visible improvement in the water stability of the nanofibres as they did not dissolve immediately after immersion in water and PBS solution. However, the differences in the structural transformation, as reflected in the FTIR studies, resulted in variations in water solubility of the nanofibre mats treated by the different solvents. Chloroform and acetone treated nanofibres completely dissolved within 12 h when immersed in PBS solution. The nanofibres treated with the other solvents showed better water resistance as they were virtually insoluble in water with less than 10 % weight loss after immersion for 7 days. It can be concluded that the higher content of β-sheets hinders penetration and interaction of water with the silk structure hence the increased stability.

6.8   Thermal properties of silk nanofibres

Structural modifications induced by solvent treatment usually affect physical properties such as thermal behaviour of silk nanofibres. TGA and DSC analyses were used to investigate the thermal behaviour of the treated and untreated nanofibres. Chloroform treated nanofibres were excluded from further analyses because of the complete degradation of the nanofibre structure. Using TGA, the nanofibre samples showed a similar decomposition trend with around 10 % weight loss up to 200 °C (Figure 6.11). The weight loss continued steadily with increasing temperature and the nanofibres had lost at least 60 % weight at 400 °C. Figure 6.12 shows the DTG curves which represent specific thermal decompositions accompanying weight losses of the SF nanofibres.
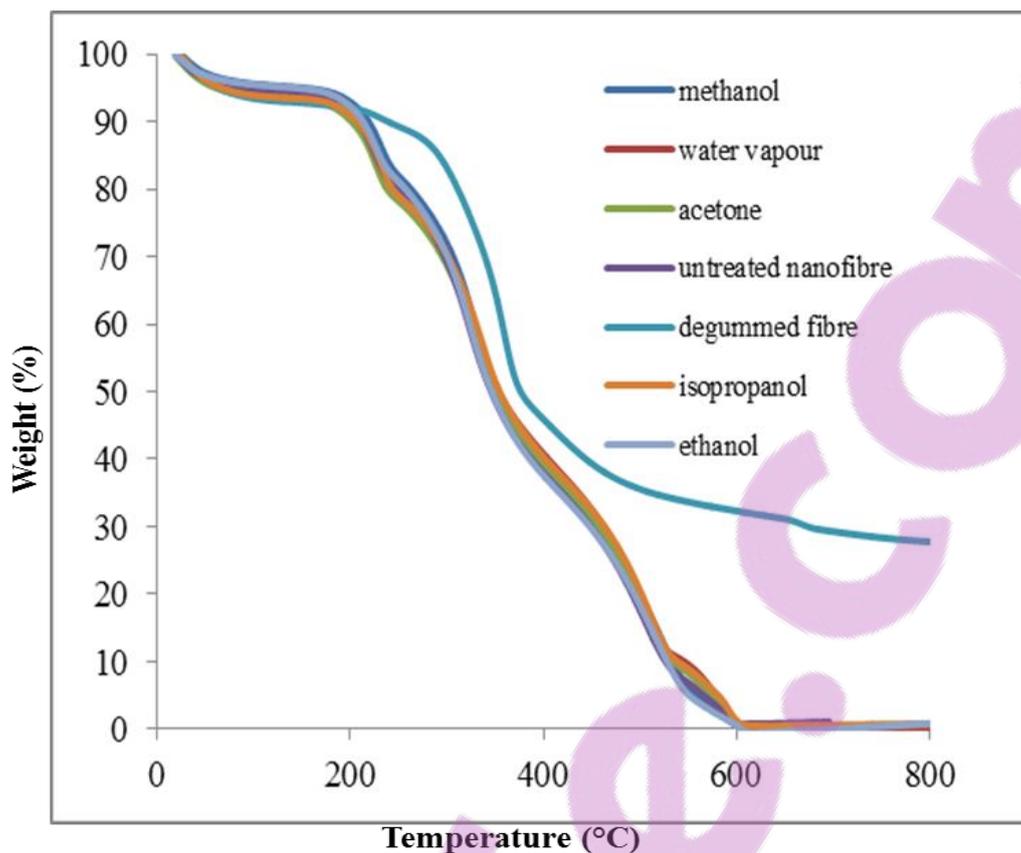
Figure 6.11. TGA curves of the untreated and solvent treated SF nanofibres

The first significant observed weight loss was around 220 to 227 °C which is attributed to breakdown of side chain groups of amino acid residues and as well as the cleavage of peptide bonds [313]. This occurs at a slightly higher temperature of 230 °C for the degummed silk fibre. The major weight loss associated with the degradation of the crystalline structure of the fibroin was observed between 320 and 340 °C for the nanofibres.

The untreated and acetone treated nanofibres showed the fastest degradation (321 °C & 322 °C respectively), which is an indication of lower thermal stability than the nanofibres treated with the other solvents. The solvents that showed the most transition to β-sheet structure (water vapour, isopropanol, ethanol and methanol) showed higher degradation at 332, 333, 335 and 337 °C respectively. This supports the theory that the higher the crystallinity, the

higher the degradation temperature. The maximum degradation of the degummed silk fibre is almost 30 °C higher, suggesting higher crystallinity in the native fibroin than any of the solvent treated nanofibres.
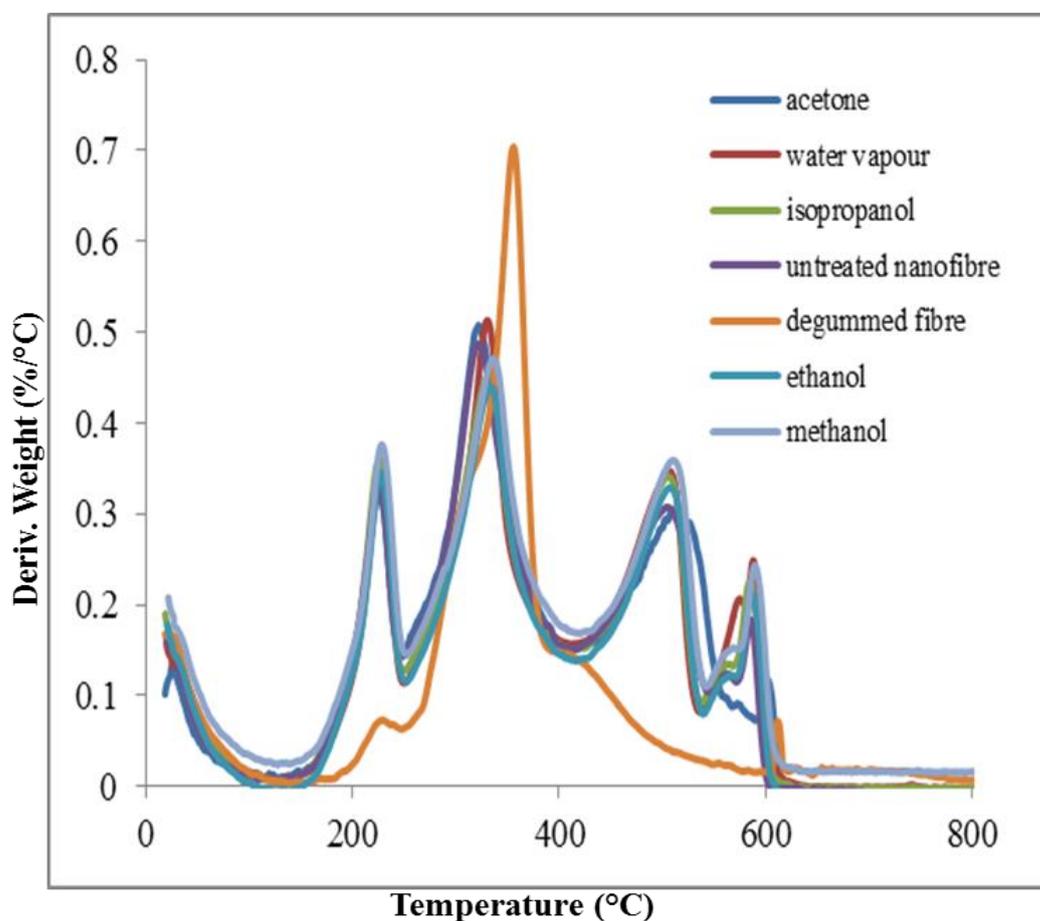
Figure 6.12.   DTG curves for untreated and solvent treated SF nanofibres

Using DSC, more data could be obtained about the effect of the different treatments on the structure of the nanofibres. The initial weight loss observed for all samples at ≈ 80 °C is due to loss of moisture. The weak endothermic shift around 168 °C indicates the glass transition (Tg) of silk [347]. However, the Tg peak was not very evident in the graphs of the nanofibres treated with the other solvents indicating the presence of more β-sheets. Though there may be differences in peak temperatures, reports from various researchers indicate that endotherms seen around 242 °C are attributed to molecular motion within the α-helix region and

crystallization of the random coil structure [305, 345, 348]. This was however observed at a lower temperature (228 ºC) for the degummed fibre. Weaker crystallization endotherms were observed for the alcohol and water vapour treated nanofibres as compared to the untreated and acetone treated nanofibres. The varied intensity of the peaks observed is probably due to the differences in the crystallinity imposed by the different solvents.
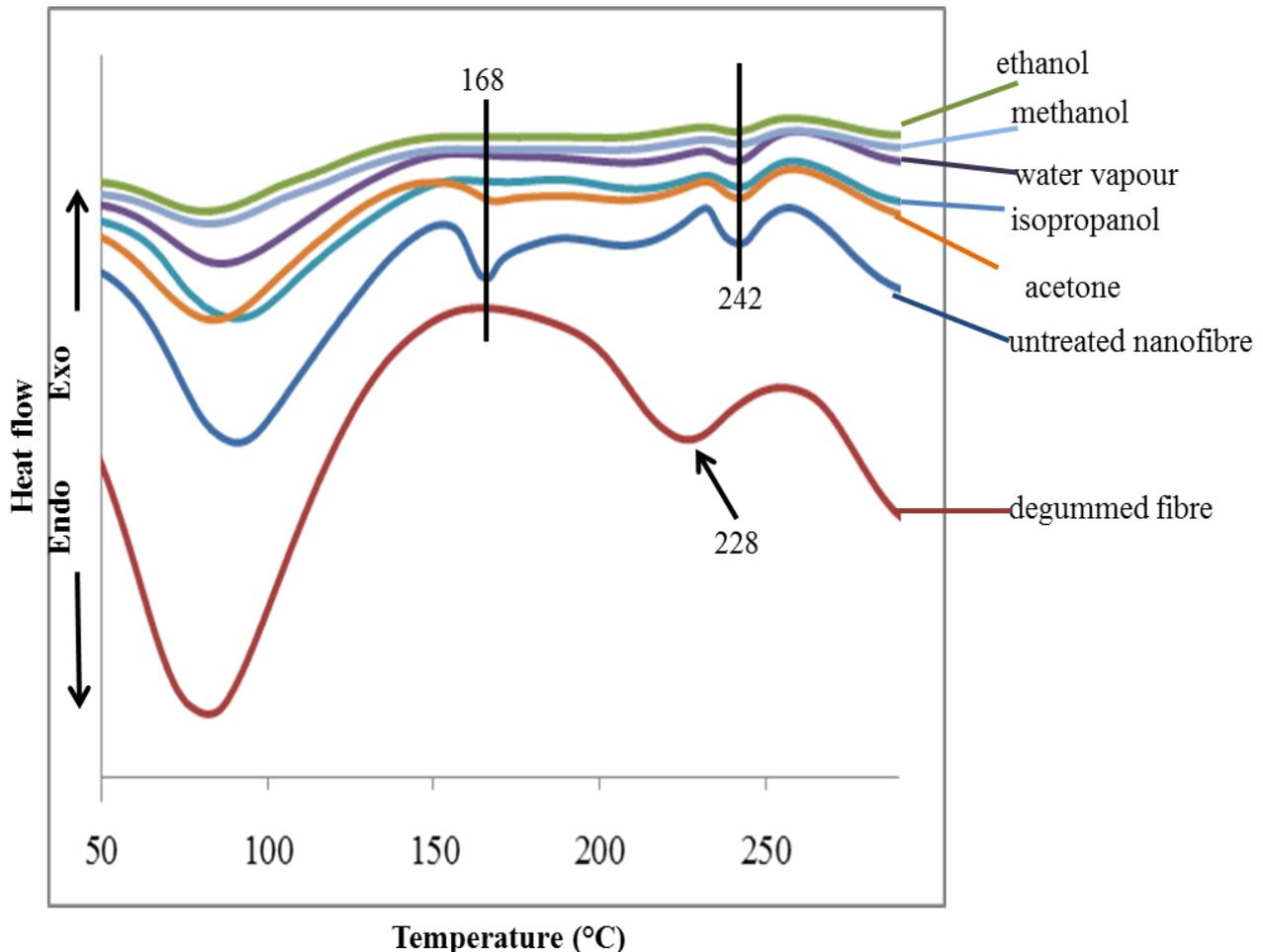
Figure 6.13.   DSC analysis of treated and untreated SF nanofibres

The more extensive transformation to β-sheets by these solvents restricts thermally induced motion of SF polypeptide chains [349] thus weak thermal transitions were observed in this temperature range. This clearly shows reduced α-helix and random coil content in these nanofibres. Overall, the DSC results show that the untreated and acetone treated nanofibres

mats were less thermally stable than the solvent treated nanofibres due to differences in crystallinity. The results are in agreement with data obtained using TGA as well as FTIR.

6.9   Loading of resveratrol onto *Gonometa* SF nanofibres

Considering the interesting chemical composition of *Gonometa* SF, we carried out a short study to assess its potential as a carrier for the bioactive phenolic compound resveratrol for wound care application. Resveratrol is mainly hydrophobic but the presence of the hydroxyl groups introduces the possibility of polar interactions, particularly considering the significant amount of polar groups in *Gonometa* fibroin. It is this dual hydrophobic and hydrophilic nature we sought to exploit in our attempt to evaluate the potential of *Gonometa* SF nanofibres as a carrier for the compound. Ethanol was used as a solvent as resveratrol is highly soluble in it and it is also a good solvent for inducing crystallization of silk fibroin matrices. In essence, in one reaction we attempted to simultaneously crystallize SF nanofibres whilst incorporating and stabilizing the resveratrol into the nanofibre matrix. The primary purpose of this study therefore was to examine the ability of *Gonometa* SF nanofibres to adsorb and stabilize resveratrol in one single easy step.

Drug loading was determined indirectly by measuring the resveratrol remaining in solution after the adsorption experiments. Mass of the nanofibres instead of size was used in the experiments in an attempt to mitigate variances due to non-uniformity and porosity differences from sample to sample. All reactions were conducted in the dark with minimum exposure to light as it has been reported that resveratrol in solution can be unstable when exposed to elements such as light [350]. CE was used to determine the change in resveratrol concentration for the tests. Figure 6.14 shows the run time for the analysis was less than 5 min with the resveratrol clearly resolved from the solvent peak.
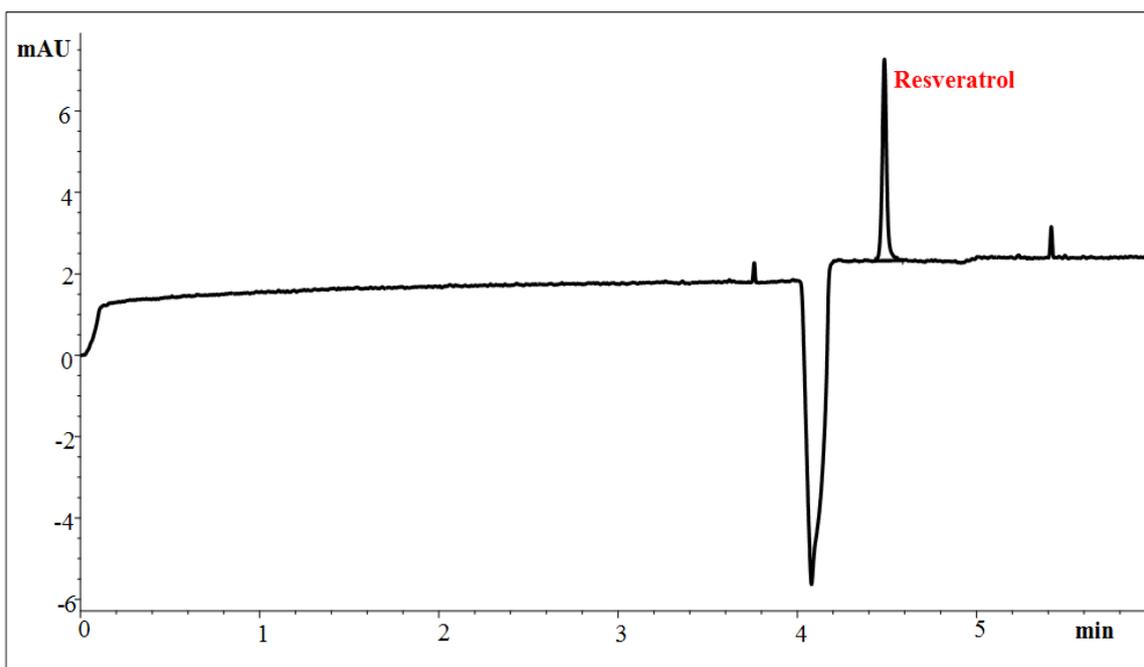
Figure 6.14. CE analysis of 20 ppm concentration resveratrol using 30 mM phosphate buffer at pH 8.0. Conditions: Capillary, 30 cm effective length (total 37.5 cm) x 50 μm i.d; voltage +26 kV, temperature 27 °C; UV-Vis detection at 285 nm

6.9.1 Effect of contact time on loading of resveratrol

We examined the influence of immersion time on the adsorption of resveratrol onto the nanofibres. A control containing just the resveratrol solution was analyzed parallel to the loading experiments to ensure stability of resveratrol under the experimental conditions in the study. Results for the control showed that the resveratrol content did not change significantly (at 5% confidence interval) and was sufficiently stable during the analysis. Aliquots were drawn at several intervals between 0 to 2 h. The loading occurred rapidly during the first 10 min of contact as observed in Figure 6.15. There was no further significant adsorption observed after 20 min. It was thus assumed that 20 min was the equilibrium point and no significant amount of resveratrol could be adsorbed after that time. There were no significant differences seen for adsorption time when different concentrations of resveratrol solutions were used.

122
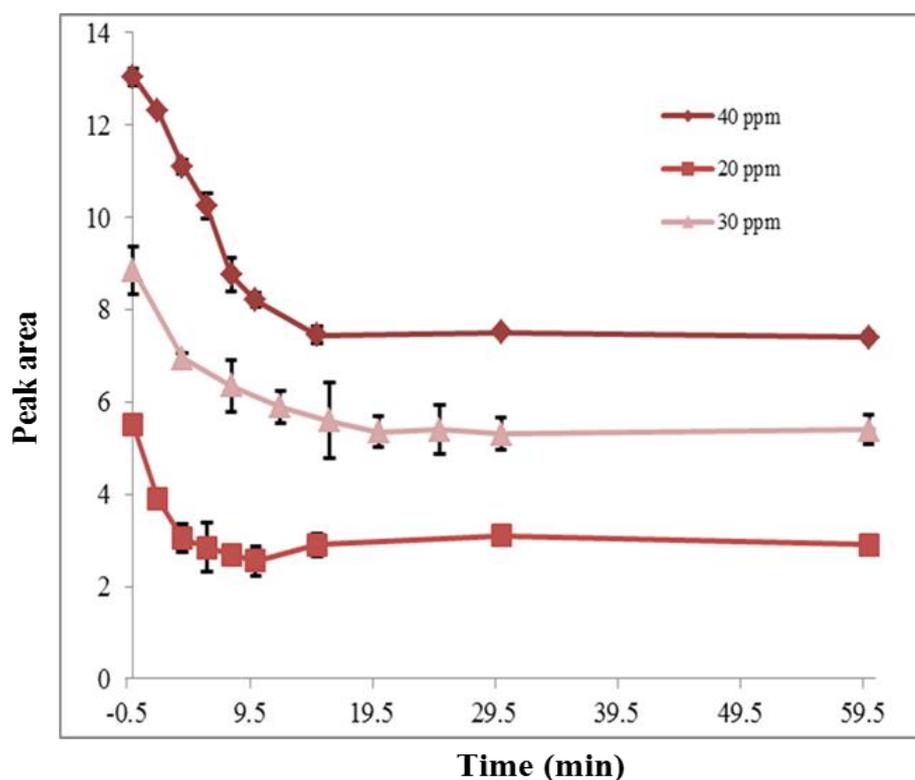
Figure 6.15. Effect of contact time on adsorption of resveratrol on SF nanofibres using 20 ppm, 30 ppm and 4 0ppm resveratrol solutions

CE electrophoregrams also revealed the reduction in peak area at different time intervals during the loading (Figure 6.17) which indicated adsorption of resveratrol onto the nanofibres had occurred. Our observations are similar to those reported by Baycin *et al*. where adsorption of phenolics from olive leaf was rapid in the first 5 min and the adsorption reached equilibrium around 40 min, though silk fibres instead of nanofibres were used in their work [351]. In the same work, the authors also concluded that the adsorption of the phenolics onto the surface of SF occurred via hydrophobic interactions [351].
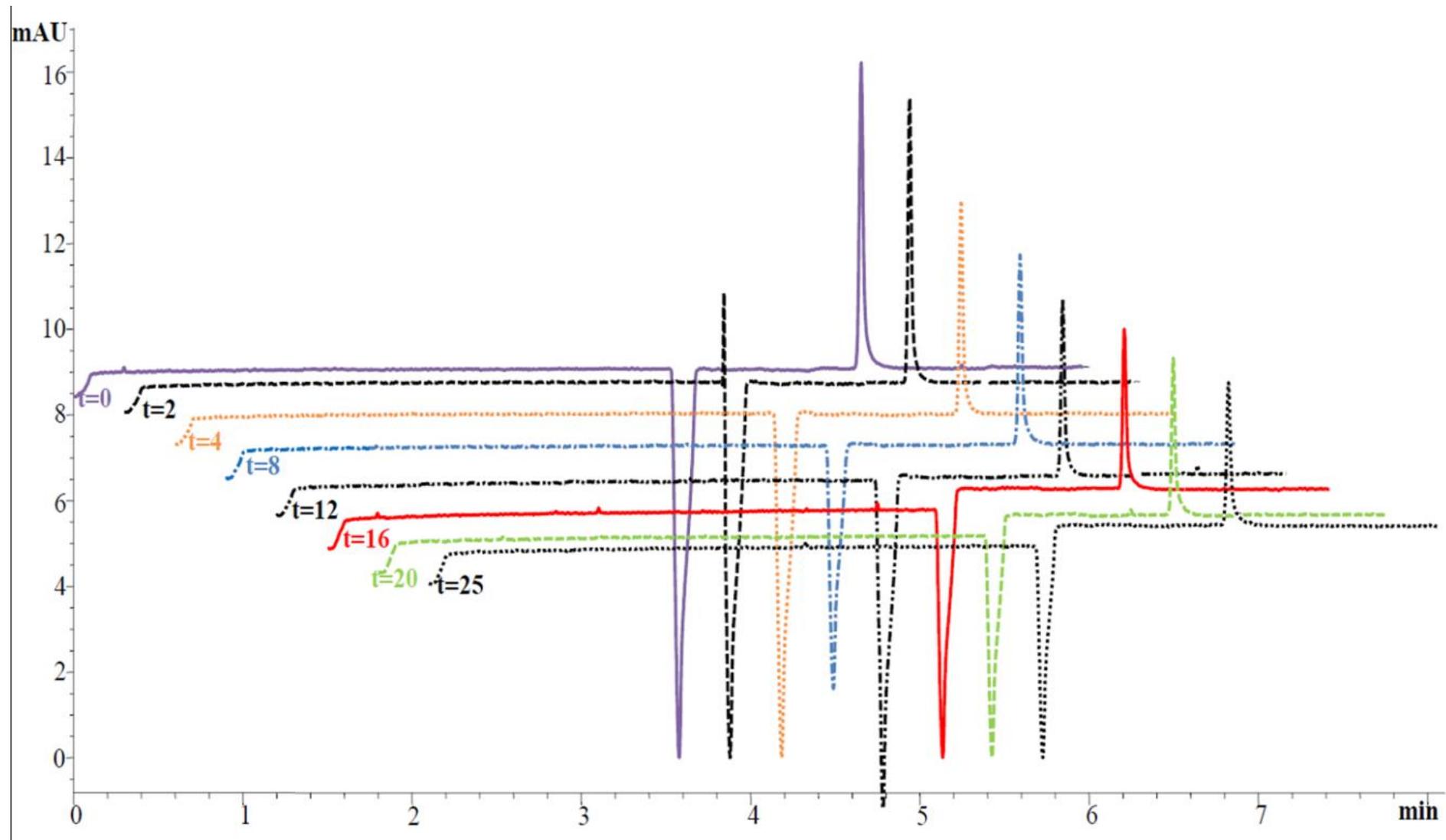
Figure 6.16. Variation of peak area of resveratrol during loading onto nanofibres using 20 ppm resveratrol solution

Using ethanol, crystallization of SF nanofibres occurs within 15 min. We presume that this proceeded simultaneously with various hydrophilic and hydrophobic interactions being formed between the SF and resveratrol. It is thus possible that the resveratrol was also incorporated into the main silk structure during this process. Structure-activity relationships of polyphenols with biopolymers carried out by Tang *et al.* showed however that the interactions between the biopolymers and polyphenols were mainly hydrophobic when hydrophilic solvents were used and vice versa [352]. It is possible in this instance that as the resveratrol was present during the crystallization process; it may have formed hydrophilic interactions via hydrogen bonds with the SF molecules and thus incorporated into the main silk structure. To further study our assumption that the resveratrol may have incorporated into the main silk structure, we examined the adsorption of resveratrol on pre-crystallized nanofibres.

6.9.2   Effect of pre-crystallization of nanofibres on loading of resveratrol

Pre-crystallized nanofibres were prepared by immersing the nanofibre mats in ethanol for 15 min and then drying under vacuum for 24 h. The dried nanofibres were then immersed in ethanolic resveratrol and the analysis done in the same way as for the uncrystallized nanofibre mats. Results showed that the decrease of resveratrol in the test solution (Figure 6.17) was less than that observed for the uncrystallized nanofibre mats (Figure 6.16). This suggests that loading capacity of pre-crystallized nanofibres is less than that of uncrystallized nanofibres, thus supporting our theory that the resveratrol is incorporated into the main silk structure during crystallization of the silk nanofibres.
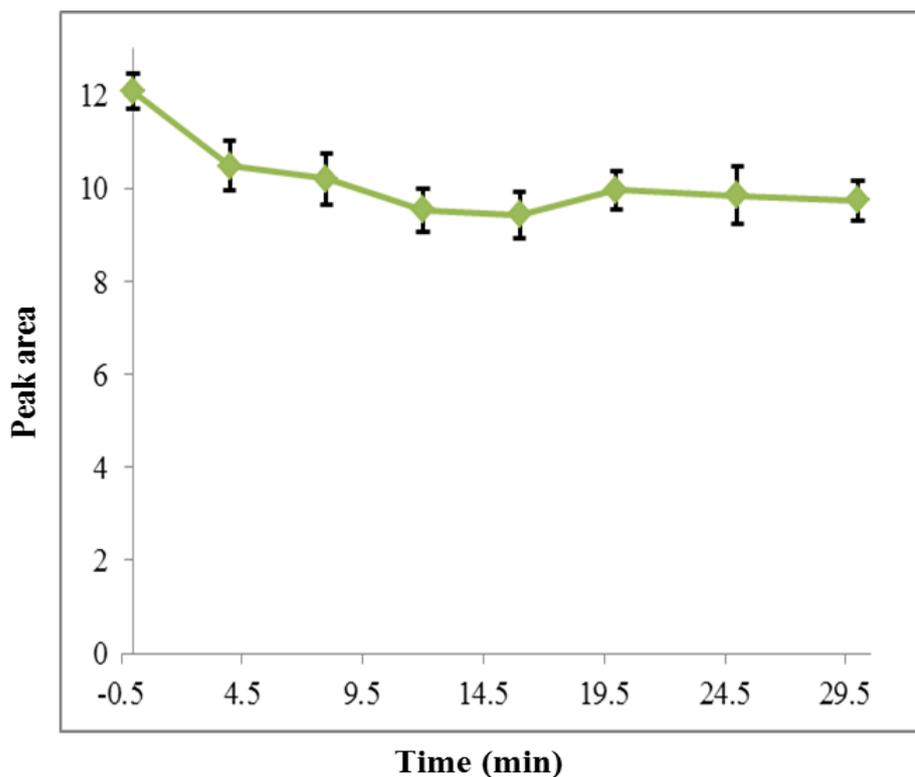
Figure 6.17.   Adsorption of resveratrol on pre-crystallized SF nanofibres using 40 ppm resveratrol solution

6.9.3   Effect of initial solution concentration on loading of resveratrol

Loading of resveratrol onto the nanofibres was investigated over a concentration range of 10 to 50 ppm as shown in Figure 6.18. Results did not clearly show any loading of the resveratrol when 10 ppm resveratrol solution was used. The lower concentrations may have been insufficient for significant interactions with SF. High variance also seen at 10 ppm may have also been compounded by poor instrument response at low concentrations. When higher concentration of 20 ppm was used, there was an increase in the incorporation of resveratrol into the SF nanofibres (Figure 6.18b). Again it was noted that the concentration rapidly decreased within the first 15 min where crystallization of the random coil segments in the SF occurs. This suggests that the availability of more resveratrol molecules during crystallization increased the loading onto the nanofibres.
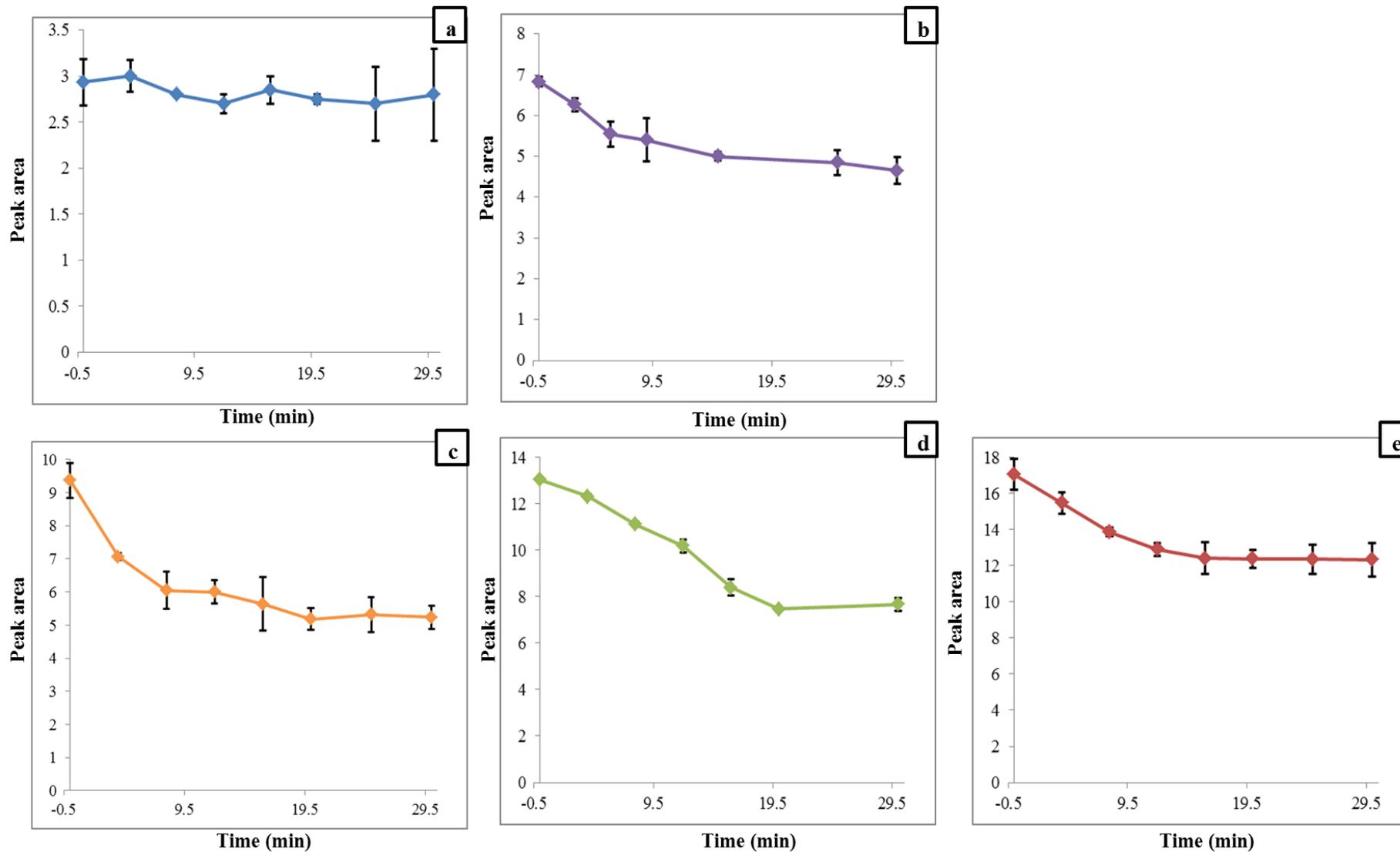
Figure 6.18. Effect of initial concentration on loading resveratrol onto SF nanofibres a) 10 ppm, b) 20 ppm, c) 30 ppm, d) 40 ppm and e) 50 ppm

127

Similar results were obtained using silk fibres and olive oil polyphenols. The authors reported a significant increase in the adsorption of the olive plant phenolic oleuropein was observed when its initial concentration in solution was increased [351].

The most resveratrol incorporated into the SF nanofibres was when 30-50 ppm solutions were used and the adsorption ranged from 8 to18 µg/mg of nanofibre. The large variances seen in the amount of resveratrol adsorbed can be attributed mainly to non-uniformity of the nanofibre mats in terms of porosity and fibre diameter. This makes it a challenge to optimize and standardize loading of the compound onto the nanofibres via adsorption. The results however show that a more thorough and extensive study of the exact type and extent interactions between resveratrol and SF under the conditions utilized in this work still need to be done to optimize the process. Upscaling the process to use larger amounts of the nanofibres may also help in providing better results.

6.10 Release of resveratrol from the nanofibres

Release studies are important for a drug delivery scaffold to determine delivery rate of the drug to target organs. The release of compounds embedded in SF matrices is determined by characteristics of both the incorporated drug and SF such as nature and size of the compound, degree of crosslinking and pore size of the SF matrix [353-355]. The release of resveratrol was evaluated in phosphate buffered saline (PBS) at pH 7.4. PBS was selected for the release studies to closely simulate human physiological pH condition of 7.2–7.4 and would therefore give an indication of release of the resveratrol under when in contact with physiological fluids. However, there was no evidence of release of any resveratrol from the SF nanofibres and this could be due to a number of reasons. Firstly, it is possible that the larger amount of resveratrol is actually incorporated into the main silk structure and release is not possible.

128

There have been reports of polyphenols interacting irreversibly with some dietary proteins [356]. It is also possible that, as resveratrol is a photosensitive compound, surface interactions may have not been sufficient enough to stabilize the compound and it therefore degraded hence no compound was present to be released. The adsorbed quantity could also have been too low.

FTIR studies could also not confirm the presence of any new interactions in the SF nanofibres (Figure 6.19). Characteristic peaks of resveratrol found at 966, 1383, 1585 and 1607 cm^{-1} [357] are in amide regions where the SF itself exhibits peaks and therefore no conclusive evidence was presented using this technique. The absence of these characteristic peaks is however not a clear sign that the resveratrol is not present in the nanofibres. Murugesh & Babu reported similar results with SF and curcumin [358]. They attributed the absence of signals to either one or a combination of the following phenomena. Firstly, the compound could simply have not been adsorbed on the surface of scaffold; rather, it possibly interacted with the core pockets of fibroin. The interactions of the compound with fibroin could be via noncovalent bonds and would therefore not exhibit any new peak or significant shift in peaks. It is also possible if interactions with the compound occurred in the regions of amide moieties or β-sheet components, it could lead to a decrease in the intensity of corresponding characteristic signals [358].

Crystallographic techniques of samples with and without resveratrol may provide more information to help understand interactions between the SF and resveratrol.
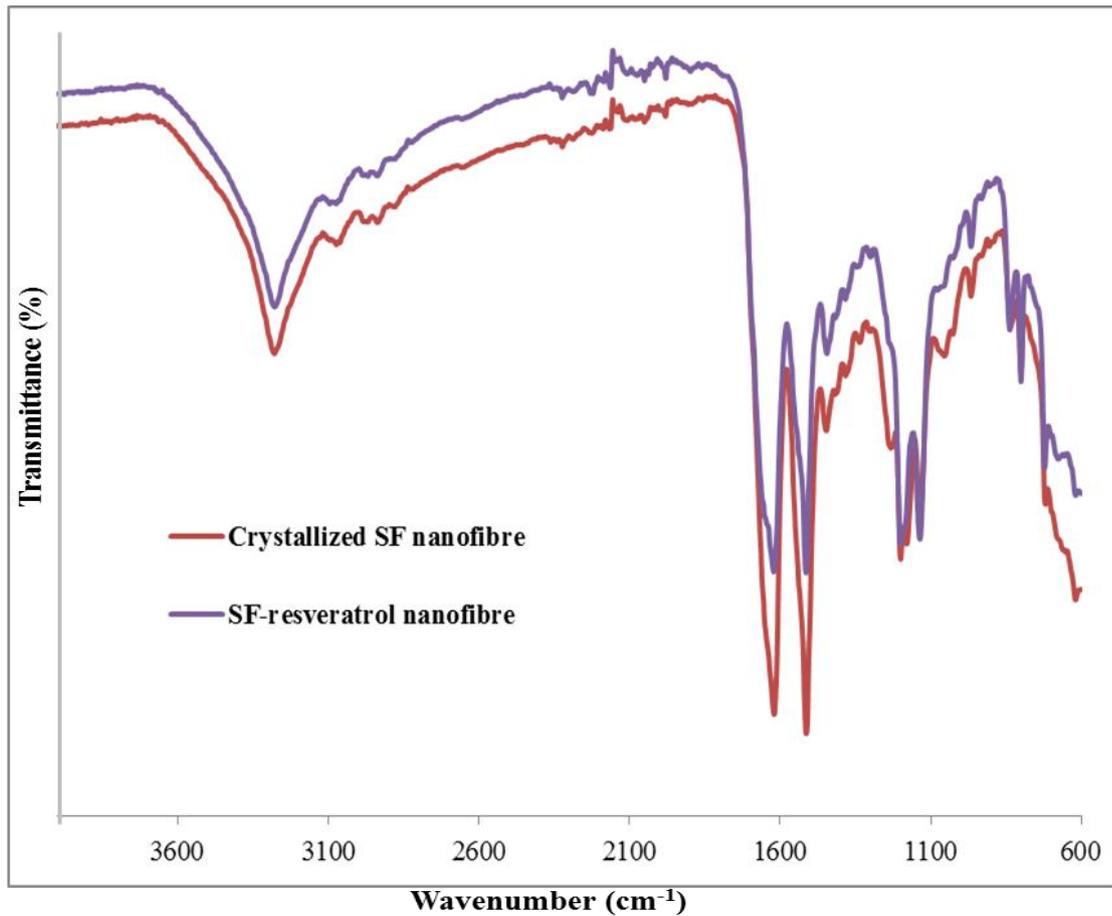
Figure 6.19. FTIR spectrum of resveratrol-SF and plain SF nanofibres

6.11 Cytotoxicity of nanofibres

Biomaterials may have different levels of potential risk to humans depending on the type and the extent contact with a patient. It is therefore imperative to assess cytotoxicity of new biomaterials.

Table 6.4. Cytotoxicity of SF nanofibres, and etoposide

Concentration (µg/ml)	Log Conc.	%Viability	SD	
100	2.0	98.41	2.98	Plain NANOFIBRE
50	1.7	98.98	1.20	
25	1.4	98.79	3.15	
12.5	1.1	98.58	3.55	
6.25	0.8	100.59	2.76	

Concentration (µg/ml)	Log Conc.	%Viability	SD	
100	2.0	102.32	1.18	Res NANOFIBRE
50	1.7	107.92	5.52	
25	1.4	109.19	4.14	
12.5	1.1	116.72	4.90	
6.25	0.8	117.03	3.84	

Concentration (µg/ml)	Log Conc.	%Viability	SD	
100	2	9.24	0.02	Etoposide
33.3	1.52	15.9	0.12	
11.1	1.05	33.3	0.27	
3.7	0.57	58.5	0.21	
1.23	0.09	74.9	0.27	

According to the cytotoxicity grading for the study, low hazard or non-toxic materials present a 50% of cell growth inhibition (IC50) at a concentration greater 100 µg/ml of the test material. Results showed IC50: >100 µg/ml for plain and resveratrol-loaded nanofibres whilst IC50 for the etoposide standard was 5.1 µg/ml. These results indicate that the plain and resveratrol-loaded silk nanofibres produced were not toxic to cells presenting at least 98% cell viability (Table 6.4). The cell's viability for the resveratrol loaded silk nanofibres was practically the same as positive control (cells, no drug) for highest concentration tested. We can therefore conclude that *Gonometa* nanofibres qualify as a non-toxic biomaterial.

6.12 Antibacterial, antioxidant and anticancer properties of resveratrol loaded silk nanofibres

Antibacterial, antioxidant and anticancer properties of the nanofibres was also examined. Despite the inconclusive results on the release of the resveratrol, it was necessary to carry out these tests as some clinical studies have revealed resveratrol to produce positive results even though the active resveratrol was not measurable [359]. However, negative results were also obtained for the tests.

For the antibacterial tests, a simple disc diffusion method was used to determine the susceptibility of *S. aureus* (gram positive) and *E. coli* (gram negative) to the nanofibre samples. The activity of the antimicrobial is determined by observing zones of no bacterial growth around the sample. Both the plain and resveratrol-loaded nanofibres did not show any inhibition zone indicating the antimicrobial effect was either very ineffective or non-existent against the bacteria used in the study.

For the antioxidant tests, gallic acid which possesses good radical scavenging properties was used as a standard. According to criterion used for the experiments, a sample is considered inactive if radical scavenging is < 80% for a concentration of 100 µg/ml. Both the nanofibre samples can therefore be considered to have no useful antioxidant properties as they showed significantly less activity than the reference compound, gallic acid (Table 6.5).

Table 6.5.   Antioxidant activity of SF nanofibres and gallic acid

Concentration, µg/ml	Radical scavenging,%	
100	20.90	Plain NANOFIBRE
50	3.99	
25	3.29	
12.5	0.92	
6.25	0.18	

Concentration, µg/ml	Radical scavenging,%	
100	7.82	ResNANOFIBRE
50	6.84	
25	5.51	
12.5	5.29	
6.25	2.46	

Concentration, µg/ml	Radical scavenging,%	
100	96.92	Gallic Acid
50	96.73	
25	96.42	
12.5	96.60	
6.25	95.28	

TK10 (renal), UACC62 (melanoma) and MCF7 (breast) cancer cells, were used to assess anticancer activity of the nanofibres. TGI (total growth inhibition) signifies a cytostatic effect. Samples are considered inactive if parameter TGI for two or three cell lines is higher than 50 µg/ml and potent activity (TGI <6.25 µg/ml). Therefore, both the plain and resveratrol-loaded nanofibres can be considered inactive against cancer cells (Table 6.6).

Table 6.6.   Anticancer activity of SF nanofibres against three cancer cell lines

Conc, µg/ml	Etoposide				Plain SF nanofibre				Resveratrol loaded SF nanofibre			
	Cell Growth,% TK10	Cell Growth,% UACC62	Cell Growth, % MCF7	SD	Cell Growth,% TK10	Cell Growth,% UACC62	Cell Growth, % MCF7	SD	Cell Growth,% TK10	Cell Growth,% UACC62	Cell Growth, % MCF7	SD
100	-52.14	-44.87	9.48	0.003-0.023	134.02	76.93	86.34	0.009-0.068	102.18	58.48	64.56	0.017-0.021
50	-43.33	-31.63	13.19	0.001-0.017	123.36	95.62	98.83	0.023-0.063	112.46	82.45	87.41	0.005-0.045
25	-10.39	6.43	20.16	0.003-0.033	119.38	99.85	97.25	0.015-0.051	105.03	89.73	94.63	0.037-0.090
12.5	19.71	20.56	27.23	0.006-0.015	117.52	99.40	113.34	0.003-0.241	101.59	97.90	98.24	0.002-0.044
6.25	43.58	26.39	34.13	0.008-0.015	111.90	107.74	99.06	0.072-1.330	99.78	97.11	98.69	0.046-0.063

We can thus conclude that using the experimental conditions in this study, SF nanofibres did not perform well as a carrier for resveratrol for drug delivery purposes.

CHAPTER SEVEN

CONCLUSIONS AND FUTURE PERSPECTIVES

7.1   Introduction

The gap in the information concerning the properties as well as biomaterial applications of fibroin from African silkworm species led to the research conducted in this thesis. This chapter presents the conclusions drawn from the work under each of the objectives set out at the beginning of the study. Although this research has addressed most of the set objectives, to further understand and develop fibroins from African silkworm species as biomaterials, further work is needed. Recommendations put forward for future work encompass work not done due to unavailability of some facilities during the study as well as questions that arose during the study.

7.2   Conclusions

Silk fibroin from *G. rufobrunnae, G. postica, A. mimosae, E. bahuniae* and *A. panda* silkworm species was successfully characterized. Much like most fibroins, the major amino acids were glycine, alanine and serine which promote formation of extensive β-sheet crystalline structures. *A. panda* was the most crystalline amongst the fibroins with a very unique composition consisting almost entirely of glycine and alanine. *G. rufobrunnae, G. postica, A. mimosae* and *E. bahuniae* fibroin are potentially more reactive than *B. mori* and *A. panda* fibroin due to a higher polar amino acid content. *A. mimosae* and *E. bahuniae* SF showed similar characteristics to those reported for species in the *Saturniidae* family. The chemical composition had a significant influence on the physical properties of the fibroins with differences observed in thermal and mechanical properties of the fibroins. Overall, the

differences in properties between the African silk fibroins and *B. mori* fibroin can offer diversity in their application as textiles and biomaterials.

The fibroins have different solubilities mostly dependant on the type and concentration of the salt. Aqueous LiBr and $Ca(NO_3)_2$ solutions were good solvents for *Gonometa* fibroin with just over 20 % (w/v) solutions obtained. Contrary to reports for other species, incorporation of organic solvents into aqueous LiBr and $Ca(NO_3)_2$ solutions reduced solubility of *Gonometa* fibroin. The solvents examined in this study were however not of practical use for the quantitative dissolution of *A. mimosae*, *A. panda* and *E. bahuniea* fibroin. This suggests the dissolution of silk is governed by several factors including the structural characteristics of the individual fibroins.

Electrospinning was successful in producing nanofibres from *Gonometa* RSF using trifluoroacetic acid as a solvent. This achievement sees the first time a biomaterial scaffold is prepared from this species. SF concentration was the most significant parameter in producing uniform and continuous fibres. The choice of solvent was also influential as trifluoroacetic acid electrospun at lower concentrations than formic acid and no electrospinning was observed using water. Other parameters such as the applied voltage, tip to collector distance and the feed rate had more impact on the morphology and diameter of the nanofibres produced rather than electrospinnability. At optimum conditions (0.05 mL/h flow rate, 10 cm tip to collector distance and an applied voltage of 15 kV), nanofibres with diameters ranging from 400-1000 nm and 300 to 760 nm using FD-RSF and RD-RSF respectively were produced. FD-RSF and RD-RSF were mainly composed of β-sheets, similar to the degummed fibre. Electrospun nanofibres showed reduced β-sheet content when compared to degummed fibroin and RSF resulting in poor physical properties as well as solubility in water. The type of solvent can be used to tailor the nanofibre material properties as the extent of crystallinity induced varied depending on the solvent. The more crystalline nanofibres

exhibited higher thermal degradation temperatures. Ethanol and water vapour were the most effective in inducing crystallinity whilst maintaining the physical integrity of the nanofibres. Despite restoration of crystalline structure in the nanofibres, they still exhibited differences in thermal properties compared to the degummed silk fibre thus showing organizational variances in their structures. These findings were confirmed by shifts in FTIR peaks, reduction in crystalline peaks in XRD scatterings and drop in endotherms in DSC thermograms.

Cytotoxicity tests showed *Gonometa* SF nanofibres were non-toxic to cells thus indicating potential for applications requiring biocompatible materials. Further experiments were performed to assess the nanofibres as a carrier for the drug resveratrol with the aim of developing an antimicrobial wound dressing. Using ethanol as a solvent, resveratrol loading onto the SF nanofibres was a maximum of 18 μg/mg of nanofibre with over 95 % of resveratrol adsorbed within 15 min. An increase in the initial resveratrol concentration increased uptake of the compound into the SF nanofibres. While the nanofibres did not display ability to release the resveratrol, the overall results encourage further investigations into the developed *Gonometa* SF nanofibres as a drug delivery vehicle. Primary composition is therefore not a direct indicator of functionality in silks, and the search for correlations between microstructure and properties still remains an important endeavour.

In summary, the work presented in this thesis has enabled a more detailed understanding of the structure of SF from African silkworm species and their potential as biomaterials as exemplified by *Gonometa* SF nanofibres. As these are the first time studies for SF from African species as biomaterials, there is great potential for their properties to be exploited for various tissues and applications.

7.3   Future Perspectives

1. Studies to determine the sequencing of the proteins will be helpful in providing more insight into the nature of the fibroins as well as provide information that can be used for genetic engineering of valuable segments of the proteins. This is important considering one of the challenges that could hinder the use of SF from wild African silk species is lack of continuous supply as their population dynamics are still being established.

2. While appreciable progress was made by producing *Gonometa* SF nanofibres, a lot of work remains as the rest of the fibroins were not investigated as biomaterial scaffolds. Further studies are required to fully understand the dissolution process of fibroin and to also determine solvents suitable for the other fibroins in order to produce RSF needed to fabricate the biomaterial scaffolds. Ionic liquids have proven to be very effective solvents for various natural polymers that are difficult to dissolve and it would be interesting to investigate them as candidate solvents.

3. Drug loading is a promising objective to extend the applications of the *Gonometa* SF nanofibres, especially considering its hydrophilic moieties. In addition to the resveratrol, other bioactive molecules with differing characteristics such as size, hydrophobicity or water solubility should be investigated to further understand the interactions with SF. The knowledge of these interactions may lead to better control of the loading and release processes of the incorporated components thus enabling further development of the ideas introduced in this study. In addition, release data can be assessed with various models to appropriately determine the release mechanism and kinetics. Determination of adsorption isotherms will also provide important data

as the isotherms give insight into the interactions and the maximum capacity of the adsorbents.

4. Different morphologies such as nanoparticles, hydrogels can be developed from the African fibroins and investigated for different applications. This will also be beneficial in identifying how the different constructs affect drug loading and release if used for drug delivery.

5. Mechanical properties of the fabricated nanofibres should be investigated to determine the load bearing capabilities of the nanofibres.

6. Biodegradation and cell interaction studies of the SF nanofibres would be valuable in cementing the biomaterial status of the *Gonometa* SF nanofibres and extend their applications for various tissues.

References

1.   Y. Bar-Cohen, *Bioinsp. Biomim*, **1**, P1–P12 (2006).

2.   P. Fratzl, *J. R. Soc. Interface*, **4**, 637–642 (2007).

3.   T. Scheibel, *Curr. Opin. Biotechnol.*, **16**, 427–433 (2005).

4.   T.D. Sutherland, J.H. Young, S. Weisman, C.Y. Hayashi, D.J. Merritt, *Annu. Rev. Entomol.*, **55**, 171-188 (2010).

5.   F. Vollrath, D. Porter, *Soft Matter*, **2**, 377–385 (2006).

6.   M. Arami, S. Rahimi, L. Mivehie, F. Mazaheri, N.M. Mahmoodi, *J. Appl. Polym. Sci.*, **106**, 267-275 (2007).

7.   Y. Liu, Z.Z. Shao, F. Vollrath, *Nat. Mater.,* **4**, 901–905 (2005).

8.   F. Vollrath, D.P. Knight, *Int. J. Biol. Macromol.*, **24**, 243–249 (1999).

9.   K.Y. Lee, L. Jeong, Y.O. Kang, S.J. Lee, W.H. Park, *Adv. Drug Deliv. Rev.*, **61**, 1020–1032 (2009).

10.   B. Dhandayuthapani, Y. Yoshida, T. Maekawa, D. Sakthi Kumar, *International Journal of Polymer Science*, Article ID 290602 (2011).

11.   G.H. Altman, F. Diaz, C. Jakuba, T. Calabro, R.L. Horan, J. Chen, H. Lu, J. Richmond, D.L. Kaplan, *Biomaterials*, **24**, 401–416 (2003).

12.   C. Vepari & D.L. Kaplan, *Prog. Polym. Sci.*, **32**, 991-1007 (2007).

13.   Y. Wang, H.J. Kim, G. Vunjak-Novakovic, D.L. Kaplan, *Biomaterials*, **27**, 6064–6082 (2006).

14.   X. Zhang, M.R. Reagan, D.L. Kaplan, *Adv. Drug Deliv. Rev.*, **61**, 988–1006 (2009).

15.   H.S. Yoo, T.G. Kim, T.G. Park, *Adv. Drug Deliv. Rev.*, **61**, 1033–1042 (2009).

16. J.K. Jayaraman, M. Kotaki, Y. Zhang, X. Mo, S. Ramakrishna, *J. Nanosci. Nanotechnol.*, **4**, 52-65 (2004).

17. Z.M. Huang, Y.Z. Zhang, M. Kotaki, S. Ramakrishna, *Compos. Sci. Technol.*, **63**, 2223-2253 (2003).

18. A. Greiner & J.H. Wendorff, *Angew. Chem. Int. Ed.*, **46**, 5670 – 5703 (2007).

19. J.D. Schiffman & C.L. Schauer, *Polym. Rev.*, **48**, 317-352 (2008).

20. B. Kundu, R. Rajkhowa, S.C. Kundu, X.Wang, *Adv. Drug Deliv. Rev.*, **65**, 457–470 (2013).

21. N.A. Ayoub, J.E. Garb, R.M. Tinghitella, M.A. Collin, C.Y. Hayashi, PLoS ONE 2(6): e514. doi:10.1371/journal.pone.0000514 (2007).

22. R.E. Marsh, R.B. Corey, L. Pauling, *Biochim. Biophys. Acta*, **16**, 1–34 (1955).

23. C.Z. Zhou, F. Confalonieri, N. Medina, Y. Zivanovic, C. Esnault, T. Yang, M. Jacquet, J. Janin, M. Duguet, R. Perasso, Z.G. Li, *Nucleic Acids Res.*, **28**, 2413–2419 (2000).

24. K.U. Sprague, *Biochemistry*, **14**, 925–931 (1975).

25. A. Datta A.K. Ghosh, S.C. Kundu, *Insect Biochem. Mol. Biol.*, **31**, 1013–1018 (2001).

26. J. Warwicker, *J. Mol. Biol.*, **2**, 350-362 (1960).

27. C. Acharya, S.K. Ghosh, S.C. Kundu, *Acta Biomaterialia*, **5**, 429-437 (2009).

28. Y. Srisuwan, P. Srihanam, *J. Appl. Sci.*, **9**, 978-982 (2009).

29. K. Ohgo, C. Zhao, M. Kobayashi, T. Asakura, *Polymer*, **44**, 841-846 (2003).

30. S. Zarkoob, R.K. Ebya, D.H. Reneker, S.D. Hudson, D. Ertley, W.W. Adams, *Polymer*, **45**, 3973–3977 (2004).

31.   A.A. Walker, S. Weisman, J.S. Church, D.J. Merritt, S.T. Mudie, T.D. Sutherland, PLoS ONE 7(2): e30408. doi:10.1371/journal.pone.0030408 (2012).

32.   N. Reddy & Y. Yang, *Int. J. Biol. Macromol.*, **46**, 419-424 (2010).

33.   S. Sunarintyas, W. Siswomihardjo, A.E. Tontowi, *International Journal of Biomaterials*, Article ID 493075 (2012).

34.   G. Freddi, A. Bianchi Svilokos, H. Ishikawa, M. Tsukada, *J. Appl. Polym. Sci.*, **48**, 99-106 (1993).

35.   C. Holland, D. Porter, F. Vollrath, *Biopolymers*, **97**, 362-7 (2012).

36.   A. Teshome, J.M. Onyari, S.K. Raina, J.M. Kabaru, F. Vollrath, *J. Appl. Polym. Sci.*, **127**, 289–297 (2013).

37.   R. Veldtman, M.A. McGeoch, C.H. Scholtz, *Afric. Entomol.*, **10**, 127-136 (2002).

38.   B.M. Ngoka, E.N. Kioko, S.K. Raina, J.M. Mueke, D.M. Kimbu, *Int. J. Trop. Insect Sci.*, **27**, 183–190 (2008).

39.   N. Mbahin, S.K. Raina, E.N. Kioko, J.M. Mueke, *J. Insect Sci.*, **10**, 1-10 (2010).

40.   T. Gheysens, A. Collins, S. Raina, F. Vollrath, D.P. Knight, *Biomacromolecules*, **12**, 2257-2266 (2011).

41.   A. Teshome, S.K. Raina, F. Vollrath, J.M. Kabaru, J. Onyari, E.K. Nguku, *J. Entomol.*, **8**, 450-458 (2011).

42.   C.L. Craig, *Annu. Rev. Entomol.*, **42**, 231–67 (1997).

43.   F.Vollrath, *Int. J. Biol. Macromol.*, **24**, 81-88 (1999).

44.   F.Vollrath, *J. Biotechnol.*, **74**, 67-83 (2000).

45. J.G. Dingle, E. Hassan, M. Gupta, D. George, L. Anota, H. Bugum, Silk production in Australia. A Report for the Rural Industries Research and Development Corporation RIRDC Publication, 2005.

46. Y-Q Liu, L. Qin, Y-P Li, H. Wang, R-X Xia, Y-H Qi, X-S Li, C. Lu, Z-H Xiang, *Neotrop. Entomol.*, **39**, 967-976 (2010).

47. N.G. Ojha, R.M. Reddy, G. Hansda, M.K. Sinha, N. Suryanarayana, N.B.V. Prakash, *Acad. J. Entomol.*, **2**, 80-84 (2009).

48. C.C. Gowdey, *Bull. Entomol. Res.*, **3**, 269-274 (1953).

49. S.K. Raina, E. Kioko, O. Zethner, S.Wren, *Ann. Rev. Entomol.*, **56**, 465–485 (2011).

50. D. Goswami & H.I. Singh, *Munis Entomology & Zoology*, **7**, 274-283 (2012).

51. M. Deka & M. Kumari, *Int. J. Res. Chem. Environ.*, **1**, 99-104 (2013).

52. R. Peigler, *Amer. Entomol.*, **39**, 151-161 (1993).

53. E.N. Kioko, S.K. Raina, J.M. Mueke, *E. Afr. J. Sci.*, **2**, 1-6 (2000).

54. R. Veldtman, M.A. McGeoch, C.H.Scholtz, *Bull. Entomol. Res.*, **97**, 15–27 (2007).

55. R.M. Robson, Silk; Composition, Structure and Properties in Handbook of Fibre Science and Technology, Vol. IV, M. Lewin & E.M. Pearce (Eds), Mercel Dekker Inc., New York, 1985, p. 649-700.

56. H.J. Jin & D.L. Kaplan, *Nature*, , 424, 1057-61 (2003).

57. A. Ochi, K.S. Hossain, J. Magoshi, N. Nemoto, *Biomacromolecules*, **3**, 1187-1196 (2002).

58. R. Dash, S. Mukherjee, S.C. Kundu, *Int. J. Biol. Macromol.*, **38**, 255– 258 (2006).

59. J-H. Wu, Z. Wang, S-H. Xu, *Food Chem.*, **103**, 1255-1262 (2007).

60. K. Kodama, *Biochem. J.*, **20**, 1208–1222 (1926).

61. K. Tanaka, S. Inoue, S.Mizuno, *Insect Biochem. Mol. Biol.*, **29**, 269-276 (1999).

62. S. Inoue, K.Tanaka, F. Arisaka, S. Kimura, K. Ohtomo, S.J. Mizuno, *Biol. Chem.*, **275**, 40517-40528 (2000).

63. F. Sehnal & M. Zurovec, *Biomacromolecules*, **5**, 666–74 (2004).

64. K. Komatsu, *JARQ*, **13**, 64-72 (1979).

65. T. Gamo, T. Inokuchi, H. Laufer, *Insect Biochem.*, **7**, 285-295 (1977).

66. R. Dash, S.K. Ghosh, D.L. Kaplan, S.C. Kundu, *Comp. Biochem. & Physiol. Part B*, **147**, 129-134 (2007).

67. D. Kaplan, W. Wade Adams, B. Farmer, C. Viney, Silk: Biology, Structure, Properties, and Genetics, In Silk Polymers; ACS Symposium Series; American Chemical Society, Washington DC, 1993, p 2-16.

68. Y. Takasu, H. Yamada, K.Tsubouchi, *Biosci. Biotechnol. Biochem.*, **66**, 2715-2718 (2002).

69. H. Yamada, K. Tsubouchi, *Int. J. Wild Silkmoth Silk*, **6**, 47–54 (2001).

70. C. Holland, D. Porter, F. Vollrath, *Biopolymers*, **97**, 362-367 (2012).

71. V. Mhuka, S. Dube, M.M. Nindi, *Int. J. Biol. Macromol.*, **52**, 305–311 (2013).

72. A.T. Kebede, S.K. Raina, J.M. Kabaru, *Int. J. Insect Sci.*, **6**, 9–14 (2014).

73. R.V. Lewis, *Acc. Chem. Res.*, **25**, 392-398 (1992).

74. H. Yano, K. Aso, A. Tsugita, *J. Biochem.*, **108**, 579-582 (1990).

75. W.J.M. Underberg & J.C.M. Waterval, *Electrophoresis*, **23**, 3922-3933 (2002).

76. K. Blau, A. Darbre, in Handbook of Derivatives for Chromatography, K. Blau, J. M. Halket (Eds), Wiley, New York, 1993, p 151-153.

77.   S. Moore & W.H. Stein, *Methods Enzymol.*, **6**, 819-831 (1958).

78.   A. Fabiani, A.Versari, G.P. Parpinello, M. Castellari, S. Galassi, , *J. Chromatogr. Sci.*, **40**, 14-18 (2002).

79.   T. Erbe & H.J Bruckner, *J. Chromatogr. A*, **881**, 81-91 (2000).

80.   V. Poinsot, M. Lacroix, D. Maury, G. Chataigne, B. Feurer and F. Couderc, *Electrophoresis*, **27**, 176-194 (2006).

81.   H.Watzig, S. Gunter, *Clin. Chem. Lab. Med.*, **41**, 724-738 (2003).

82.   J.H. Issaq, *J. Liq. Chrom. & Rel. Technol.*, **25** , 1153-1170 (2005).

83.   A. Varenne, S. Descroix, *Anal. Chim. Acta*, **628**, 9–23 (2008).

84.   http://academics.keene.edu/rblatchly/Chem220/hand/npaa/aawpka.htm

85.   M.G. Khaledi, in Handbook of Capillary Electrophoresis. P. Oda & J. P. Landers (Eds), CRC Press, FL, 1994, p. 46.

86.   P. Iadarola, F. Ferrari, M. Fumagalli, S. Viglio, *Electrophoresis*, **29**, 224-236 (2008).

87.   C.L. Craig & C. Riekel, *Comp. Biochem. & Physiol. Part B*, **133**, 493-507 (2002).

88.   O. Hakimi, D.P. Knight, M.M. Knight, M.F. Grahn, P. Vadgama, *Biomacromolecules*, **7**, 2901-2908 (2006).

89.   E. Sashina, A. Bochek, N. Novoselov, D. Kirichenko, *Russ. J. Appl. Chem.*, **79**, 869-876 (2006).

90.   T. Asakura, A. Kuzuhara, R. Tabeta, H. Saito, *Macromolecules*, **18**, 1841-1845 (1985).

91.   K. Okuyama, K. Takanashi, Y. Nakajima, Y. Hasegawa, K. Hirabayashi, N. Nishi, *J. Seric. Sci. Jpn.*, **57**, 23-30 (1988).

92.   B. Lotz, A. Brack, G. Spach, *J. Mol. Biol.*, **87**, 193-203 (1974).

93. S.J. He, R. Valluzzi, S.P. Gido, *Int. J. Biol. Macromol.*, **24**, 187-195 (1999).

94. B. Lotz & F. C. Cesari, *Biochimie*, **61**, 205- 214 (1979).

95. S.A. Fossey, G. Nemethy, K.D. Gibson, H.A. Scheraga, *Biopolymers*, **31**, 1529-1541 (1991).

96. J. Magoshi, M. Mizuide, Y. Magoshi, K. Yakahashi, M. Kubo, S. Nakamura, *J. Polym. Sci. Polym. Phys. Ed.*, **17**, 515- 520 (1979).

97. H. Saito, R. Tabeta, T. Asakura, Y. Iwanaga, A. Shoji, T. Ozaki, I. Ando, *Macromolecules*, **17**, 1405-1412 (1984).

98. L.K. Nicholson, T. Asakura, M. Demura, T. A. Cross, *Biopolymers*, **33**, 847- 861 (1993).

99. J. Yao, Y. Nakazawa, T. Asakura, *Biomacromolecules*, **5**, 680-688 (2004).

100. R. Valluzzi & S.P. Gido, *Biopolymers*, **42**, 701-705 (1997).

101. S. Putthanarat, N. Stribeck, S.A. Fossey, R.K. Eby, W.W. Adams, *Polymer*, **41**, 7735–7747 (2000).

102. C. Wong Po Foo, E. Bini, J. Hensman, D.P. Knight, R.V. Lewis, D.L. Kaplan, *Appl. Phys. A*, **82**, 223–233 (2006).

103. K. Nuanchai, S. Wilaiwan, S. Prasong, *Current Research in Chemistry*, **2**, 1-9 (2010).

104. L. Jeong, K.Y. Lee, J.W. Liu, W.H. Park, *Int. J. Biol. Macromol.*, **30**, 140-144 (2006).

105. T. Asakura, J. Ashida, T. Yamane, T. Kameda,; Nakazawa, K. Ohgo, K. Komatsu, *J. Mol. Biol.*, 3**06**, 291-305 (2001).

106. J.O. Warwicker, *Acta Crystallogr.*, **7**, 565–73 (1955).

107. K. Yukuhiro, T. Kanda, T. Tamura, *Insect. Mol. Biol.*, **6**, 89–95 (1997).

108. J.T.B. Shaw & S.G. Smith, *Biochim. Biophys. Acta*, **52**, 305-318 (1961).

109. A.R. Murphy & D.L. Kaplan, *J. Mater. Chem.*, **19**, 6443-6450 (2009).

110. E. Bini, D.P. Knight, D.L. Kaplan, *J. Mol. Biol.*, **35**, 27-40 (2004).

111. Y. Yang, X. Chen, Z. Shao, P. Zhou, D. Porter, D.P. Knight, *Adv. Mater.*, **17**, 84–88 (2005).

112. A.F. Von Recum & M. LaBerge, *J. Appl. Biomater.*, **6**, 137-144 (1995).

113. L.R. Moy, A. Lee, A. Zalka, *Am. Fam. Physician*, **44**, 2123-2128 (1991).

114. R.L. Horan, K. Antle, A.L. Collette, Y. Wang, J. Huang, J.E. Moreau, V. Volloch, D.L. Kaplan, G.H. Altman, *Biomaterials*, **26**, 3385-3393 (2005).

115. L. Meinel, S. Hofmann, V. Karageorgiou, C. Kirker-Head, J. McCool, G. Gronowicz, *Biomaterials*, **26**,147–55 (2005).

116. Y. Wang, H.J. Kim, G. Vunjak-Novakovic, D.L. Kaplan, *Biomaterials*, **27**, 6064-6082 (2006).

117. K. Cai, K. Yao, Y. Cui, Z. Yang, X. Li, H. Xie, T. Qing, L. Gao, *Biomaterials*, **23**, 1603-1611 (2002).

118. B.M. Min, L. Jeong, Y.S. Nam, J.M. Kim, J.Y. Kim, W.H. Park, *Int. J. Biol. Macromol.*, **34**, 223-230 (2004).

119. R.E. Unger, K. Peters, M. Wolf, A. Motta, C. Migliaresi, C.J. Kirkpatrick, *Biomaterials*, **25**, 5137-5146 (2004).

120. X. Zhang, C.B. Baughman, D.L. Kaplan, *Biomaterials*, **29**, 2217–2227 (2008).

121. M. Li, M. Ogiso, N. Minoura, *Biomaterials*, **24**, 357-365 (2003).

122. P. Taddei, T. Arai, A. Boschi, P. Monti, M. Tsukada, G. Freddi, *Biomacromolecules*, **7**, 259-267 (2006).

123. T. Arai, G. Freddi, R. Innocenti, M. Tsukada, *J. Appl. Polym. Sci.*, **91**, 2383-2390 (2004).

124. J. Kundu, M. Dewan, S. Ghoshal, S.C. Kundu, *J. Mater. Sci. Mater. Med.*,**19**, 2679-2689 (2008).

125. M.L. Gulrajani, R. Purwar, R.K. Prasad, M. Joshi., *J. Appl. Polym. Sci.*, **113**, 2796–2804 (2009).

126. A. Ajisawa, *J. Seric. Sci. Jap.*, **67**, 91-94, (1998).

127. X. Chen, D.P. Knight, Z. Shao, F. Vollrath, *Polymer*, **42**, 9969-9974 (2001).

128. H. Kweon, Y.H. Park, *J. Appl. Polym. Sci.*, **82**, 750-758 (2001).

129. D.M. Phillips, L.F. Drummy, D.G. Conrady, D.M. Fox, R.R. Naik, M.O. Stone, P.C. Trulove, H.C. De Long, R.A. Mantz „*J. Am. Chem. Soc.*, **126**, 14350-14351 (2004).

130. Q. Wang, Q. Chen,Y. Yang, Z. Shao, *Biomacromolecules*, **13**, 1875−1881 (2012).

131. M. Agostini de Moraes G.M. Nogueira, R.F. Weska, M.M. Beppu, *Polymers*, **2**, 719-727 (2010).

132. M.K. Gupta, S.K. Khokhar, D.M. Phillips, L.A. Sowards, L.F. Drummy, M.P. Kadakia, R.R. Naik, *Langmuir*, **23**, 1315-1319 (2007).

133. M.Z. Li, W. Tao, S. Lu, S. Kuga, *Int. J. Biol. Macromol.*, **32**, 159–163 (2003).

134. N. Minoura, M. Tsukada, M. Nagura, *Biomaterials*, **11**, 430-434 (1990).

135. U.J. Kim, J. Park, C. Li, H.J. Jin, R.Valluzzi, D.L. Kaplan, *Biomacromolecules*, **5**, 786-792 (2004).

136. A. Motta, C. Migliaresi, F. Faccioni, P. Torricelli, M. Fini, R. Giardino, *J. Biomater. Sci. Polym. Edn*, **15**, 851-864 (2004).

137. T. Hino, M. Tanimoto, S. Shimabayashi, *J. Colloid. Interface Sci.*, **266**, 68-73 (2003).

138. U. Kim, J. Park, H. Kim, M. Wadac, D. Kaplan, *Biomaterials*, **26**, 2775–2785 (2005).

139. J.R. Mauney, T. Nguyen, K. Gillen, C. Kirker-Head, J.M. Gimble, D.L. Kaplan, *Biomaterials*, **28**, 5280-5290 (2007).

140. R.L. Horan, A.L. Collette, C. Lee, K. Antle, J. Chen, G.H. Altman, *J. Biomech.*, **39**, 2232-2240 (2006).

141. J. Chen, G.H. Altman, V. Karageorgiou, R.L. Horan, A.L. Collette, V. Volloch, T. Colabro, D.L. Kaplan, *J. Biomed. Mat. Res. Part A*, **67**, 559-570 (2003).

142. S.R. Bhattarai, N. Bhattarai, H.K. Yi, P.H. Hwang, D. Cha, H.Y. Kim, *Biomaterials*, **25**, 2595–2602 (2002).

143. C. Chen, C. Chuanbao, M. Xilan, T. Yin, Z. Hesun, *Polymer*, **47**, 6322-6327 (2006).

144. H. Wang, H. Shao, X. Hu, *J. Appl. Polym. Sci.*, **101**, 961–968 (2006).

145. N. Minoura, S.I. Aiba, Y. Gotoh, M. Tsukada, Y. Imai, *J. Biomed. Mater. Res.*, **29**, 1215-1221 (1995).

146. C. Acharya, S.K. Ghosh, S.C. Kundu, *J. Mater. Sci. Mater. Med.*, **19**, 2827-2836 (2008).

147. C. Acharya, S.K. Ghosh, S.C. Kundu, *Acta Biomaterialia*, **5**, 429-437 (2009).

148. N. Reddy & Y. Yang, *Int. J. Biol. Macromol.*, **46** 419-424 (2010).

149. N. Reddy & Y. Yang, *J. Mater. Sci.*, **45**, 6617–6622 (2010).

150. S. Kundu, B. Kundu, S. Talukdar, S. Bano, S. Nayak, J. Kundu, B.B. Mandal, N. Bhardwaj, M. Botlagunta, B.C. Dash, C. Acharya, A.K. Ghosh, **97**, 455-467 (2012).

151. J-H. He, Y-Q. Wan, L. Xu, *Chaos, Soliton. Fract.*, **33**, 26–37 (2007).

152. L. Feng, N. Xie, J. Zhong, *Materials*, **7**, 3919-3945 (2014).

153. H. Schreuder-Gibson, P.G.K. Senecal, M. Sennett, J.E. Walker, W. Yeomans, D. Ziegler, P. P. Tsai, *J. Adv. Mater.*, **34**, 44 (2002).

154. R.S. Barhate, S. Ramakrishna, *J. Membrane Sci.*, **296**, 1—8 (2007).

155. M.M. Demir, M.A. Gulgun, Y.Z. Menceloglu, *Macromolecules*, **37**, 1787—1792 (2004).

156. Z. Ma, M. Kotaki, R. Inai, S. Ramakrishna, *Tissue Eng.*, **11**, 101—109 (2005).

157. W.J. Li, C.T. Laurencin, E.J. Caterson, R.S. Tuan, F.K. Ko, *J. Biomed. Mater. Res.*, **60**, 613–21 (2002).

158. X. Li, G. Cheruvally, J.K. Kim, J.W. Choi, J.H. Ahn, K.W. Kim, H.J. Ahn, *J. Power Sources*, **167**, 491—498 (2007).

159. X. Wang, Y-G. Kim, C. Drew, B-C Ku, J Kumar, L.A. Samuelson, *Nano Lett.*, **4**, 331—334 (2004).

160. H. Jia, *Methods Mol. Biol.*, **743**, 205-12 (2011).

161. S. Ramakrishna, K. Fujihara, W.E. Teo, T.C. Lim, Z. Ma, Introduction to Electrospinning and Nanofibres, World Scientific Publishing Company, Incorporated, Singapore, 2005.

162. H. Li, Y. Ke, Y. Hu, *J. Appl. Polym. Sci.*, **99**, 1018—1023 (2006).

163. Z. Yang & B.Xu, *J. Mater. Chem.*, **17**, 2385—2393 (2007).

164. P.X. Ma & R. Zhang, *J. Biomed. Mater. Res. Part A*, **46**, 60—72 (1999).

165. T. Ondarcuhu & C. Joachim, *Europhys. Lett.*, **42**, 215-220 (1998).

166. C.J. Ellison, A. Phatak, D.W. Giles, CW. Macosko, F.S. Bates, *Polymer*, **48**, 3306—3316 (2007).

167. H.P. Zhao, X.Q. Feng, H.J. Gao, *Appl. Phys. Lett.*, **90**, 073112 (2007).

168. A.A. Tseng, A. Notargiacomo, T.P. Chen, *J. Vac. Sci. Technol. B*, **23**, 877-894 (2005).

169. B. Ding, M. Wang, J. Yu, G. Sun, *Sensors*, **9**, 1609-1624 (2009).

170. S. Ramakrishna, K. Fujihara, W-E. Teo, T. Yong, Z. Ma, R. Ramaseshan, *Mater. Today*, **9**, 40-50 (2006).

171. F. Jian, N. HaiTao, L. Tong, W. XunGai, *Chin. Sci. Bull.*, **53**, 2265-2286 (2008).

172. J. F. Cooley, Patent US 692,631, 1902.

173. A. Formhals, Patent US 1,975,504, 1934.

174. B. Taylor, *Proc. Roy. Soc. London A*, **313**, 453-475 (1969).

175. J. Doshi, D. Reneker, *J. Electrostat.*, **35**, 151-160 (1995).

176. I. Chun, D.H. Reneker, H. Fong, X. Fang, J. Dietzel, N.B. Tan, K.J. Kearns, *Adv. Mater.*, **31**, 36-41 (1999).

177. D. Li& Y. Xia, *Adv. Mater.*, **16**, 1151-1170 (2004).

178. W-E. Teo & S. Ramakrishna, *Nanotechnology*, **17**, R89─R106 (2006).

179. A. Martins R.L. Reis, N.M. Neves, *Int. Mater. Rev.*, **53**, 257-274 (2008).

180. N.L. Lala, V. Thavasi, S. Ramakrishna, *Sensors*, **9**, 86–101 (2009).

181. T.Subbiah, G.S. Bhat, R.W. Tock, S. Parameswaran, S.S. Ramkumar, *J. Appl. Polym. Sci.*, **96**, 557-569 (2005).

182. L. Huang, K. Nagapudi, R.P. Apkarian, E. Chaikof, *J. Biomat. Sci. Polym. Ed.*, 12, 979-993 (2001).

183. J. Kameoka, R. Orth, Y. Yang, D. Czaplewski, R. Mathers, G. Coates, H. G. Craighead, *Nanotechnology*, **14**, 1124-1129 (2003).

184. S. Sukigara, M. Gandhi, J. Ayutsede, M. Micklus, F. Ko, *Polymer*, **44**, 5721–5727 (2003).

185. T. Jarusuwannapoom, W. Hongrojjanawiwat, S. Jitjaicham, L. Wannatong, M. Nithitanakul, C. Pattamaprom, P. Koombhongse, R. Rangkupan, P. Supaphol, *Euro. Polym. J.*, **41**, 409-421 (2005).

186. A. Koski, K. Yim, S. Shivkumar, *Mater. Lett.*, **58**, 493-497 (2004).

187. M.M. Hohman, M. Shin, G. Rutledge, M.P. Brenner, *Phys. Fluids*, **13**, 2201-2220 (2001).

188. X.H. Zhong, K. S. Kim, D.F. Fang, S.F. Ran, B.S. Hsiao, B. Chu, *Polymer*, **43**, 4403-4412 (2002).

189. J. Ayutsede, M. Gandhi, S. Sukigara, M. Micklus, H.E. Chen, F. Ko, *Polymer*, **46**, 1625–1634 (2005).

190. T.J. Sill & H.A. Recum, *Biomaterials*, **29**, 1989-2006 (2008).

191. D. Li & Y. Xia, *Nano Lett.*, **3**, 555-560 (2003).

192. C Mit-uppatham, M.Nithitanakul, P. Supaphol, *Macromol. Chem. Physic.*, **205**, 2327-2338 (2004).

193. O.O. Dosunmu, G.G. Chase, W. Kataphinan, D.H. Reneker, *Nanotechnology*, **17**, 1123-1127 (2006).

194. M.S. Khil, S.R. Bhattari, H.Y. Kim, S.Z. Kim, K.H. Lee, *J. Biomed. Mater. Res. B*, **72**, 117-123 (2005).

195. S. Zarkoob, D.H. Reneker, R.K. Eby, S.D. Hudson, D. Ertley, W.W. Adams, *Polym. Prepr.*, **39**, 244–245 (1998).

196. S. Sukigara, M. Gandhi, J.Ayutsede, M. Micklus, F.Ko, *Polymer*, **45** 3701–3708 (2004).

197. K. Ohgo, C.H. Zhao, M. Kobayashi, T. Asakura, *Polymer*, **44**, 841–846 (2003).

198. C. Meechaisue, P. Wutticharoenmongkol, R. Waraput, T. Huangjing, N. Ketbumrung, P. Pavasant, and P. Supaphol, *Biomed. Mater.*, **2**, 181-188 (2007).

199. F. Zhang, B.Q. Zuo, H.X. Zhang, L. Bai, *Polymer*, **50**, 279-285 (2009).

200. P. Wadbua B. Promdonkoy, S. Maensiri, S. Siri, *Int. J. Biol. Macromol.*, **46**, 493–501 (2010).

201. M. Mohammadian, A.K. Haghi, *Mater. Plast.*, **49**, 301-311 (2012).

202. K. Wei, B-S. Kim, I-S. Kim, *Membranes*, **1**, 275-298 (2011).

203. C.R. Yoo, I.S. Yeo, K.E. Park, J.H. Park, S.J. Lee, W.H. Park, B.M. Min, *Int. J. Biol. Macromol.*, **42**, 324–334 (2008).

204. T. Elakkiya, G. Malarvizhi, S Rajiv, T. S. Natarajan, *Polym. Int.*, **63**, 100–105 (2014).

205. H. Wang, Y. Zhang, H. Shao, X. Hu, *J. Mater. Sci.*, **40**, 5359–5363 (2005).

206. J. Zhu, H. Shao, X. Hu, *Int. J. Biol. Macromol.*, **41**, 469–474 (2007).

207. H. Cao, X. Chen, L. Huang, Z. Shao, *Mater. Sci. Eng. C*, **29**, 2270–2274 (2009).

208. H.J. Jin, J. Chen, V. Karageorgiou, G.H. Altman, D.L. Kaplan, *Biomaterials*, **25**, 1039–1047 (2004).

209. D.M. Fox, P. Flystra, M. Hanley, W. Henderson, P. C. Trulove, S. Bellayer, J.W. Gilman, H.C. DeLong, *ECS Trans.*, **3**, 11–20 (2007).

210. H. Pan Y. Zhang, Y. Hang, H. Shao, X. Hu, Y. Xu, C. Feng, *Biomacromolecules*, **13** , 2859–2867 (2012).

211. W-H. Park, L. Jeong, D. Yoob, S. Hudson, *Polymer*, **45**, 7151–7157 (2004).

212. W. Zhou, J. He, S. Cui, W. Gao, *Fibres Polym.*, **12**, 431-437 (2011).

213. B-M. Min, L. Jeong L, K.Y. Lee, W.H. Park., *Macromol. Biosci.*, **6**, 285–292 (2006).

214. K.H. Zhang, Q.Z. Yu, X.M. Mo, *Int. J. Mol. Sci.*, **12**, 2187-99 (2011).

215. A. Schneider, X.Y. Wang, D.L. Kaplan, J.A. Garlick, C. Egles, *Acta Biomaterialia*, **5**, 2570-2578 (2009).

216. L-P. Fan, H. Wang, K. Zhang, Z-X. Cai, C. He, X. Sheng, X. Mo, *RSC Advances*, **2**, 4110–4119 (2012).

217. Z-X. Cai, X-M Mo, K-H Zhang, L-P. Fan, A-L Yin, C-L. He, H-S. Wang, *Int. J. Mol. Sci.*, **11**, 3529-3539 (2010).

218. J.P. Chen, S.H. Chen, G.J. Lai, *Nanoscale Res. Lett.*, **7**, 170 (2012).

219. J. He, N. Guo, S. Cui, *Iran. Polym. J.*, **20**, 713-724 (2011).

220. T. Cohen-Karni, K.J. Jeong, J.H. Tsui, G. Reznor, M. Mustata , M. Wanunu , A. Graham , C. Marks, D.C. Bell, R. Langer, D.S. Kohane, *Nano Lett.*, **12**, 5403-5406 (2012).

221. M. Gandhi, H. Yang, L. Shor, F. Ko, *J. Biobased Mater. Bio.*, **1**, 274–281 (2007).

222. C.S. Ki, E.H. Gang, I.C. Um, Y.H. Park, *J. Membr. Sci.*, **302**, 20–26 (2007).

223. C. Li, C. Vepari, H.J. Jin, H.J. Kim, D.L. Kaplan, *Biomaterials*, **27**, 3115–3124 (2006).

224. F. Zhang, R. Liu, B.Q. Zuo, J.Z. Qin, Bioinformatics and Biomedical Engineering (iCBBE), 2010 4th International Conference, IEEE, 1-4.

225. J. Wang, R. Ye, Y. Wei, H. Wang, X. Xu, F. Zhang, J. Qu, B. Zuo, H. H. Zhang, *J. Biomed. Mater. Res. Part A*, **100A**, 632–645 (2012).

226. K.H. Lee, C.S. Ki, D.H. Baek, G.D. Kang, D.W. Ihm, Y.H. Park, *Fibre Polym.*, **6**, 181-185 (2005).

227. G.B. Yin, Y.Z. Zhang, W.W. Bao, J.L. Wu, B. Shi, . Z.H. Dong, W.G. Fu, , *J. Appl. Polym. Sci.*, , **111**, 1471–1477 (2009).

228. W. Li, J Wang, H. Chi, G. Wei, J. Zhang, L. Dai, *J. Appl. Polym. Sci.*, **123**, 20–25 (2012).

229. T. Damrongrungruang, M. Siritapetawee, K. Kamanarong, S. Limmonthon, A. Rattanathongkom, S. Maensiri, *J. Oral Tissue Eng.*, **5**, 1-6 (2007).

230. S. Putthanarat, R.K. Eby, W. Kataphinan, S. Jones, R. Naik, D.H. Reneker, B. L. Farmer, *Polymer*, **47**, 5630–5632 (2006).

231. J. Nam & Y.H. Park, *J. Appl. Polym. Sci.*, **81**, 3008-3021 (2001).

232. A. Motta, L. Fambri, C. Migliaresi, *Macromol. Chem. Physic.*, **203**, 1658-1665 (2002).

233. B.B. Mandal & S.C. Kundu, *Macromol. Biosci.*, **8**, 807–818 (2008).

234. V. Kearns, A. Crawford, P.V. Hatton, Silk-based biomaterials for tissue engineering, in Topics in tissue engineering, R.R.N. Ashammakhi, F. Chiellini (Eds.), 2008, p 1-19.

235. E. Kharlampieva, V Kozlovskaya, B Wallet, V.V. Shevchenko , R.R. Naik, R. Vaia, D.L. Kaplan, V. V. Tsukruk, *ACS Nano*, **4**, 7053–7063 (2010).

236. S.S. Silva, D.M., Antonella Motta, J.F. Mano, R.L. Reis, C. Migliaresi, *Macromol. Biosci.*, **8**, 766-774 (2008).

237. P. Petrini, C. Parolari, M.C. Tanzi, *J. Mater. Sci.- Mater. Med.*, **12**, 849-853 (2001).

238. N. Minoura, M. Tsukada, M. Nagura, *Polymer*, **31**, 265-269 (1990).

239. H.J. Jin, S.V. Fridrikh, G.C. Rutledge, D.L. Kaplan, *Biomacromolecules*, **3**, 1233–1239 (2002).

240. B.M. Min, G. Lee, S.H. Kim, Y.S. Nam, T.S. Lee, W.H. Park, *Biomaterials*, **25**, 1289-97 (2004).

241. Y. Shen, Y. Qian, H. Zhang, B. Zuo, Z. Lu, Z. Fan, P. Zhang, F. Zhang, C. Zhou. *Cell Transplant*, **19**, 147-57 (2010).

242. H. Kim, U. Kim, G. Vunjak-Novakovic, B. Min, D. Kaplan, *Biomaterials*, **26**, 4442-4452 (2005).

243. J.H. Wendorff, S. Agarwal, A. Greiner, Electrospinning: Materials, Processing, and Applications, 1st Ed., Wiley-VCH, Weinheim, Germany, 2012, p 3.

244. J. Fang, X. Wang, T. Lin, Functional Applications of Electrospun Nanofibers, in Nanofibers -Production, Properties and Functional Applications, L. Tong (Ed.), InTech – Open Access Publisher, Rijeka, Croatia, 2011, p 293.

245. J.S. Boateng, K.H. Matthews, H.N.E. Stevens, G.M. Eccleston, *J. Pharm. Sci.*, **97**, 2892–2923 (2008).

246. P. Zahedi, I. Rezaeian, S.O. Ranaei-Siadat, S.H. Jafari, P. Supaphol, *Polym. Adv. Technol.*, **21**, 77-95 (2010).

247. A. Demir Sezer, E. Cevher, Biopolymers as Wound Healing Materials: Challenges and New Strategies in Biomaterials Applications for Nanomedicine, Prof. Rosario Pignatello (Ed.), 2011, 661-664.

248. S. Kanokpanont, S. Damrongsakkul, J. Ratanavaraporn, P. Aramwit, *Int. J. Pharm.*, **436**, 141-53 (2012).

249. L. Jeong, I.S. Yeo, H.N. Kim, Y.I. Yoon, H. Jang da, S.Y. Jung, B.M. Min, W.H. Park, *Int. J. Biol. Macromol.*, **44**, 222–228 (2009).

250. N. Minoura, S.I. Aiba, M. Higuchi, Y. Gotoh, Y. Tsukada, Y. Imai, *Biochem. Biophys. Res. Commun.*, **208**, 511-516 (1995).

251. I.D. Pra, P. Petrini, A. Charini, S. Bozzini, S. Fare, U. Armato, *Tissue Eng.*, **9**, 1113-1121 (2003).

252. A. Chiarini, P. Petrini, S. Bozzini, I.D. Pra, *Biomaterials*, **24**, 789-799 (2003).

253. E. Servoli, D. Maniglio, A. Motta, R. Predazzer, C. Migliaresi, *Macromol. Biosci.*, **5**, 1175-1183 (2005).

254. P. Zahedi, Z. Karami, I. Rezaeian, S-H. Jafari, P. Mahdaviani, A.H. Abdolghaffari, M. Abdollahi, *J. Appl. Polym. Sci.*, **124**, 4174–4183 (2012).

255. A.A. Elzatahry, A.M. Al-Enizi, E.A. Elsayed, R.R. Butorac, S.S. Al-Deyab, M.A. Wadaan, A.H. Cowley, *Int. J. Nanomed.*, **7**, 2829–2832 (2012).

256. J. Qin Y. Jiang, J. Fu, Y. Wan, R. Yang, W. Gao, H. Wang, *Iran. Polym. J.*, **22**, 729-737 (2013).

257. G. Verreck, I. Chun, J. Rosenblatt, J. Peeters, A. van Dijck, J. Mensch, M. Noppe, M.E. Brewster, *J Controlled Release*, **92**, 349-360 (2003).

258. R.A. Takur, C.A. Florek, J. Kohn, B.B. Michniak, *Int. J. Pharm.*, **19**, 87-93 (2008).

259. V.K.M. Poon & A. Burd, *Burns*, *30*, 140–147 (2004).

260. P.V. AshaRani, G.L.K. Mun, M.P. Hande, S. Valiyaveettil, *ACS Nano*, **3**, 279–290 (2009).

261. A.B. Lansdown & A. Williams, *J. Wound Care*, **13**, 131–136 (2004).

262. H.C. Neu, *Science*, **257**, 1064–1073 (1992).

263. R.A. Bonomo, *Clin. Infect. Dis.*, **31**, 1414-1422 (2000).

264. X-Z. Li, H. Nikaido, S. Silver, L.T. Phung, G. Silver, *J. Ind. Microbiol. Biotechnol.*, **33**, 627–634 (2006).

265. J.A. Ross, C.M. Kasum, *Annu. Nutr.*, **22**, 19–34 (2002).

266. A. Svobodová, J. Psotová, D. Walterová, *Biomed. Papers*, **147**, 137–145 (2003).

267. M. Buderer, P. Ford, G. Roentcsh, R. Cervelli, H. Joyce, Patent EP1663132 A1.

268. A.Y. Mensah, P.J. Houghton, R.A. Dickson, T.C. Fleischer, *Phytother. Res.*, **20**, 941-944 (2006).

269. G. Basal, D. Altiok, O. Bayraktar, *Fibres Polym.*, **11**, 21-27 (2010).

270. N. Kasoju & U. Bora, *J. Biomed. Mater. Res. B*, **100B**, 1854–1866 (2012).

271. M. Jang, J.M. Pezzuto, *Drugs Exp. Clin. Res.*, **25**, 65–77 (1999).

272. V. Filip, M. Plocková, J. Šmidrkal, Z. Špičková, K. Melzoch, Š. Schmidt, *Food Chem.*, **83**, 585-593 (2003).

273. J.J. Docherty, M.M. Fu, M. Tsai. *J. Antimicrob. Chemother.*, **47**, 239-246 (2001).

274. M. M-Y Chan, *Biochem. Pharmacol.*, **63**, 99-104 (2002).

275. J.J. Docherty, H.A. McEwen, T.J. Sweet, E. Bailey, T.D. Booth. *J. Antimicrob. Chemother.*, **59**, 1182–1184 (2007).

276. M. Jang, L. Cai, G.O. Udeani, K.V. Slowing, C.F. Thomas, C.W. Beecher, H.H. Fong, N.R. Farnsworth, A.D. Kinghorn, R.G. Mehta, R.C. Moon, J.M. Pezzuto, *Science*, **275**, 218-220 (1997).

277. L. Frèmont, *Life Sci.*, **66**, 663-673 (2000).

278. Z.M. Huang, C.L. He, A.Yang, Y. Zhang, X.J. Han, J. Yin, Q. Wu, *J. Biomed. Mater. Res. Part A*, **77**, 169-179 (2006).

279. D.S. Katti, K.W. Robinson, F.K. Ko, C.T. Laurencin, *J. Biomed. Mater. Res. Part B*, **70**, 286-296 (2004).

280. N. Bolgen, I. Vargel, P. Korkusuz, Y.Z. Menceloglu, E. Piskin, *J. Biomed. Mater. Res. Part B*, **81B,** 530–543 (2007).

281. T.G. Kim, T.G. Park, *Tissue Eng.*, **12**, 221–233 (2006).

282. J. Zeng, X. Xu, X. Chen, Q. Liang, X. Bian, L. Yang, X. Jing, *J. Controlled Release*, **92**, 227-231 (2003).

283. K. Kim, Y.K. Luu, C. Chang, C.D. Fang, B.S. Hsiao, B. Chu, B.M. Hadjiargyrou, *J. Controlled Release*, **98**, 47–56 (2004).

284. B.A. Bidlingrneyer, S.A. Cohen, Z.L, Tarvin, *J. Chromatogr.B*, **336**, 93-104 (1984).

285. S. Dube, M.T. Khumalo, N. Torto, J.A. Nyati, *J. Sep. Sci.*, **29**, 1245-1250 (2006).

286. J.R. Mazzeo, in Handbook of capillary electrophoresis, 2nd Ed., J.M. Landers (Ed.), CRC Press, Florida, 1997, p 51.

287. E. Zahou, H. Jörnvall, T. Bergman, *Anal. Biochem.*, **281**, 115-122 (2000).

288. B.X. Mayer, *J. Chromatogr. A*, **907**, 21-37 (2001).

289. T.Y. Liu & Y.H. Chang, *J. Biol. Chem.*, **246**, 2842-2848 (1971).

290. K. Sen & M.K. Babu *J. Appl. Polym. Sci.*, **92**, 1080 (2004).

291. N.V. Bhat & G.S. Nadiger, *J. Appl. Polym. Sci.*, **25** 921–932 (1980).

292. K. Komatsu, in Structure of Silks, N. Hojo (Ed.), Shinkyo, Ueda, 1980, p. 353.

293. G. Freddi, Y. Gotoh, T. Mori, I. Tsutsui, M. Tsukada, *J. Appl. Polym. Sci.*, **52** 775-781 (1994).

294. J.C. Chang, M.J. Fletcher, G.M. Gurr, D.S. Kent, R.G. Gilbert, *Polymer,* **46** 7909-7917 (2005).

295. M. Levitt, *Biochemistry*, **17**, 4277–4285 (1978).

296. L. Shimoni, & J. P. Glusker, *Protein Sci.*, **4**, 65–74 (1995).

297. C.L. Borders,, J.A. Broadwater, P.A. Bekeny, J.E. Salmon, A.S. Lee, A.M. Eldridge, V.B. Pett, *Protein Sci.* **3**, 541 – 548 (1994).

298. A. Teshome, F. Vollrath, S.K. Raina, J.M. Kabaru, J. Onyari, *Int. J. Biol. Macromol.*, **50**, 63–68 (2012).

299. F.J. Chen, D. Porter, f. Vollrath, *Mater. Sci. Eng. C*, **32**, 772–778 (2012).

300. R. Chattopadhyay, *J. Text. Eng.*, **54** 179-190 (2008).

301. J.T. Pelton & L.R. McLean, *Anal. Biochem.*, **277**, 167–176 (2000).

302. D. Devi, N.S. Sarma, B. Talukdar, P. Chetri, K. Baruah, N.N. Dass, *J. Text. Inst.*, **102** 527–533 (2011).

303. W. Zhou, X. Chen, Z.Z. Shao, *Prog. Chem.*, **18**, 1514–1522 (2006).

304. X. Chen, D.P. Knight, Z.Z. Shao, *Soft Matter*, **5**, 2777–2781 (2009).

305. M. Tsukada, *J. Appl. Polym. Sci. Part B*, **32**, 1407-1412 (1994).

306. Y . Gotoh, H. Tsukada, N. Minoura, *Biomaterials*, **59**, 402-409 (1990).

307. W. Tao, Y-Q. Wei, M-Z. Li, *JFBI*, **2**, 114-119 (2009).

308. M.E. Rousseau, T. Lefèvre, L. Beaulieu, T. Asakusa, M. Pézolet, *Biomacromolecules*, **5**, 2247–2257 (2004).

309. M. Preghenella, G. Pezzotti, C. Migliaresi, *J. Raman Spectrosc.*, **38**, 522-536 (2007).

310. P. Monti, P. Taddei, G. Freddi, T. Asakura, M. Tsukada *J. Raman Spectrosc.*, **32**, 103-107 (2001).

311. R. Valluzzi & H.J. Jin, *Biomacromolecules*, **5**, 696–703 (2004).

312. J.O. Warwicker, *Trans. Farady Soc.*, **52**, 556-562 (1956).

313. G. Freddi, M. Tsukada, S. Beretta, *J. Appl. Polym. Sci.*, **71**, 1563–1571(1999).

314. H.Y. Kweon, I.C. Um, Y.H. Park, *Polymer*, **41**, 7361 –7367 (2000).

315. M. Tsukada, M. Nagura, H. Ishikawa, *J. Appl. Polym. Sci.Phys. Ed.*, **25**, 1325–1329 (1987).

316. C.Y. Hayashi, N.H. Shipley, R.V. Lewis, *Int. J. Biol. Macromol.*, **24**, 271–275 (1999).

317. R. Meridith, *J. Text. Inst.*, **36**, T107-T130 (1945).

318. R.M. Robson, Silk in Handbook of Fibre Chemistry, 2nd Ed, M. Lewin & E.M. Pearce (Eds), Marcel Dekker, NY, USA, 1998, p 446.

319. S. Kushal & B.K. Murugesh, *J. Appl. Polym. Sci.*, **92**, 1098-1115 (2004).

320. G. Freddi, R. Mossotti, R. Innocenti, *J. Biotechnol.*, **106** 101–112 (2003).

321. J. Perez-Rigueiro, M. Elices, J. Llorca, C. Viney, *J. Appl. Polym. Sci.*, **84**, 1431-1437 (2002).

322. P. Jiang, H. Liu, C. Wang, L. Wu, J. Huang, C. Guo, *Mater. Lett.*, **60**, 919-925 (2006).

323. V. Mhuka S. Dube, M.M. Nindi, N. Torto *Macromol. Res.*, **21**, 995-1003 (2013).

324. A.I. Sarabia, M.C. Gómez-Guillén, P. Montero, *Food Chem.*, **70**, 71–76 (2000).

325. K.T. Addis & S.K. Raina, *Pak. J. Biol. Sci.*, **16**, 1199-1203 (2013).

326. A. Dér, L. Kelemen, L. Fábián, S. G. Taneva, E. Fodor, T. Páli, A. Cupane, M.G. Cacace, J.J. Ramsden, *J. Phys. Chem. B*, **111**, 5344-5350 (2007).

327. K.D. Collins, *Methods*, **34**, 300–311 (2004).

328. W.N.L. Zhang, Y. Wenhua, X. Shiying, *J Chin. Inst. Food Sci. Technol.*, **1**, 56 (2001).

329. Y. Miyaguchi, J. Hu, *Food Sci. Technol. Res.*,**11**, 37-42 (2005).

330. Tomoaki Hino, *J. Colloid Interface Sci.*, **266**, 68–73 (2003).

331. A.S. Bommarius, B.R. Riebel, Biocatalysis: Fundamentals and Applications, Wiley, New York, 2004, p 228.

332. J. Perez-Rigueiro, C. Viney, J. Llorca, M.J. Elices, *J. Appl. Polym. Sci.* **82**, 1928–1935 (2001).

333. J.M. Deitzel, J. Kleinmeyer, D. Harris, N.C. Beck Tan, *Polymer*, **42**, 261, (2001).

334. S.H. Tan, R. Inai, M. Kotaki, S. Ramakrishna, *Polymer*, **46**, 6128-6134 (2005).

335. D. H. Reneker, I. Chun, *Nanotechnology*, **7**, 216-223 (1996).

336. L Jeong, K.Y. Lee, W.H. Park, *Key Eng. Mater.*, **342-343**, 813-816 (2007).

337. Y. Liu, S. Xiong, R. You and M. Li, *Mater. Sci. Appl.*, **4**, 365-373 (2013).

338. Z.W. Zhou, J. He, S. Cui, W. Gao, *Open Mater. Sci. J.*, **5**, 51 (2011).

339. E.R. Kenawy, J.M. Layman, J.R. Watkins, G.L. Bowlin, J.A. Matthews, D.G. Simpson, G.E. Wnek, *Biomaterials*, **24**, 907-913 (2003).

340. Y. Tamada, *Biomacromolecules*, **6**, 3100-3106 (2005).

341. N. Bhardwaj & S.C. Kundu, *Biotechnol. Adv.*, **28**, 325–347 (2010).

342. A. L. Andrady, Science and Technology of Polymer Nanofibers, John Wiley & Sons, Hoboken, 2007, p 105.

343. W. Wei, Y. Zhang, H. Shao, X. Hu, *J. Mater. Res.*, **26**, 1100-1106 (2011).

344. W. Tao, M. Li, C. Zhao, *Int. J. Biol. Macromol.*, **10**, 472-478 (2007).

345. M. Li, W. Tao, S. Kuga, Y. Nishiyama, *Polym. Adv. Technol.*, **14**, 694–698 (2003).

346. M. Ishida, T. Asakura, M. Yokoi, H. Saito, *Macromolecules*, **23**, 88-94 (1990).

347. J. Zhu, Y. Zhang, H Shao, X. Hu, *Polymer*, **49**, 2880–2885 (2008).

348. M. Zoccola, A. Aluigi, C. Vineis, C. Tonin, F. Ferrero, M.G. Piacentino, *Biomacromolecules*, **9**, 2819–2825 (2008).

349. A. Alessandrino, B. Marelli, C. Arosio, S. Fare, M.C. Tanzi, G. Freddi, *Eng. Life Sci.*, **8**, 219–225 (2008).

350. Y.B. Chen, B.X. Sun, J.X.Chen, *Zhong Yao Cai.* **30**, 805–807 (2007).

351. D. Baycin, E. Altiok, S. Ulku, and O. Bayraktar, *J. Agric. Food Chem.*, **55**, 1127-1136 (2007).

352. H.R. Tang, A.D. Covington, R.A. Hancock, *Biopolymers*, **70**, 403-413 (2003).

353. S. Hofmann, C.T. Foo, F. Rossetti, M. Textor, G. Vunjak-Novakovic, D.L. Kaplan, *J. Controlled Release*, **111**, 219-227 (2006).

354. E. Wenk, A.J. Wandrey, H.P. Merkle, L. Meinel, *J. Controlled Release*, **132**, 26-34 (2008).

355. A. Vasconcelos A.C. Gomes, A. Cavaco-Paulo, *Acta Biomaterialia*, **8** 3049–3060 (2012).

356. A. Scalbert, *Phytochemistry*, **30**, 3875–3883 (1991).

357. S Das, K.Y. Ng, P.C. Ho, *AAPS Pharm. Sci. Tech.*, **11**, 729–742 (2010).

358. M.K Babu & K. Sen, *RJTA,* **11**, 21-27 (2007).

359. S.S. Karuppagounder, J.T. Pinto, H. Xu, H.L. Chen, M.F. Beal, G.E. Gibson, *Neurochem. Int.*, **54**, 111–118 (2009).